Hybrid Macro-Particle Moment Accelerator Tracking Algorithm

by

Paul Matthew Jung

B.Sc., University of Waterloo, 2017

A Thesis Submitted in Partial Fulfilment of the
Requirements for the Degree of

MASTER OF SCIENCE

in the Department of Physics and Astronomy

Hybrid Macro-Particle Moment Accelerator Tracking Algorithm

by

Paul Matthew Jung

B.Sc., University of Waterloo, 2017

Supervisory Committee

Prof. Richard A. Baartman, Co-Supervisor
(Department of Physics and Astronomy & TRIUMF)

Dr. Dean Karlen, Co-Supervisor
(Department of Physics and Astronomy & TRIUMF)

Abstract

A particle accelerator simulation which straddles the gap between multi-particle and moment codes is derived. The hybrid approach represents the beam using macro-particles which contain discrete longitudinal coordinates and transverse second moments. The discretization scheme for the macro-particles is derived using variational principles, as a natural extension of well known variational approaches. This variational discretization allows for exact transverse emittance conservation. The electrostatic self-potential is discrete in the longitudinal direction and solved semi-analytically in the transverse direction using integrated Green's functions. The algorithm is implemented and tested against both a moment and multi-particle code.

Table of Contents

List of Figures

Chapter 1

Introduction

1.1 Particle Accelerator Simulation

Particle accelerators are machines that use electromagnetic fields to accelerate and contain charged particles for a variety of scientific, medical and industrial applications. To build new machines and improve the existing ones, we construct mathematical models. These models are used in the design process to predict performance and to guide design decisions. For machines that are already operating, models are used to identify and diagnose problems, and to gain a more nuanced understanding of the intricacies of the machine with the goals to improve their reliability and extend their capabilities.

The laws that govern the dynamics of charged particles in electromagnetic fields have been well known since Lorentz published in 1895 [2]. Even with the added refinement of Special Relativity by Einstein, the study of motion of individual charged particles remains managable. The difficulty arises from the electromagnetic field that is produced by the particles themselves. This so-called 'self field' (as opposed to external field), depends on the position and velocity of each of the particles, and therefore requires a detailed model of the beam to reproduce. Directly modelling every individual charged particle in a realistic machine would require tracking the an immense number of individual particles including the exact electromagnetic interaction between each of them. This approach is impractical.

The complexity of the problem can be reduced by viewing the distribution of particles as a continuum of charge. By taking this continuous approximation, the system can be described by partial differential equations.

The system of interest in accelerator and plasma physics is the the Maxwell Vlasov system, a set of non-linear partial differential equations. This system was first presented by Vlasov in Ref. [3]. The ensemble of particles is represented by a continuous particle density function in six-dimensional phase space. This distribution of charge generates electric and magnetic fields that influences itself. There are many methods both analytic and numerical to solve such a system. I will restrict the scope to specific numerical schemes.

Detailed Discretizations

One numerical approach to discretize the continuum of charge is the method of 'macro-particles'. This method tracks the flow of continuous media by tracking a set of points in phase space as they evolve in time. This is often referred to as the Lagrangian specification of fluid flow. This discretization scheme is used in many areas including fluid dynamics, plasma dynamics and astrophysics. Many of these applications are discussed in the seminal textbook by Hockney and Eastwood [4] which presents a unified picture of the method. In accelerator and plasma physics, the macro-particles represent some number of real particles and hence have the same mass to charge ratio as them as well.

One of the most widely used tools for studying space charge effects in particle accelerators is the particle-in-cell (PIC) method, where macro-particles are tracked through discretized electric and magnetic fields. The PIC scheme has among the best time-stepping performance, conserves particle momentum, and is second-order accurate in space and time. [4]. With the PIC method, using modern hardware, accelerator physicists have recently been able to simulate systems with a realistic number of particles. However the computing requirements are tremendous. See the discussion of the use of high performance parallel computing by Ryne Ref. [5].

Reduced Discretizations

An alternative approach to solving such a system is to track a set of macroscopic variables that broadly describe the evolution of the system, while neglecting the minutiae. Kapchinskij and Vladimirskij derived a self-consistent system of equations (KV equations) that described the transverse size of a continuous beam in a transport line [6]. Their system assumes the beam is a particular idealized distribution in phase-space, which produces a linear

space-charge force. Sacherer generalized the KV equations to beams with ellipsoidal symmetry showing that for such a beam, the linear force depends almost entirely on the second moments, in 1, 2 and 3 dimensions [7]. The size of the ellipsoidal beam is described by a collection of statistical second moments, the dynamics for which is derived by averaging over the collection of discrete particle equations of motion.

There are computer codes that track the size of the ellipsoidal beam in phase space such as `TRANSPORT` [8] and `TRANSOPTR` [9, 10, 11]. These codes are still in use today, as they offer unrivalled performance. However, these methods are limited in that they cannot model the degradation of beam quality from the non-linear components of external and space-charge forces. To extend the method of moments, work was done to derive systems of statistical moments of arbitrary order by Channell [12]. While the second order moment method remains in use, higher-order moment methods have not. The preferred models of detailed dynamics are usually multi-particle.

Errors in Mathematical Modelling

The dynamics in particle accelerators is precisely governed by well-known physical laws. Even so, in the early years of accelerators, the limited computing power led accelerator physicists to rely heavily on reduced models and approximations, often having to leave large margins of error in the design process. Hence the popularity of the envelope codes like `TRANSPORT`. Even with the use of multi-particle codes, many simplifying assumptions had to be made to make implementation and computation time tractable. In more recent years, with the accessibly of high performance computing facilities, the modelling of entire machines with high resolution is possible. It has enabled physicists to develop designs with significantly more precision. This leads to the temptation to include every detail of the accelerator in the model.

However, the short article written by Saltelli [1], cautions that care must be taken when building and testing mathematical models. From this article, Fig 1.1 outlines the fundamental trade off between model error and complexity that has to be considered when designing mathematical models. By including many details not essential to the area of interest, we may introduce sources of uncertainty into the simulation, which can increase the model error overall.

The software used in accelerator physics is high quality: having been well tested, and the underlying physics is well understood, however, the mod-

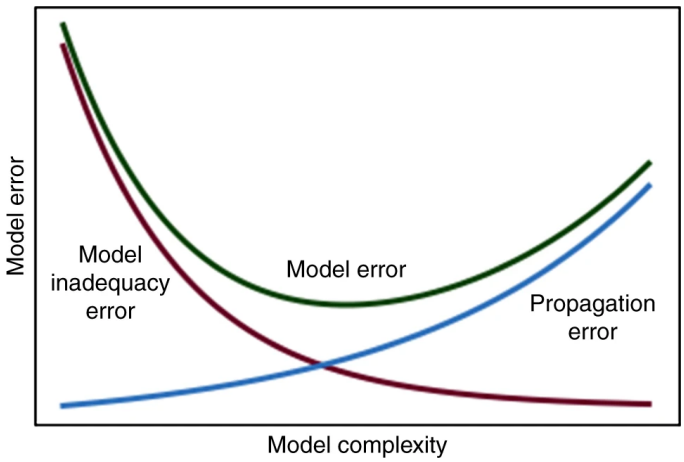

Figure 1.1: Saltelli [1], the total error in a model as function of the complexity. The total error is a combination of the errors made by the simplicity of the model as well as the errors made due to uncertainty present in the inputs to the model.

elling of the machines done in the input to the software may diverge from reality. This divergence arises from many different sources of input error which may be due to manufacturing errors, incorrect alignment or faulty control software, among many others. To build a detailed model which accurately represents an as-built machine, all of these sources of error must be taken into account.

This consideration of mathematical modelling is a motivating factor behind the work of this thesis. That is, to build a model with reduced complexity, by removing some unnecessary details and leaving fewer inputs which are more robust to statistical and systematic error.

Variational Discretizations

Direct discretization of the system of equations of motion is known to lead to difficulties. The equations of motion have underlying mathematical structure such as conservation laws for energy, momentum and symplecticity. This underlying structure is often important to the validity of the results and often ends up being neglected by directly discretizing the equations of motion. The underlying mathematical structure is expressed by the variational formulation of the system. In mechanics, this is Hamilton's principle

of stationary action. The first variational formulation of the Vlasov-Maxwell system was done by Low [13] as a classical field theory Lagrangian which led eventually to work done by Morrison and collaborators [14, 15, 16] to discover the Hamiltonian formulation of the Maxwell-Vlasov system using a non-canonical Poisson bracket. This approach, based on the stationary action principle, enabled plasma physicists to produce a class of energy conserving macro-particle algorithms. These are also presented in the textbook by Hockney and Eastwood [4]. These early variational algorithms had limitations such as requiring an implicit time step at a specific integration order and their performance scaled poorly with discretization parameters, which overall resulted in a large computational cost that prevented adoption in the accelerator physics community.

The work of Evstatiev and Shadwick in Ref.[17, 18] marks a turning point for variational macro-particle algorithms. Their methods for deriving new algorithms loosens the restrictions previously applied to these algorithms. Of particular importance to accelerator physics, the variational algorithms can be integrated with an arbitrary order and accuracy, while conserving many of the desirable properties of the underlying mechanics.

The variational formalism also had consequences for moment methods. The work done by Shadwick and collaborators [19, 20] presents an elegant moment expansion and truncation using the non-canonical Hamiltonian formulation of the Vlasov system. In the conclusion to the 1999 conference paper [19] they suggest:

> It is also possible to construct "semi-discrete" models; for example, by averaging only over the transverse phase space, one obtains a system where the transverse dynamics are determined by moments while a full kinetic description is retained longitudinally.

1.2 Outline of Thesis

The purpose of the thesis is to derive and test a "semi-discrete" space charge algorithm. This algorithm consists of a macro-particle discretization in the longitudinal direction and moments transversely. This chapter covers the underlying mathematical model which is the Hamiltonian formulation of the Vlasov Poisson system, and its application in accelerator physics.

Chapter 2 is a review that presents the variational derivation of three separate one-dimensional algorithms. The first two schemes are macro-particle methods: the particle-particle method as well as the particle-in-cell method. The third scheme is the moment method. The derivations in Chapter 2 serve as pedagogical examples, as well as the basis for the next chapter. Chapter 3 presents the derivation for the three-dimensional hybrid macro-particle moment method. The details of the self-field discretization and calculation can be found in Appendix C. Chapter 4 presents the tests of the implementation of the hybrid scheme including the comparison to another code. The analytic results used in testing are derived in Appendix D.

1.3 The Vlasov Poisson System

The Vlasov Poisson system of partial differential equations describes the time evolution of a distribution of charged particles in the continuum limit. The continuum limit, in this case, considers the charge to be smoothly distributed, this removes the singularities in the potential from individual charged particles. It has a few underlying assumptions, the first being that the particles are non-relativistic. The second assumption is that the collisions between particles is negligible. Consider a distribution of identical particles with mass, denoted by m, and charge, denoted by q. This distribution of particles can be described by the particle distribution function $f(\mathbf{x}, \mathbf{p}, t)$. This is a number density in phase space and has units of number of particles per phase-space volume. Integrating over a phase-space volume $\mathcal{V}$, we find the total number of particles in the volume.

$$N(t) = \int_{\mathcal{V}} \mathrm{d}^3\mathbf{x}\, \mathrm{d}^3\mathbf{p}\, f(\mathbf{x}, \mathbf{p}, t)\,. \tag{1.1}$$

Let $\phi(\mathbf{x}, t)$ denote the electrostatic potential that satisfies the Poisson equation:

$$\Delta_{\mathbf{x}}\phi(\mathbf{x}, t) = -\frac{q}{\epsilon_0}\int \mathrm{d}^3\mathbf{p}\, f(\mathbf{x}, \mathbf{p}, t) = -\frac{q}{\epsilon_0} n(\mathbf{x}, t)\,, \tag{1.2}$$

where $n(\mathbf{x}, t)$ is the spatial number density. Then, the force on a particle with charge, q is:

$$\mathbf{F} = -q\nabla_{\mathbf{x}}\phi(\mathbf{x}, t)\,. \tag{1.3}$$

So the Vlasov Poisson system in its entirety is:

$$\begin{aligned} \frac{\partial f}{\partial t} + \frac{\mathbf{p}}{m} \cdot \nabla_{\mathbf{x}} f - q \nabla_{\mathbf{x}} \phi \cdot \nabla_{\mathbf{p}} f = 0, \\ \Delta_{\mathbf{x}} \phi + \frac{q}{\epsilon_0} n = 0 \,. \end{aligned} \tag{1.4}$$

Note, that the above equations are for a single particle species, however, it may easily be extended to include an arbitrary number of different particle distributions.

The system of equations (1.4) is the basis for many of the high-performance particle-in-cell codes written today. To continue in the direction of Evstatiev and Shadwick [17, 18], we need to study the variational formulation of this system.

1.3.1 Hamiltonian Formulation

The Hamiltonian formulation of the Vlasov Poisson system was first derived by Morrison in Ref. [15]. This section presents a broad overview of this system. Although, it is the underlying mathematical model of this thesis, the details of the classical field theory formulation are not crucial as the focus of this work is on discretization. The intrepid reader may refer to Appendix A which derives the equations of motion yielding the Vlasov Poisson equations.

The phase space is comprised of the position vector $\mathbf{x}$, and the canonical momentum vector $\mathbf{p}$. This system is constructed using the Eulerian description of a fluid. In this case, the variables $\mathbf{x}$ and $\mathbf{p}$ are considered independent variables like time. An excellent summary on the Hamiltonian fomulation of an Eulerian fluid is given by Salmon in Ref. [21].

The Hamiltonian is the energy of the system, which for the Vlasov Poisson system may be written as:

$$\mathrm{H} = \int \mathrm{d}^3\mathbf{x}\, \mathrm{d}^3\mathbf{p}\, f(\mathbf{x}, \mathbf{p}, t) \left(\frac{\mathbf{p}^2}{2m} + \frac{q}{2} \phi[f](\mathbf{x}, t) \right) . \tag{1.5}$$

the sum of the kinetic and potential energy.[1]

[1]Note that the factor of $\frac{1}{2}$ on the electrostatic potential relates to the sum of two terms in the Lagrangian, the interaction energy of the charge distribution with the electric potential and the energy in the field itself.

To use this Hamiltonian to find equations of motion, the non-canonical Poisson bracket is defined as:

$$\{F, G\} = \int \mathrm{d}^3\mathbf{x}\, \mathrm{d}^3\mathbf{p}\, f(\mathbf{x}, \mathbf{p}, t) \left[\frac{\delta F}{\delta f}, \frac{\delta G}{\delta f}\right] , \tag{1.6}$$

where F and G are functionals of f, and may be functions of time. The terms $\frac{\delta F}{\delta f}$ and $\frac{\delta G}{\delta f}$ are functional derivatives of F and G with respect to the particle density function, for more information see the Appedix A.1. Also, the expression, $[\,\cdot\,,\cdot\,]$ is the familiar canonical Poisson bracket with respect to $\mathbf{x}$ and $\mathbf{p}$ given by:

$$[a, b] = \nabla_{\mathbf{x}} a \cdot \nabla_{\mathbf{p}} b - \nabla_{\mathbf{p}} a \cdot \nabla_{\mathbf{x}} b\,, \tag{1.7}$$

where a and b are general functions of the canonical variables $(\mathbf{x}, \mathbf{p})$. Then, Morrison in section 1.2 of Ref. [15] defines a system to be Hamiltonian if the time derivative of a functional is given by the Poisson bracket:

$$\frac{\delta F}{\delta t} = \{F, H\}\,. \tag{1.8}$$

This Poisson bracket obeys the usual properties of anti-symmetry and bi-linearity it also satisfies Leibniz's Rule and the Jacobi Identity. For more specifics, see the paper in which it was first derived by Morrison in section 6 of Ref. [15]. Note that while the overall bracket is called non-canonical, the phase-space coordinates $(\mathbf{x}, \mathbf{p})$ are canonically conjugate.

Self Field

An important subtlety of this formalism is that the electrostatic potential is defined as a functional, as well as a function:

$$\phi[f](\mathbf{x}', t) = -\frac{q}{\epsilon_0} \int \mathrm{d}^3\mathbf{x}\, \mathrm{d}^3\mathbf{p}\, f(\mathbf{x}, \mathbf{p}, t) G(\mathbf{x}', \mathbf{x})\,, \tag{1.9}$$

where the function $G(\mathbf{x}', \mathbf{x}'')$ is called the Green's function for the Poisson equation. The Green's function follows from Poisson's equation:

$$\Delta_{\mathbf{x}} \phi[f](\mathbf{x}, t) = -\frac{q}{\epsilon_0} \int \mathrm{d}^3\mathbf{p}\, f(\mathbf{x}, \mathbf{p}, t)\,, \tag{1.10}$$

where we may write the solution as:

$$\phi[f](\mathbf{x},t) = -\frac{q}{\epsilon_0}\int \mathrm{d}^3\mathbf{x}'\,\mathrm{d}^3\mathbf{p}'\,f(\mathbf{x}',\mathbf{p}',t)G(\mathbf{x},\mathbf{x}')\,. \tag{1.11}$$

Since $G(\mathbf{x},\mathbf{x}')$ is defined as the Green's function that satisfies

$$\Delta_{\mathbf{x}}G(\mathbf{x},\mathbf{x}') = \delta^{(3)}(\mathbf{x}-\mathbf{x}') \tag{1.12}$$

inside the domain of interest, and it must also satisfy any boundary conditions. See Arfken and Weber, Ref. [22], for existence and uniqueness proofs of the Poisson equation.

Using the explicit form of the potential, (1.11), the Hamiltonian may be written more explicitly as two terms:

$$\mathrm{H}_p = \int \mathrm{d}^3\mathbf{x}\,\mathrm{d}^3\mathbf{p}\,f(\mathbf{x},\mathbf{p},t)\frac{\mathbf{p}^2}{2m}\,, \tag{1.13}$$

$$\mathrm{H}_\phi = -\frac{q^2}{2\epsilon_0}\int \mathrm{d}^3\mathbf{x}'\,\mathrm{d}^3\mathbf{x}''\,\mathrm{d}^3\mathbf{p}'\,\mathrm{d}^3\mathbf{p}''\,f(\mathbf{x}',\mathbf{p}')f(\mathbf{x}'',\mathbf{p}'')G(\mathbf{x}',\mathbf{x}'')\,, \tag{1.14}$$

such that the total Hamiltonian: $\mathrm{H} = \mathrm{H}_p + \mathrm{H}_\phi$, the sum of kinetic and potential energy terms respectively. This is the expression for the Hamiltonian that will be used most commonly in this thesis.

1.3.2 From Plasmas to Electrostatic Optics

The motivating problem for this work is to model the bunching process in the injection line to the TRIUMF 520 MeV cyclotron. This beamline transports and bunches H^- ions at a relatively low energy of 300 keV, well below the relativistic regime. However, it can transport relatively high current; up to around 500 µA, which makes it heavily influenced by the effects of space-charge.

To apply the Poisson Vlasov model to such a problem in accelerator physics, we will need to determine where it is valid. In particle accelerators, the beam moves coherently in one direction, the 'longitudinal' direction, in which most of the kinetic energy is carried. The plane perpendicular to the longitudinal direction is called the 'transverse' plane. The beam is assumed to travel through a system of vacuum chambers so that it does not degrade in quality due to interactions with the atmosphere. Colloquially, the vacuum

chamber is often called the 'beam-pipe', as it is often a metallic pipe.

The main limitation of the model is that it is non-relativistic. It will only be valid for relatively heavy particles at lower energy. The extension to a relativistic model would have to be done similarly to Shadwick and Wurtele [19] but that extension is outside the scope of this thesis. The non-relativistic limitation is not a concern for our application since the average velocity of the beam in the injection line is around 2.5% the speed of light.

The feature often distinguishing accelerator modelling from plasma physics is the tracking through the electromagnetic field that is produced by the machine to contain and control the beam. Since the injection line consists of only electrstatic optical elements, we only need to model the electric potential of these elements. Let the external potential be $\varphi(\mathbf{x}, t)$. The energy of the particle distribution in this potential, hence the Hamiltonian is the integral:

$$\mathrm{H}_{\text{external}} = \int \mathrm{d}^3\mathbf{x}\, \mathrm{d}^3\mathbf{p}\, f(\mathbf{x}, \mathbf{p}, t) q\varphi(\mathbf{x}, t)\,. \tag{1.15}$$

This is a general model able to represent arbitrary electrostatic and radio-frequency devices neglecting magnetic fields. It may extended to include some magnetic elements in certain regimes.[2]

[2]For systems with a constant longitudinal velocity, v_0, it is possible to represent some magnetic elements using the longitudinal component of the magnetic vector potential. In this case, the external potential has the form:

$$\varphi(\mathbf{x}, t) = \varphi_{\text{external}}(\mathbf{x}, t) - v_0 A_z(\mathbf{x}, t)\,. \tag{1.16}$$

This approximation works well for common magnetic optical elements like dipoles, quadrupoles, and octopoles.

Chapter 2

A Tutorial on Macro-particle and Moment Algorithms

To be able to implement an algorithm on a computer, the system of partial differential equations must be reduced to a system with finite number of discrete degrees of freedom. This chapter is a pedagogical exercise to show that this formalism allows for the unified description of very different techniques of discretization.

The macro-particle discretization scheme splits the particle density function into many sub-distributions with a fixed shape and charge. Each of these distributions represents many real particles and each has the same charge-to-mass ratio as the real particles. The set of these macro-particles is equivalent to a statistical sampling of the density function. The macro-particles obey equations of motion similar to those of real particles, and can be integrated as such. The fixed shape of each macro-particle distributes its charge smoothly in space to avoid creating artificial collisions between the macro-particles. This approach is used to derive the particle-particle method in Section 2.2.1 as well as the particle-in-cell method in Section 2.2.2.

The moment discretization scheme represents the particle density distribution by a collection of its statistical moments. We can expand and truncate the Hamiltonian, so that it is an explicit expression of the moments. Then, the Poisson bracket is used to compute the equation of motion for each of these moments. The result is a linear system of first order ordinary differential equations. This approach is used to derive the 1D KV equation in Section 2.3.

2.1 One Dimension Simplification

For simplicity, throughout this chapter, I work with the Vlasov Poisson system in one transverse dimension: (x, p). The particle density function, $f(x, p, t)$, is a number density in phase space. The Hamiltonian is then:

$$\mathrm{H} = \int \mathrm{d}x\, \mathrm{d}p\, f(x,p,t) \left(\frac{p^2}{2m} + q\varphi(x,t) \right) - \frac{q^2}{2\epsilon_0} \int \mathrm{d}x'\, \mathrm{d}x''\, \mathrm{d}p'\, \mathrm{d}p''\, f(x',p') f(x'',p'') G(x',x'')\,, \quad (2.1)$$

and the Poisson bracket is

$$\{F, G\} = \int \mathrm{d}x\, \mathrm{d}p\, f(x,p,t) \left[\frac{\delta F}{\delta f}, \frac{\delta G}{\delta f} \right], \quad (2.2)$$

where the one-dimensional Poisson bracket defined with respect to phase-space functions, $a(x, p)$ and $b(x, p)$ is:

$$[a, b] = \frac{\partial a}{\partial x}\frac{\partial b}{\partial p} - \frac{\partial a}{\partial p}\frac{\partial b}{\partial x}\,. \quad (2.3)$$

2.2 Macro-particle Discretization

The work by Evstatiev and Shadwick, Ref. [17], was the first to present a Hamiltonian formulation of a variational macro-particle algorithm. This section restates the presentation by Evstatiev and Shadwick, with the goal of providing explicit derivations.

First consider the particle density function $f(x, p, t)$. The first step is to divide this distribution function into different groupings:

$$f(x,p,t) = \sum_{i=1}^{N_p} f_i(x,p,t)\,, \quad (2.4)$$

where each f_i interacts only though the self-field, i is the macro-particle index and N_p is the total number of macro-particles. Furthermore, assume

that each f_i has an explicit form:

$$f_i(x,p,t) = w_i R(x - x_i(t))\delta\left(p - \frac{p_i(t)}{w_i}\right) , \tag{2.5}$$

where the coordinate pair (x_i, p_i) is position and momentum of the macro-particle in phase space. Here, I have assumed that this grouping of particles contains a constant number, w_i, of real particles. The macro-particle is distributed over a fixed spatial distribution $R(x)$ with an exact momentum. [1]

The density function is explicitly:

$$f(x,p,t) = \sum_{i=1}^{N_p} w_i R(x - x_i(t))\delta\left(p - \frac{p_i(t)}{w_i}\right) . \tag{2.6}$$

The spatial distribution, $R(x)$, is a function that satisfies the norming condition [17]:

$$\int_{-\infty}^{\infty} \mathrm{d}x\, R(x) = 1 . \tag{2.7}$$

This results in the total charge being a conserved quantity.

The shape of the spatial distribution of the macro-particle is a choice left to the creator of the algorithm. The smoothness of the distribution function will influence the smoothness of the force between particles. In particular, by choosing some distribution other than a Dirac δ-function, we may avoid hard-edge collisions that can introduce an artificial level of noise into the computation. Even though smoother distribution functions are more desirable, they have a the greater implementation and computation time cost, so a delicate balance must be achieved. Usually, first and second order polynomials are chosen as they provide sufficient smoothness while being cheap to evaluate. The macro-particle shape distribution is usually chosen to be an even function. For further discussion on macro-particle shape see Evstatiev and Shadwick, Ref. [17].

[1] Note that the coordinate x_i is the centre of mass position of the macro-particle and the momentum, p_i, is the total momentum of the macro-particle. This choice differs from that of Evstatiev and Shadwick so that these are canonicly conjugate variables, as shown in Appendix B. The term p_i/w_i in (2.5) is the average momentum of the constituent particles in the macro-particle.

2.2.1 A Particle-Particle Algorithm

For the purpose of simplicity we will assume that the particle shape function is given by the Dirac δ-function. This choice is the most natural for the purpose of explanation, however in practice it leads to simulations plagued by numerical noise and instability, see the discussion on macro-particle shape by Evstatiev and Shadwick, Ref. [17]. The particle density function is then:

$$f(x,p,t) = \sum_{i=1}^{N_p} w_i \delta(x - x_i(t)) \delta\left(p - \frac{p_i(t)}{w_i}\right) . \tag{2.8}$$

Recall the one dimensional Hamiltonian is:

$$\begin{aligned} \mathrm{H} = \int \mathrm{d}x\, \mathrm{d}p\, f(x,p,t) \left(\frac{p^2}{2m} + q\varphi(x,t)\right) \\ - \frac{q^2}{2\epsilon_0} \int \mathrm{d}x'\, \mathrm{d}x''\, \mathrm{d}p'\, \mathrm{d}p''\, f(x',p') f(x'',p'') G(x',x'') \,, \end{aligned} \tag{2.9}$$

substituting (2.8) directly, taking care to use unique indices for the summations and straightforward integration of the δ-functions gives:

$$\widetilde{\mathrm{H}} = \sum_i \left(\frac{{p_i}^2}{2m w_i} + q w_i \varphi(x_i,t)\right) - \frac{q^2}{2\epsilon_0} \sum_{j,k} w_j w_k G(x_j, x_k) \,, \tag{2.10}$$

this is almost identical to a single particle Hamiltonian, but for the weight factors of w_i, w_j and w_k. The Green's function may be interpreted as the potential energy between two infinitesimal charges, which will give the familiar Coulomb force between the particles. This Hamiltonian is equivalent to the one constructed by Qiang in Ref. [23].

To see how the equations of motion are derived variationally from this discretization scheme, refer to Appendix B. Section B.2 in particular, shows that the non-canonical Poisson bracket reduces to Hamilton's equations for the (x_i, p_i) pairs. Hamilton's equations are:

$$\frac{\mathrm{d}x_\ell}{\mathrm{d}t} = \frac{\partial \widetilde{\mathrm{H}}}{\partial p_\ell} \,, \qquad\qquad \frac{\mathrm{d}p_\ell}{\mathrm{d}t} = -\frac{\partial \widetilde{\mathrm{H}}}{\partial x_\ell} \,.$$

Starting with the equation of motion for the position, the only dependence

on p_ℓ is in the kinetic energy term:

$$\frac{\mathrm{d}x_\ell}{\mathrm{d}t} = \frac{p_\ell}{mw_\ell}\,. \tag{2.11}$$

Similarly for the momentum,

$$\frac{\mathrm{d}p_\ell}{\mathrm{d}t} = -\left(qw_\ell \frac{\partial \varphi(x_\ell, t)}{\partial x_\ell} - \frac{q^2}{2\epsilon_0} \sum_{j,k} \left[w_\ell w_k \frac{\partial G(x_\ell, x_k)}{\partial x_\ell} + w_j w_\ell \frac{\partial G(x_j, x_\ell)}{\partial x_\ell} \right] \right)\,. \tag{2.12}$$

Note that the self-potential term is split into two terms. However, the Green's function is symmetric so, swapping the arguments in the Green's function and relabelling the indices, $k \to j$, gives:

$$\frac{\mathrm{d}p_\ell}{\mathrm{d}t} = -\left(qw_\ell \frac{\partial \varphi(x_\ell, t)}{\partial x_\ell} - \frac{q^2}{\epsilon_0} \sum_{j} w_j w_\ell \frac{\partial G(x_j, x_\ell)}{\partial x_\ell} \right)\,. \tag{2.13}$$

Further simplification gives:

$$\frac{\mathrm{d}p_\ell}{\mathrm{d}t} = -qw_\ell \frac{\partial}{\partial x_\ell} \left(\varphi(x_\ell, t) - \frac{q}{\epsilon_0} \sum_{j} w_j G(x_j, x_\ell) \right)\,. \tag{2.14}$$

So the overall system of equations for the particle-particle scheme is:

$$\frac{\mathrm{d}x_\ell}{\mathrm{d}t} = \frac{p_\ell}{mw_\ell}\,, \tag{2.15}$$

$$\frac{\mathrm{d}p_\ell}{\mathrm{d}t} = -qw_\ell \frac{\partial}{\partial x_\ell} \left(\varphi(x_\ell, t) - \sum_{j} \frac{q}{\epsilon_0} w_j G(x_j, x_\ell) \right)\,. \tag{2.16}$$

This system of equations is the same as any system of non-relativistic particles in an external potential with interaction terms. The factors of w_ℓ show that the macro-particle has mass mw_ℓ and charge qw_ℓ, the mass and charge of the total number of real particles it represents.

2.2.2 A Particle-In-Cell Algorithm

This method is similar to the previous method, however, it involves also discretizing the self-potential. This derivation diverges slightly from the work of Evstatiev and Shadwick, Ref. [17], and takes inspiration from Qiang Ref. [24]. This approach involves finding the discrete form of the Green's function by solving the discrete Poisson equation, which will be derived separately from variational principles.

Discrete Green's Function

Since the potential formulation of the electric field is degenerate (there is no explicit time dependence), the Hamiltonian formalism cannot produce the equations of motion for the electrostatic potential. To overcome this, I will use the Lagrangian formulation of the electrostatic potential to variationally derive and solve the resulting discrete equations of motion following directly the one dimensional Lagrangian of Evstatiev and Shadwick in Ref [17], but with a general charge density function $\rho(x,t)$. The Lagrangian is:

$$\mathrm{L} = -\int \mathrm{d}x\, \rho(x,t)\phi(x,t) + \frac{\epsilon_0}{2}\int \mathrm{d}x\, \left(\nabla_x \phi(x,t)\right)^2 . \tag{2.17}$$

First, let us approximate the self-potential by projecting it onto a set of local basis functions on a uniform spatial grid with grid points labelled by $i = 1, 2, \ldots, N_g$, the grid spacing is h and the basis function is denoted $\psi_i(x)$. The potential is then:

$$\phi(x,t) = \sum_{i=1}^{N_g} \phi_i(t)\psi_i(x)\,, \tag{2.18}$$

where $\phi_i(t)$ is the value of the potential at grid point i and $\psi_i(x)$ is the finite element function centred at that grid point. For details on the linear finite element basis functions refer to Appendix C. Similar to previous discretization schemes, substitute this directly into the Lagrangian to find:

$$\mathrm{L} = -\sum_i \phi_i \int \mathrm{d}x\, \rho(x,t)\psi_i(x) + \frac{\epsilon_0}{2}\sum_{j,k}\phi_j\phi_k \int \mathrm{d}x \nabla_x\psi_j(x)\nabla_x\psi_k(x)\,. \tag{2.19}$$

Note that the remaining integral in the second term is a constant that only depends on the shape of the basis functions so may be computed directly. For now, this integral is defined to be:

$$D_{jk} = -\frac{1}{h}\int \mathrm{d}x \nabla_x \psi_j(x) \nabla_x \psi_k(x)\,, \tag{2.20}$$

which may be written as a symmetric matrix. Therefore the discrete Lagrangian is:

$$\mathrm{L} = -\sum_i \phi_i \int \mathrm{d}x\, \rho(x,t)\psi_i(x) - h\frac{\epsilon_0}{2}\sum_{j,k}\phi_j\phi_k D_{jk}\,. \tag{2.21}$$

Since this does not depend on the time derivative of ϕ_i, the Euler-Lagrange equation is simply:

$$\frac{\partial \mathrm{L}}{\partial \phi_\ell} = 0\,, \tag{2.22}$$

for all $\ell = 1, 2, \ldots, N_g$. Therefore, we have that:

$$-\int \mathrm{d}x\, \rho(x,t)\psi_\ell(x) - h\frac{\epsilon_0}{2}\sum_{j,k}\left(\delta_{j\ell}\phi_k + \phi_j\delta_{k\ell}\right) D_{jk} = 0 \tag{2.23}$$

$$-\int \mathrm{d}x\, \rho(x,t)\psi_\ell(x) - h\frac{\epsilon_0}{2}\sum_{k}\phi_k D_{\ell k} - h\frac{\epsilon_0}{2}\sum_{j}\phi_j D_{j\ell} = 0\,, \tag{2.24}$$

since $\mathbf{D}$ is symmetric, we can relabel $k \to j$ to find:

$$\int \mathrm{d}x\, \rho(x,t)\psi_\ell(x) + h\epsilon_0\sum_j \phi_j D_{j\ell} = 0 \tag{2.25}$$

$$\sum_j \phi_j D_{j\ell} = -\frac{1}{h\epsilon_0}\int \mathrm{d}x\, \rho(x,t)\psi_\ell(x)\,. \tag{2.26}$$

Which is the discrete Poisson equation. On the left hand side, $\mathbf{D}$ represents a discrete second order differentiation and the right hand side is the charge density projected onto the basis functions.

Now, this system may be solved. Since $\mathbf{D}$ can be written as a symmetric matrix, assume that it has an inverse $\mathbf{D}^{-1}$. Written with indices this may be

expressed as:

$$\sum_j D_{ij} D^{-1}_{jk} = \delta_{ik}\,, \tag{2.27}$$

that is, matrix multiplying the matrix with its inverse gives the identity matrix. So, contracting the discrete Poisson equation with the inverse gives:

$$\sum_\ell \sum_j \phi_j D_{j\ell} D^{-1}_{\ell k} = -\sum_\ell D^{-1}_{\ell k} \frac{1}{h\epsilon_0} \int \mathrm{d}x\, \rho(x,t)\psi_\ell(x) \tag{2.28}$$

$$\sum_j \phi_j \delta_{jk} = -\sum_\ell \frac{1}{h\epsilon_0} D^{-1}_{\ell k} \int \mathrm{d}x\, \rho(x,t)\psi_\ell(x) \tag{2.29}$$

$$\phi_k = -\frac{1}{h\epsilon_0} \sum_\ell D^{-1}_{\ell k} \int \mathrm{d}x\, \rho(x,t)\psi_\ell(x)\,, \tag{2.30}$$

the explicit solution for each basis function. Now, substituting this solution into the self-potential to find the analytic solution for the potential:

$$\phi(x,t) = -\frac{1}{h\epsilon_0} \sum_{i,\ell} \psi_i(x) D^{-1}_{\ell i} \int \mathrm{d}x'\, \rho(x',t)\psi_\ell(x')\,, \tag{2.31}$$

and written in a more suggestive form:

$$\phi(x,t) = -\frac{1}{\epsilon_0} \int \mathrm{d}x'\, \rho(x',t) \left(\frac{1}{h} \sum_{i,j} \psi_i(x) D^{-1}_{ij} \psi_j(x') \right)\,. \tag{2.32}$$

Compare this to the equation for the potential with respect to the Green's function:

$$\phi(x,t) = -\frac{1}{\epsilon_0} \int \mathrm{d}x' \rho(x',t) G(x,x')\,. \tag{2.33}$$

Thus, the discrete form of the Green's function is:

$$G_D(x,x') = \frac{1}{h} \sum_{i,j} D^{-1}_{ij} \psi_i(x)\psi_j(x')\,. \tag{2.34}$$

Note that this function is also symmetric with respect to its arguments since $\mathbf{D}^{-1}$ is a symmetric matrix. The continuous Green's function may be interpreted as the energy stored between two infinitesimal points with unit-charge; the infinitesimal points are labelled x and x'. The discrete Green's function

projects the points onto the basis of finite elements and the matrix $\mathbf{D}^{-1}$ describes the energy stored between each combination of basis functions, for a unit charge.

For details on the basis functions, see Appendix C and for the proof of the symmetry of $\mathbf{D}^{-1}$, see Section C.1.2.

Discrete Hamiltonian

Substituting the discrete Green's function (2.34) into the discrete macro-particle Hamiltonian (2.10) and after simplifying we have:

$$\widetilde{\mathrm{H}} = \sum_i w_i \left(\frac{{p_i}^2}{2m} + q\varphi(x_i, t) \right) + \frac{q^2}{2\epsilon_0 h} \sum_{j,k} \sum_{n,m} w_j w_k D^{-1}_{nm} \psi_n(x_j) \psi_m(x_k) \,. \tag{2.35}$$

The derivation of the equations of motion follows the exact same steps as the previous algorithm. Note that this derivation relies on the symmetry of the discrete Green's function. The equations of motion are:

$$\frac{\mathrm{d}x_\ell}{\mathrm{d}t} = \frac{p_\ell}{m w_\ell} \,, \tag{2.36}$$

$$\frac{\mathrm{d}p_\ell}{\mathrm{d}t} = -q w_\ell \frac{\partial}{\partial x_\ell} \left(\varphi(x_\ell, t) - \sum_{j,n,m} \frac{q w_j}{\epsilon_0 h} D^{-1}_{nm} \psi_n(x_\ell) \psi_m(x_j) \right) \,, \tag{2.37}$$

where the equations are the same as the particle-particle method, with the discrete Green's function substituted for the analytic one.

2.2.3 Discussion

To compare the computational complexity of these methods, independent of the choice of integration scheme, consider the numerical evaluation of the derivatives. The particle-particle method has time complexity $\mathcal{O}({N_p}^2)$. This is because for each macro-particle, there is a second sum over all of the other macro-particles to find the internal forces. As for the particle-in-cell scheme, even though it has a greater number of sums in the equations of motion, the time complexity may be $\mathcal{O}(N_p + {N_g}^2)$ if implemented optimally. The optimal implementation first involves computing the contribution of each macro-particle to each basis function in $\mathcal{O}(N_p)$ time since each basis function has finite length. Then, solve the linear system with D_{ij} for the potential

values which would take $\mathcal{O}({N_g}^2)$ time. (This is opposed to the non-optimal solution which involves matrix multiplying with the inverse D_{ij}^{-1}, which would take $\mathcal{O}({N_g}^3)$ time.) Lastly, applying the potential values to the equations of each macro-particle takes $\mathcal{O}(N_p)$ time. The potential grid stores information in an intermediate data structure to reduce the time complexity, this is a common feature of many algorithms in computer science. Typically, $N_p > N_g$ so the particle-in-cell method is generally preferred.

The initial particle density distribution is a smooth function. The macro-particles are initialized with phase space coordinates which are statistically sampled from the initial particle density distribution. Integrating the system in time, the set of macro-particles represent a sampling distribution of the particle density function at the later time. From the set of macro-particles, sample statistics may be calculated. The error of sample statistics scales with $N_p^{-1/2}$, so a well bounded error requires many macro-particles.

The discrete equations for both methods are left as continuous functions of time. They can then be integrated using any desired integration method, including symplectic integration schemes.

2.3 Moment Discretization

The goal of this section is to study the reduction of the density function using moments. In principle, the set of infinitely many statistical moments contains adequate information for describing an arbitrary distribution. In practice, we must work with a finite number of moments, so the system of moments needs to be carefully truncated so that the system of equations of motion is closed.

A difficulty that has often arisen in previous work on deriving moment systems is that the only naturally closed system of moments are the first and second order systems of moments [7, 12, 19]. When computing the equation of motion for any moment of third order or higher, it will always depend on some moment of higher order than itself [7]. Thus, when expanding such a system from the equations of motion directly, there appears to be no natural method of truncation.

However, this drawback was overcome by Shadwick and Wurtele in Ref. [19]. One can create a truncation of such a system by Taylor expansion of the Hamiltonian to a chosen arbitrary order. Then, the non-canonical Poisson bracket of Morrison in Ref. [15], as seen in the previous sections can be used

to compute the equations of motion for all of the moments up to the chosen order. This will yield a closed system of equations for the moments.

This section presents a highly simplified version of the derivation in Ref. [19], considering only one dimensional motion in the non-relativistic and electrostatic regimes. Furthermore, the discussion of the self-field is left until the end of this section.

For convenience, moments are denoted using angle brackets:

$$\langle a \rangle = \int \mathrm{d}x\, \mathrm{d}p\, f(x,p)\, a(x,p)\,, \tag{2.38}$$

where $a(x,p)$ is an arbitrary function of the phase space coordinates. Note that such a moment is a functional of $f(x,p)$.

An important simplifying assumption is that the first order moments are zero. This is equivalent to asserting that the beam is well centred on the design-axis, or reference-trajectory, of the accelerator. This assumption is not required for general modelling but it is useful for reducing the errors in mathematical modelling as discussed in Section 1.1.

2.3.1 Moment Expansion

Starting from the one-dimensional Hamiltonian without space charge:

$$\mathrm{H} = \int \mathrm{d}x\, \mathrm{d}p\, f(x,p,t) \left(\frac{p^2}{2m} + q\varphi(x,t) \right) . \tag{2.39}$$

Note that the momentum term of the Hamiltonian is already written in terms of a second moment:

$$\mathrm{H}_p = \int \mathrm{d}x\, \mathrm{d}p\, f(x,p)\, \frac{p^2}{2m} = \frac{\langle p^2 \rangle}{2m}\,. \tag{2.40}$$

However, the external potential term does not depend explicitly on moments. So, taking the Taylor expansion of $\varphi(x,t)$ with respect to x gives:

$$\varphi(x,t) \approx \varphi(0,t) + x \left.\frac{\partial \varphi}{\partial x}\right|_{x=0} + \frac{1}{2} x^2 \left.\frac{\partial^2 \varphi}{\partial x^2}\right|_{x=0} + \mathcal{O}(x^3)\,. \tag{2.41}$$

Substituting this expansion and dropping the higher order terms leaves:

$$\mathrm{H}_\varphi = \int \mathrm{d}x\,\mathrm{d}p\, f(x,p)\, q\varphi(x,t) \approx\; q\langle 1\rangle\, \varphi(0) + q\langle x\rangle\, \frac{\partial\varphi}{\partial x}\bigg|_{x=0} + \frac{q}{2}\langle x^2\rangle\, \frac{\partial^2\varphi}{\partial x^2}\bigg|_{x=0}\,, \tag{2.42}$$

where the moment $\langle 1\rangle$ is the particle number, a constant. The first moment $\langle x\rangle$ is the beam centroid which is zero because of the on-axis assumption. The final moment, $\langle x^2\rangle$ relates to the square of the beam size, up to a multiplicative factor. Dropping the constant terms we are left with:

$$\mathrm{H} = \frac{\langle p^2\rangle}{2m} + \frac{q}{2}\langle x^2\rangle\, \frac{\partial^2\varphi}{\partial x^2}\bigg|_{x=0}\,. \tag{2.43}$$

This reduced Hamiltonian is a functional of f that depends only on $\langle x^2\rangle$ and $\langle p^2\rangle$. Now we need to check that the set of second order moments paired with this Hamiltonian form a closed system of equations.

Using the Poisson bracket to compute the time derivatives for the moments, the functional derivatives are given by (A.6):

$$\frac{\delta\langle x^2\rangle}{\delta f} = x^2\,, \qquad \frac{\delta\langle xp\rangle}{\delta f} = xp\,, \qquad \frac{\delta\langle p^2\rangle}{\delta f} = p^2\,, \tag{2.44}$$

as well as the functional derivative of the Hamiltonian:

$$\frac{\delta\mathrm{H}}{\delta f} = \frac{p^2}{2m} + \frac{q}{2}x^2\, \frac{\partial^2\varphi}{\partial x^2}\bigg|_{x=0}\,, \tag{2.45}$$

which just recovers the single particle Hamiltonian. The equations of motion follow:

$$\begin{aligned}\frac{\mathrm{d}\langle x^2\rangle}{\mathrm{d}t} &= \int \mathrm{d}x\,\mathrm{d}p\, f(x,p)\left[x^2, \frac{\delta\mathrm{H}}{\delta f}\right] \\ &= \int \mathrm{d}x\,\mathrm{d}p\, f(x,p)\left(2x\,\frac{p}{m}\right) \\ &= \frac{2}{m}\langle xp\rangle\,.\end{aligned} \tag{2.46}$$

$$
\begin{aligned}
\frac{\mathrm{d}\langle xp\rangle}{\mathrm{d}t} &= \int \mathrm{d}x\,\mathrm{d}p\, f(x,p)\left[xp, \frac{\delta \mathrm{H}}{\delta f}\right] \\
&= \int \mathrm{d}x\,\mathrm{d}p\, f(x,p)\left(p\,\frac{p}{m} - qx^2\,\frac{\partial^2\varphi}{\partial x^2}\bigg|_{x=0}\right) \\
&= \frac{1}{m}\langle p^2\rangle - q\langle x^2\rangle\,\frac{\partial^2\varphi}{\partial x^2}\bigg|_{x=0}\,.
\end{aligned}
\tag{2.47}
$$

$$
\begin{aligned}
\frac{\mathrm{d}\langle p^2\rangle}{\mathrm{d}s} &= \int \mathrm{d}x\,\mathrm{d}p\, f(x,p)\left[p^2, \frac{\delta \mathrm{H}}{\delta f}\right] \\
&= \int \mathrm{d}x\,\mathrm{d}p\, f(x,p)\left(-2qp\,x\,\frac{\partial^2\varphi}{\partial x^2}\bigg|_{x=0}\right) \\
&= -2q\langle xp\rangle\,\frac{\partial^2\varphi}{\partial x^2}\bigg|_{x=0}\,.
\end{aligned}
\tag{2.48}
$$

Thus, the equations of motion for the second moments without space-charge only depend on the other second moments; the system is closed.

In more compact notation, the equations of motion are:

$$
\frac{\mathrm{d}}{\mathrm{d}t}\begin{bmatrix}\langle x^2\rangle\\ \langle xp\rangle\\ \langle p^2\rangle\end{bmatrix} = \begin{bmatrix} 0 & \frac{2}{m} & 0\\ -q\,\frac{\partial^2\varphi}{\partial x^2}\Big|_{x=0} & 0 & \frac{1}{m}\\ 0 & -2q\,\frac{\partial^2\varphi}{\partial x^2}\Big|_{x=0} & 0\end{bmatrix}\begin{bmatrix}\langle x^2\rangle\\ \langle xp\rangle\\ \langle p^2\rangle\end{bmatrix}, \tag{2.49}
$$

which is a first order matrix ordinary differential equation. This system is identical to the one derived by Sacherer in Ref. [7], without the space charge terms. The matrix is a function of time since the external potential may be time dependent. The integration of such a system is well studied, however we would like to integrate in such a way as to maintain the structure from which it derives.

Canonical Coordinates

Using the theory of general Poisson systems presented in Appendix B we may find a symplectic integration scheme for our moment method. General Poisson systems are defined by a Poisson bracket that uses a generalization of the symplectic matrix: the structure matrix. For details on the structure matrix, refer to Appendix B.1.

Computing the structure matrix involves taking the Poisson bracket between each pair of coordinates. Our system of coordinates is defined by the triplet $\langle x^2 \rangle$, $\langle xp \rangle$, $\langle p^2 \rangle$ which we may write as a coordinate vector:

$$\mathbf{y} = \begin{bmatrix} \langle x^2 \rangle \\ \langle xp \rangle \\ \langle p^2 \rangle \end{bmatrix} . \tag{2.50}$$

The components of the structure matrix is given by the Poisson bracket between each of the coordinates:

$$\mathbf{B}(\mathbf{y}) = \begin{bmatrix} 0 & 2\langle x^2 \rangle & 4\langle xp \rangle \\ -2\langle x^2 \rangle & 0 & 2\langle p^2 \rangle \\ -4\langle xp \rangle & -2\langle p^2 \rangle & 0 \end{bmatrix} , \tag{2.51}$$

the explicit derivation is presented in Section B.3 in the appendix. Note that this structure matrix depends on the state $\mathbf{y}$, however it has familiar properties of the symplectic matrix, those being anti-symmetry and it satisfies Jacobi's identity, which is straightforward to verify. Given these properties, this system of moments is a valid Poisson system.

One property of canonical systems is that they are always even-dimensional. Our moment system has three dimensions so we can surmise that it will be reduced to one position coordinate and its canonical momentum as well as an additional conserved quantity. This kind of conserved quantity is called a Casimir [25] and is described by:

$$\nabla_{\mathbf{y}} C \cdot \mathbf{B}(\mathbf{y}) = 0 , \tag{2.52}$$

for all states $\mathbf{y}$ and where C is the Casimir. That is, regardless of what the Hamiltonian is, the Casimir is invariant, it is a property of the Poisson bracket structure.

One of the set of canonical coordinates will be the Casimir. In general, there is no mechanistic method of solving for them, besides guessing and checking. A candidate for the constant of motion in linear optics is the emittance, which is given by:

$$\mathcal{E} = \sqrt{\langle x^2 \rangle \langle p^2 \rangle - \langle xp \rangle^2} . \tag{2.53}$$

We can determine if it is a Casimir by taking the left side of the Poisson

bracket, (2.52) which gives:

$$\begin{aligned}\nabla_{\mathbf{y}}\mathcal{E}\cdot\mathbf{B}(\mathbf{y}) &= \begin{bmatrix}\frac{\langle p^2\rangle}{2\mathcal{E}} & -\frac{\langle xp\rangle}{\mathcal{E}} & \frac{\langle x^2\rangle}{2\mathcal{E}}\end{bmatrix}\begin{bmatrix}0 & 2\langle x^2\rangle & 4\langle xp\rangle\\ -2\langle x^2\rangle & 0 & 2\langle p^2\rangle\\ -4\langle xp\rangle & -2\langle p^2\rangle & 0\end{bmatrix}\\ &= \frac{1}{\mathcal{E}}\begin{bmatrix}2\langle xp\rangle\langle x^2\rangle - 2\langle x^2\rangle\langle xp\rangle\\ \langle p^2\rangle\langle x^2\rangle - \langle x^2\rangle\langle p^2\rangle\\ 2\langle p^2\rangle\langle xp\rangle - 2\langle xp\rangle\langle p^2\rangle\end{bmatrix}\\ &= \mathbf{0}\,,\end{aligned} \tag{2.54}$$

and it is indeed a Casimir.

In general, there is no straightforward method to determine the coordinates besides by ansatz motivated by dimensional analysis. For our system, dimensional analysis leads us to the new coordinates and the Casimir, labelled $(Q, P, \mathcal{E})$ where the coordinate transformation is given by:

$$Q = \sqrt{\langle x^2\rangle}\,, \qquad P = \frac{\langle xp\rangle}{\sqrt{\langle x^2\rangle}}\,, \qquad \mathcal{E} = \sqrt{\langle x^2\rangle\langle p^2\rangle - \langle xp\rangle^2}\,. \tag{2.55}$$

The physical interpretation of the new coordinates is shown in Fig. 2.1.

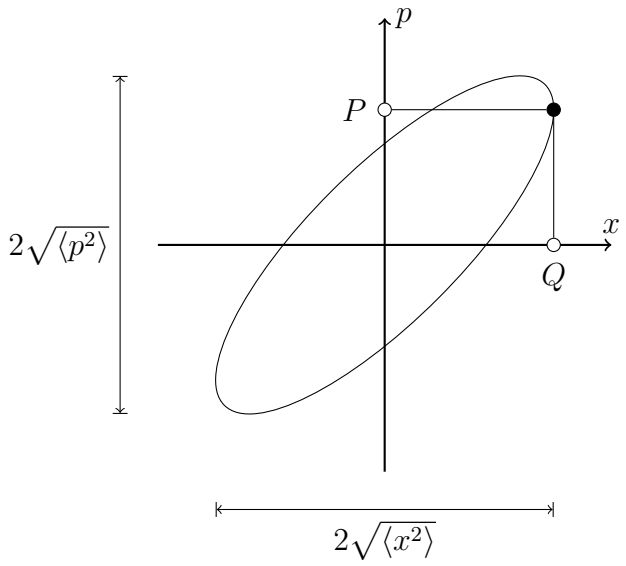

Figure 2.1: Canonical coordinates on the uniformly distributed phase space ellipse. The canonical position and momentum correspond to the right-most point of the ellipse in phase space. The emittance multiplied by π is the area of the ellipse.

By computing the Poisson bracket between each of these coordinates, we find the new structure matrix:

$$\widetilde{\mathbf{B}}(\mathbf{y}) = \begin{bmatrix} \{Q,Q\} & \{Q,P\} & \{Q,\mathcal{E}\} \\ \{P,Q\} & \{P,P\} & \{P,\mathcal{E}\} \\ \{\mathcal{E},Q\} & \{\mathcal{E},P\} & \{\mathcal{E},\mathcal{E}\} \end{bmatrix} = \begin{bmatrix} 0 & 1 & 0 \\ -1 & 0 & 0 \\ 0 & 0 & 0 \end{bmatrix}, \tag{2.56}$$

where the upper left-hand corner is the symplectic matrix, $\mathbf{J}$, with a zero row and column corresponding to the conserved emittance. This verifies that the coordinates Q and P are canonically conjugate, and the Casimir is a conserved quantity. For convenience, the inverse transformation is given by:

$$\langle x^2 \rangle = Q^2\,, \qquad \langle xp \rangle = QP\,, \qquad \langle p^2 \rangle = \frac{\mathcal{E}^2}{Q^2} + P^2\,. \tag{2.57}$$

We may express the Hamiltonian in terms of the new coordinates:

$$\mathrm{H} = \frac{P^2}{2m} + \frac{\mathcal{E}^2}{2mQ^2} + \frac{q}{2}Q^2 \left.\frac{\partial^2\varphi}{\partial x^2}\right|_{x=0} . \tag{2.58}$$

We are finally left with a canonical system of canonical coordinates which may be integrated with standard symplectic integrators. The equations of motion follow from Hamilton's equations as:

$$\frac{\mathrm{d}Q}{\mathrm{d}t} = \frac{\partial \mathrm{H}}{\partial P} = \frac{P}{m} , \tag{2.59}$$

$$\frac{\mathrm{d}P}{\mathrm{d}t} = -\frac{\partial \mathrm{H}}{\partial Q} = \frac{\mathcal{E}^2}{mQ^3} - qQ \left.\frac{\partial^2\varphi}{\partial x^2}\right|_{x=0} . \tag{2.60}$$

The above system of equations is the KV envelope equations without the space charge force. The next section completes the derivation of the 1D KV equations.

2.3.2 Kapchinskij Vladimirskij Equations

Recall the self-field term of the Hamiltonian (2.1):

$$\mathrm{H}_\phi = -\frac{q^2}{2\epsilon_0} \int \mathrm{d}x' \, \mathrm{d}x'' \, \mathrm{d}p' \, \mathrm{d}p'' \, f(x', p') f(x'', p'') G(x', x'') , \tag{2.61}$$

Since the second moments are insufficient for uniquely describing a distribution, this term cannot be computed directly. Instead, further assumptions have to be made about the form of $f(x, p)$, so that the second moments fully parametrize the shape of the real-space density function, $n(x)$.

This assumption must be carefully considered since it is only fixing the projection of the distribution, $n(x)$. In general, an external potential will transform the phase space distribution function in a way that is inconsistent with the assumption. Kapchinskij and Vladimirskij derived a set of distributions, for two and four phase-space dimensions for which the projection is always consistent, regardless of the transformations applied by linear external forces. Using the KV distribution in two phase space dimensions implies that $n(x)$ is uniformly distributed. The Green's function of the Poisson equation in one dimension is:

$$G(x, x') = \frac{1}{2}|x - x'| , \tag{2.62}$$

for open boundary conditions. The uniform distribution may be written using Heaviside step functions, in terms of our canonical variables (Q, P) it is:

$$n(x) = \frac{N}{2\sqrt{3}Q}\left[\Theta\left(\frac{x}{\sqrt{3}Q}+1\right) - \Theta\left(\frac{x}{\sqrt{3}Q}-1\right)\right], \tag{2.63}$$

where we define the step function using the Dirac delta function:

$$\Theta(x) = \int_{-\infty}^{x} \mathrm{d}x'\, \delta(x')\,. \tag{2.64}$$

The Hamiltonian self-field, (2.61), may then be integrated directly to yield:

$$\mathrm{H}_\phi = -\frac{q^2}{2\epsilon_0}\frac{N}{\sqrt{3}}Q\,. \tag{2.65}$$

So, we have an additional Hamiltonian term that describes the energy contained in a uniformly distributed beam. Now, the total Hamiltonian with space charge is:

$$\mathrm{H}_{\text{total}} = \frac{P^2}{2m} + \frac{\mathcal{E}^2}{2mQ^2} + \frac{q}{2}Q^2\left.\frac{\partial^2\varphi}{\partial x^2}\right|_{x=0} - \frac{q^2}{2\epsilon_0}\frac{N}{\sqrt{3}}Q\,. \tag{2.66}$$

and Hamilton's equations are:

$$\frac{\mathrm{d}Q}{\mathrm{d}t} = \frac{\partial \mathrm{H}}{\partial P} = \frac{P}{m}\,, \tag{2.67}$$

$$\frac{\mathrm{d}P}{\mathrm{d}t} = -\frac{\partial \mathrm{H}}{\partial Q} = \frac{\mathcal{E}^2}{mQ^3} - qQ\left.\frac{\partial^2\varphi}{\partial x^2}\right|_{x=0} - \frac{q^2}{2\epsilon_0}\frac{N}{\sqrt{3}}\,, \tag{2.68}$$

and by converting to a second order equation of motion for the size Q we find:

$$\begin{aligned}\frac{\mathrm{d}^2Q}{\mathrm{d}t^2} &= \frac{1}{m}\frac{\mathrm{d}P}{\mathrm{d}t} \\ &= \frac{\mathcal{E}^2}{m^2Q^3} - \frac{q}{m}Q\left.\frac{\partial^2\varphi}{\partial x^2}\right|_{x=0} - \frac{q^2}{2m\epsilon_0}\frac{N}{\sqrt{3}}\,,\end{aligned} \tag{2.69}$$

which, in a more familiar form is:

$$\frac{\mathrm{d}^2Q}{\mathrm{d}t^2} - \frac{\mathcal{E}^2}{m^2Q^3} + \frac{q}{m}Q\left.\frac{\partial^2\varphi}{\partial x^2}\right|_{x=0} + \frac{q^2}{2m\epsilon_0}\frac{N}{\sqrt{3}} = 0\,, \tag{2.70}$$

the well-known one dimensional envelope equation presented by Sacherer in Ref. [26]. The first analogue of which was the two-dimensional equations derived by Kapchinskij and Vladimirskij in Ref. [6]. It may be solved using any analytic or numerical methods for ordinary differential equations. Furthermore, in the Hamiltonian form, it may be integrated symplectically. Also note that the choice of the KV distribution for the explicit form of the distribution is not required. Sacherer showed in Ref. [26] that choosing other 1D distributions with the same symmetry such as a Gaussian or parabolic distribution produce a comparable force.

2.4 Discussion

Notice some important features of each of these methods. The macro-particle methods work for an arbitrary external potential, hence they are useful for studying optical elements of higher order than quadrupoles. The second order moment approach, conversely, only describes the effects from linear external forces. This limitation may be overcome by expanding to include higher order moments, as outlined by Shadwick and Wurtele in Ref. [19], however this has not been derived including the effects of space-charge.

The moment method is also significantly faster than the macro-particle methods. The moment method involves integrating one discrete degree of freedom, whereas for the macro-particle methods, there are at least as many degrees of freedom as there are macro-particles. Since, the numerical accuracy of the macro-particle method depends on the number of macro-particles the user of such a code will have to balance the computational cost with the accuracy and noise of the simulation. This problem is made more difficult in particle-in-cell methods where the fields are discrete as well. No such tension exists in moment methods.

In practice, both classes of algorithms have domains in which they are useful. Moment algorithms are very convenient for building and validating models since they require fewer inputs. Particle algorithms are needed to model details that may be important for specific machines, especially the effects of complex external fields. The moment method also requires a much simplified input which reduces the model input error significantly, compared to the macro-particle model. There are some accelerators where the relevant physics are not ideally handled by either case, so the next chapter will combine these methods to cover such an application.

Chapter 3

Hybrid Method

The motivating problem of this thesis is to self-consistently model the transition from a DC to a bunched beam. In this process, the longitudinal phase space undergoes filamentation, where non-linear forces effectively change the emittance of the beam. These non-linear forces arise from the RF bunchers, which impart a sinusoidal momentum spread, as well as the space charge force. The longitudinal distribution of the beam also directly affects the transverse dynamics. In one respect, momentum deviation will change the effective focusing strength from the quadrupoles, an effect known as chromaticity. Also, as the beam becomes bunched the transverse space charge force will increase, potentially affecting the transverse tune. Clearly, the longitudinal dynamics need to be described with a detailed discretization scheme. However, the transverse dynamics would be well described by second moments; since the beam is relatively localized and the beam is well matched though linear optics. By using the strengths of both discretization schemes the essential physics may be represented while minimizing the errors arising from model complexity.

This chapter starts with the discretization of the particle density function. The discretization assumes that the distribution is divided into macroparticles, which unlike before, have a general transverse distribution described by second moments. For simplicity, I choose to ignore the second moments that correspond to correlations between the x and y transverse directions. The discretization of the electrostatic self-field follows, using a particle-in-cell discretization in the longitudinal direction only. This discretization gives a system of partial differential algebraic equations which are solved to identify the semi-analytic Green's function. Finally, the end of

this chapter combines these components of discretization to look at the final system. This includes a discussion of some of the important implementation details, and further assumptions that have been made. One such assumption that is important to note, is that for ease of implementation and for testing performance, I break the symplectic capabilities of the algorithm by simplifying the self-field term of the Hamiltonian. All tests in the next chapter follow using this approximate implementation.

3.1 Hybrid Discretization

Starting from the three dimensional Vlasov Hamiltonian neglecting the self-field:

$$\mathrm{H} = \int \mathrm{d}^3\mathbf{x}\,\mathrm{d}^3\mathbf{p}\, f(\mathbf{x},\mathbf{p},t)\left(\frac{\mathbf{p}^2}{2m} + q\varphi(\mathbf{x},t)\right). \tag{3.1}$$

To discretize, divide the distribution function into different groupings, like a macro-particle discretization:

$$f(\mathbf{x},\mathbf{p},t) = \sum_i f_i(\mathbf{x},\mathbf{p},t)\,, \tag{3.2}$$

where each f_i interacts only through the self-field. This may be interpreted as attaching different labels to groups of particles. In this case, the Poisson bracket becomes:

$$\{F,G\} = \sum_i \int \mathrm{d}^3\mathbf{x}\,\mathrm{d}^3\mathbf{p}\, f_i(\mathbf{x},\mathbf{p},t)\left[\frac{\delta F}{\delta f_i}, \frac{\delta G}{\delta f_i}\right], \tag{3.3}$$

a sum over the normal Poisson bracket for each group of particles.

Each grouping is split into the normal macro-particle discretization in the longitudinal phase space but now the transverse distribution remains general. This gives the particular explicit distribution:

$$f_i(\mathbf{x},\mathbf{p},t) = w_i f_i^{\perp}(\mathbf{x}^{\perp},\mathbf{p}^{\perp},t) R(z - z_i(t))\delta\left(p_z - \frac{p_{zi}(t)}{w_i}\right), \tag{3.4}$$

where $f_i^{\perp}(\mathbf{x}^{\perp},\mathbf{p}^{\perp})$ is the transverse distribution of the ith group. The symbol $^{\perp}$ denotes a quantity in the transverse plane. Recall, $R(z-z_i(t))$ is the macro-particle shape function described in Section 2.2. It is an even, non-negative

function that satisfies the norming condition. Now, the longitudinal phase space of each f_i is fully described by the set of coordinates w_i, z_i, p_{zi}. By substituting (3.4) any functional of f_i can now be written as a function of the coordinates w_i, z_i, p_{zi} and a functional of $f_i^\perp$. The particle density function has discrete form:

$$f(\mathbf{x},\mathbf{p},t) = \sum_i w_i f_i^\perp(\mathbf{x}^\perp,\mathbf{p}^\perp,t) R(z - z_i(t)) \delta\left(p_z - \frac{p_{zi}(t)}{w_i}\right), \tag{3.5}$$

Let us denote the moment with respect to the ith transverse distribution with square brackets for example:

$$\langle a \rangle_i = \int \mathrm{d}^2\mathbf{x}^\perp \, \mathrm{d}^2\mathbf{p}^\perp \, f_i^\perp(\mathbf{x}^\perp,\mathbf{p}^\perp)\, a(\mathbf{x}^\perp,\mathbf{p}^\perp), \tag{3.6}$$

for some function of the transverse phase space, $a(\mathbf{x}^\perp,\mathbf{p}^\perp)$.

Once again, the transverse dynamics will be described by a system of second moments. The set of second moments consists of $\langle x^2\rangle_i$, $\langle xp_x\rangle_i$, $\langle p_x^2\rangle_i$, $\langle y^2\rangle_i$, $\langle yp_y\rangle_i$ and $\langle p_y^2\rangle_i$. I choose to neglect the other second moments correlating the x and y dimensions which are: $\langle xy\rangle_i$, $\langle xp_y\rangle_i$, $\langle yp_x\rangle_i$ and $\langle p_xp_y\rangle_i$. Therefore each macro-particle is described by the following set of non-canonical coordinates:

$$\mathbf{y}_i = (\langle x^2\rangle_i, \langle xp_x\rangle_i, \langle p_x^2\rangle_i, \langle y^2\rangle_i, \langle yp_y\rangle_i, \langle p_y^2\rangle_i, z_i, p_{zi}), \tag{3.7}$$

where, as before, each of these coordinates can be written as a functional of f_i.

The uncorrelated assumption implies that the coordinates can be described as being in their own 'subspace' of phase space. This means that the results of Chapter 2 directly apply. The Poisson bracket between each of these coordinates is the same as before, with the brackets of coordinates in

different directions being zero. The structure matrix is then:

$$\mathbf{B}(\mathbf{y}) = \begin{bmatrix} 0 & 2\langle x^2\rangle & 4\langle xp_x\rangle & 0 & 0 & 0 & 0 & 0 \\ -2\langle x^2\rangle & 0 & 2\langle p_x^2\rangle & 0 & 0 & 0 & 0 & 0 \\ -4\langle xp_x\rangle & -2\langle p_x^2\rangle & 0 & 0 & 0 & 0 & 0 & 0 \\ 0 & 0 & 0 & 0 & 2\langle y^2\rangle & 4\langle yp_y\rangle & 0 & 0 \\ 0 & 0 & 0 & -2\langle y^2\rangle & 0 & 2\langle p_y^2\rangle & 0 & 0 \\ 0 & 0 & 0 & -4\langle yp_y\rangle & -2\langle p_y^2\rangle & 0 & 0 & 0 \\ 0 & 0 & 0 & 0 & 0 & 0 & 0 & 1 \\ 0 & 0 & 0 & 0 & 0 & 0 & -1 & 0 \end{bmatrix}. \tag{3.8}$$

a block-diagonal matrix with each block corresponding to the structure matrices for 1D moments in x and y and 1D particles in z.

Now to transform to a set of canonical coordinates, using the results of Chapter 2 directly. The transformation is as follows:

$$\begin{aligned} Q_{xi} &= \sqrt{\langle x^2\rangle_i}\,, \quad P_{xi} = w_i \frac{\langle xp_x\rangle_i}{\sqrt{\langle x^2\rangle_i}}\,, \quad \mathcal{E}_{xi} = w_i\sqrt{\langle x^2\rangle_i\langle p_x^2\rangle_i - \langle xp_x\rangle_i^2}\,, \\ Q_{yi} &= \sqrt{\langle y^2\rangle_i}\,, \quad P_{yi} = w_i \frac{\langle yp_y\rangle_i}{\sqrt{\langle y^2\rangle_i}}\,, \quad \mathcal{E}_{yi} = w_i\sqrt{\langle y^2\rangle_i\langle p_y^2\rangle_i - \langle yp_y\rangle_i^2}\,, \\ Q_{z_i} &= z_i\,, \qquad\qquad P_{zi} = p_{zi}\,, \end{aligned} \tag{3.9}$$

where $\mathcal{E}_{xi}$ and $\mathcal{E}_{yi}$ the transverse emittance, in the respective direction. Note the momenta have a factor of w_i for the same reason as before, the canonical momentum is the momentum of all of the real particles that the macro-particle represents.

The new state vector of canonical coordinates for macro-particle i is:

$$\tilde{\mathbf{y}}_i = (Q_{xi}, Q_{yi}, Q_{zi}, P_{xi}, P_{yi}, P_{zi}, \mathcal{E}_{xi}, \mathcal{E}_{yi})\,. \tag{3.10}$$

With respect to these coordinates, the structure matrix becomes:

$$\widetilde{\mathbf{B}}(\mathbf{y}) = \begin{bmatrix} 0 & 0 & 0 & 1 & 0 & 0 & 0 & 0 \\ 0 & 0 & 0 & 0 & 1 & 0 & 0 & 0 \\ 0 & 0 & 0 & 0 & 0 & 1 & 0 & 0 \\ -1 & 0 & 0 & 0 & 0 & 0 & 0 & 0 \\ 0 & -1 & 0 & 0 & 0 & 0 & 0 & 0 \\ 0 & 0 & -1 & 0 & 0 & 0 & 0 & 0 \\ 0 & 0 & 0 & 0 & 0 & 0 & 0 & 0 \\ 0 & 0 & 0 & 0 & 0 & 0 & 0 & 0 \end{bmatrix}. \tag{3.11}$$

which is the symplectic matrix, with zero rows and columns for the Casismir functions. In fact, the Poisson bracket is now in symplectic form as:

$$\{F, G\} = \sum_i \left(\frac{\partial \widetilde{F}}{\partial Q_{xi}} \frac{\partial \widetilde{G}}{\partial P_{xi}} - \frac{\partial \widetilde{F}}{\partial P_{xi}} \frac{\partial \widetilde{G}}{\partial Q_{xi}} \right) + \left(\frac{\partial \widetilde{F}}{\partial Q_{yi}} \frac{\partial \widetilde{G}}{\partial P_{yi}} - \frac{\partial \widetilde{F}}{\partial P_{yi}} \frac{\partial \widetilde{G}}{\partial Q_{yi}} \right) + \left(\frac{\partial \widetilde{F}}{\partial Q_{zi}} \frac{\partial \widetilde{G}}{\partial P_{zi}} - \frac{\partial \widetilde{F}}{\partial P_{zi}} \frac{\partial \widetilde{G}}{\partial Q_{zi}} \right). \tag{3.12}$$

Thus, Hamilton's equations can be used to find the equations of motion. Although, the Hamiltonian must first be simplified to close this system.

3.1.1 Expanded Hamiltonian

Now that the Poisson bracket is in canonical form, the next step is to simplify the Hamiltonian. Following the moment method in Chapter 2, the external potential needs to be expanded so that it has an explicit dependence on the second moments transversely.

Taylor expanding the external potential to second order in x and y gives:

$$\begin{aligned} \varphi(\mathbf{x}, t) \approx\ & \varphi(\mathbf{x}, t)|_{\mathbf{x}^\perp = \mathbf{0}} + x \left. \frac{\partial \varphi(\mathbf{x}, t)}{\partial x} \right|_{\mathbf{x}^\perp = \mathbf{0}} + y \left. \frac{\partial \varphi(\mathbf{x}, t)}{\partial y} \right|_{\mathbf{x}^\perp = \mathbf{0}} \\ & + \frac{x^2}{2} \left. \frac{\partial^2 \varphi(\mathbf{x}, t)}{\partial x^2} \right|_{\mathbf{x}^\perp = \mathbf{0}} + xy \left. \frac{\partial^2 \varphi(\mathbf{x}, t)}{\partial x \partial y} \right|_{\mathbf{x}^\perp = \mathbf{0}} + \frac{y^2}{2} \left. \frac{\partial^2 \varphi(\mathbf{x}, t)}{\partial y^2} \right|_{\mathbf{x}^\perp = \mathbf{0}}. \end{aligned} \tag{3.13}$$

For notational convenience, let the on-axis external potential terms be de-

noted:

$$\varphi(z,t) = \varphi(\mathbf{x},t)|_{\mathbf{x}^\perp=\mathbf{0}}\,, \quad \varphi_x(z,t) = \left.\frac{\partial\varphi(\mathbf{x},t)}{\partial x}\right|_{\mathbf{x}^\perp=\mathbf{0}}, \quad \varphi_{xx}(z,t) = \left.\frac{\partial^2\varphi(\mathbf{x},t)}{\partial x^2}\right|_{\mathbf{x}^\perp=\mathbf{0}}, \tag{3.14}$$

such that the subscript denotes a partial derivative. Similarly, $\varphi_{yy}(z,t)$ is the second y derivative.

Thus, substituting the expansion into the Hamiltonian yields:

$$\begin{aligned}\mathrm{H} = &\frac{1}{2m}\int \mathrm{d}^3\mathbf{x}\,\mathrm{d}^3\mathbf{p}\, f(\mathbf{x},\mathbf{p},t)\left(p_x^2+p_y^2+p_z^2\right)\\ &+ q\int \mathrm{d}^3\mathbf{x}\,\mathrm{d}^3\mathbf{p}\, f(\mathbf{x},\mathbf{p},t)\left(\frac{x^2}{2}\varphi_{xx}(z,t)+xy\varphi_{xy}(z,t)+\frac{y^2}{2}\varphi_{yy}(z,t)\right)\\ &+ q\int \mathrm{d}^3\mathbf{x}\,\mathrm{d}^3\mathbf{p}\, f(\mathbf{x},\mathbf{p},t)\left(\varphi(z,t)+x\varphi_x(z,t)+y\varphi_y(z,t)\right)\,.\end{aligned} \tag{3.15}$$

Now, note that the terms in xy will lead to a correlation moment and the terms linear in x and y will give a first order moment. Given the on-axis assumption, the first order moments will remain zero as long as $\varphi_x(z) = \varphi_y(z) = 0$. This restricts the model to exclude alignment errors and steerers. Similarly, for the system to remain uncorrelated $\varphi_{xy}(z) = 0$, this means that this model is restricted to optical elements with axial-rotational symmetry, dipole symmetry and quadrupole symmetry. Note that compared to Section 2.3, the lowest order term of the Taylor expansion remains. This term will be used to model acceleration gaps both direct-current and radio-frequency devices.

To convert this from a continuous Vlasov Hamiltonian to a discrete Hamiltonian, substituting the discretization scheme, (3.5), and simplifying gives:

$$\begin{aligned}\mathrm{H} = &\sum_i \frac{1}{2mw_i}\left(\langle p_x^2\rangle_i + \langle p_y^2\rangle_i + {p_{z_i}}^2\right)\\ &+ qw_i\int \mathrm{d}z\, R(z-z_i)\left(\varphi(z)+\frac{\langle x^2\rangle_i}{2}\varphi_{xx}(z)+\frac{\langle y^2\rangle_i}{2}\varphi_{yy}(z)\right),\end{aligned} \tag{3.16}$$

Then, applying the coordinate transformation to canonical coordinates:

$$\mathrm{H} = \sum_i \frac{1}{2mw_i}\left((P_{xi})^2 + \left(\frac{\mathcal{E}_{xi}}{Q_{xi}}\right)^2 + (P_{yi})^2 + \left(\frac{\mathcal{E}_{yi}}{Q_{yi}}\right)^2 + (P_{zi})^2\right) + qw_i \int \mathrm{d}z\, R(z - Q_{zi})\left(\varphi(z) + \frac{(Q_{xi})^2}{2}\varphi_{xx}(z) + \frac{(Q_{yi})^2}{2}\varphi_{yy}(z)\right). \quad (3.17)$$

This is now a closed system of macro-particles and moments. The next step is to consider how to best represent the self-field, in this discretization scheme.

3.2 Self Field Discretization

Intuitively, the potential should be both discrete in the longitudinal direction as well as linearised in the transverse directions to make it consistent with the particle discretization. To accomplish this, I will use the same discretization scheme as in the particle-in-cell approach in Chapter 2, this time in three dimensions.

Starting from the three dimensional electrostatic Lagrangian with an externally applied charge distribution:

$$\mathrm{L} = -\int \mathrm{d}^3\mathbf{x}\,\mathrm{d}^3\mathbf{p}\,\rho(\mathbf{x},\mathbf{p})\phi(\mathbf{x}) + \frac{\epsilon_0}{2}\int \mathrm{d}^3\mathbf{x}\,|\nabla\phi|^2\,. \quad (3.18)$$

Using the same discretization scheme as the particle-in-cell algorithm in Section 2.2 but now, applying it to a full three-dimensional system. The potential is decomposed onto a uniform grid of basis functions in the z direction, with grid spacing h which is expressed as:

$$\phi(\mathbf{x},t) = \sum_{i=1}^{N_g} \phi_i(\mathbf{x}^\perp,t)\psi_i(z)\,, \quad (3.19)$$

where $\psi_i(z)$ is the finite element basis function of the ith node. Note that the coefficient of the basis function $\phi_i(\mathbf{x}^\perp,t)$ is a function of the transverse directions $\mathbf{x}^\perp$. The purpose of this section is to compute the explicit solution for each of these functions to solve the semi-analytic form of the self potential.

Substituting the discretization scheme into the Lagrangian gives:

$$\begin{aligned} \mathrm{L} = -\sum_i \int \mathrm{d}^3\mathbf{x}\, \rho(\mathbf{x},t)\phi_i(\mathbf{x}^\perp,t)\psi_i(z) \\ + \frac{h\epsilon_0}{2}\sum_{jk} M_{jk}\int \mathrm{d}^2\mathbf{x}^\perp \left(\nabla_{\mathbf{x}^\perp}\phi_j(\mathbf{x}^\perp,t)\cdot\nabla_{\mathbf{x}^\perp}\phi_k(\mathbf{x}^\perp,t)\right) \\ + \frac{\epsilon_0}{2h}\sum_{jk} D_{jk}\int \mathrm{d}^2\mathbf{x}^\perp \left(\phi_j(\mathbf{x}^\perp,t)\phi_k(\mathbf{x}^\perp,t)\right)\,, \end{aligned} \tag{3.20}$$

where

$$M_{nm} = \frac{1}{h}\int \mathrm{d}z \psi_n(z)\psi_m(z)\,, \tag{3.21}$$

$$D_{k\ell} = h\int \mathrm{d}z \frac{\mathrm{d}\psi_k(z)}{\mathrm{d}z}\frac{\mathrm{d}\psi_\ell(z)}{\mathrm{d}z}\,. \tag{3.22}$$

In the context of the finite element method, $\mathbf{M}$ is called a 'mass matrix' and $\mathbf{D}$ is a 'stiffness matrix'.

Taking the Euler Lagrange equations with respect to the set of transverse fields $\phi_i(\mathbf{x}^\perp,t)$ we find:

$$\sum_n \left(M_{\ell n}\Delta_{\mathbf{x}^\perp}\phi_n - \frac{1}{h^2}D_{\ell n}\phi_n\right) = -\frac{1}{\epsilon_0 h}\int \mathrm{d}z\, \rho(\mathbf{x},t)\psi_\ell(z)\,, \tag{3.23}$$

where $\Delta_{\mathbf{x}^\perp}\phi_n(\mathbf{x}^\perp,t)$ is the 2D Laplacian of the semi-discrete potential $\phi_n(\mathbf{x}^\perp,t)$.

This is a set of differential algebraic equations for the set of transverse fields. To solve this system, it will first have to be diagonalized then the remaining independent partial differential equations can be solved.

3.2.1 Solving the Differential Algebraic Equations

Diagonalizing the system requires that $\mathbf{M}$ and $\mathbf{D}$ be simultaneously diagonalizable. Appendix C shows that for the linear finite elements that the node mass and differentiation matrices are simultaneously diagonalizable.

Let the matrix $\mathbf{M}$ have the set of eigenvalues, λ_i^M, and eigenvectors, which form an orthogonal matrix $\mathbf{S}$. The eigenvalues of $\mathbf{D}$ are then denoted λ_i^D and are found by similarity transform using $\mathbf{S}$. This may be written in index

notation as:

$$\lambda_i^M \delta_{ijk} = \sum_{ab} S_{ja} M_{ab} S_{bk} \,, \tag{3.24}$$

$$\lambda_i^D \delta_{ijk} = \sum_{ab} S_{ja} D_{ab} S_{bk} \,, \tag{3.25}$$

where the δ_{ijk} denotes a three-index Kronecker delta symbol:

$$\delta_{abc} = \begin{cases} 1, & a = b = c \\ 0, & \text{else,} \end{cases} \tag{3.26}$$

which is used to write the vector of eigenvalues as a diagonal matrix. Contracting both free indices with $\mathbf{S}$ gives:

$$M_{nm} = \sum_{ijk} \lambda_i^M S_{nj} \delta_{ijk} S_{km} \,, \tag{3.27}$$

$$D_{nm} = \sum_{ijk} \lambda_i^D S_{nj} \delta_{ijk} S_{km} \,, \tag{3.28}$$

since $\mathbf{S}$ is orthogonal:

$$\sum_j S_{ij} S_{jk} = \delta_{ik} \,. \tag{3.29}$$

Let the particle density term be a vector of distributions $\rho_\ell(\mathbf{x}^\perp)$ which is given by:

$$\rho_\ell(\mathbf{x}^\perp, t) = \int \mathrm{d}z \, \rho(\mathbf{x}, t) \psi_\ell(z) \,, \tag{3.30}$$

then simplifying:

$$\sum_n \left(M_{\ell n} \Delta_{\mathbf{x}^\perp} - \frac{1}{h^2} D_{\ell n} \right) \phi_n(\mathbf{x}^\perp, t) = -\frac{1}{\epsilon_0 h} \rho_\ell(\mathbf{x}^\perp, t) \,, \tag{3.31}$$

where $\Delta_{\mathbf{x}^\perp}$ is the 2D Laplace operator, that commutes with numbers. Sub-

stituting the diagonalized $\mathbf{M}$ and $\mathbf{D}$ gives:

$$\sum_{ijkn}\left(\lambda_i^M S_{\ell j}\delta_{ijk}S_{kn}\Delta_{\mathbf{x}^\perp}-\frac{1}{h^2}\lambda_i^D S_{\ell j}\delta_{ijk}S_{kn}\right)\phi_n(\mathbf{x}^\perp,t)=-\frac{1}{\epsilon_0 h}\rho_\ell(\mathbf{x}^\perp,t)\,, \tag{3.32}$$

$$\sum_{ijkn}S_{\ell j}\left(\lambda_i^M\Delta_{\mathbf{x}^\perp}-\frac{1}{h^2}\lambda_i^D\right)\delta_{ijk}S_{kn}\phi_n(\mathbf{x}^\perp,t)=-\frac{1}{\epsilon_0 h}\rho_\ell(\mathbf{x}^\perp,t)\,, \tag{3.33}$$

and contracting with $\mathbf{S}$ on the left hand side:

$$\sum_{ikn}\left(\lambda_i^M\Delta_{\mathbf{x}^\perp}-\frac{1}{h^2}\lambda_i^D\right)\delta_{iak}S_{kn}\phi_n(\mathbf{x}^\perp,t)=-\frac{1}{\epsilon_0 h}\sum_\ell S_{a\ell}\rho_\ell(\mathbf{x}^\perp,t)\,. \tag{3.34}$$

So, the diagonalized potential and charge density vectors are defined as:

$$\tilde{\phi}_k(\mathbf{x}^\perp,t)=\sum_n S_{kn}\phi_n(\mathbf{x}^\perp,t)\,, \tag{3.35}$$

$$\tilde{\rho}_a(\mathbf{x}^\perp,t)=\sum_\ell S_{a\ell}\rho_\ell(\mathbf{x}^\perp,t)\,. \tag{3.36}$$

Now, by applying the definition of the Kronecker delta symbol we are left with a vector of independent partial differential equations to solve for each diagonalized transverse potential:

$$\left(\lambda_a^M\Delta_{\mathbf{x}^\perp}-\frac{1}{h^2}\lambda_a^D\right)\tilde{\phi}_a(\mathbf{x}^\perp,t)=-\frac{1}{\epsilon_0 h}\tilde{\rho}_a(\mathbf{x}^\perp,t)\,, \tag{3.37}$$

where there is no summation over indices. Dividing by the eigenvalue λ_a^M we find:

$$\left(\Delta_{\mathbf{x}^\perp}-\frac{\lambda_a^D}{\lambda_a^M h^2}\right)\tilde{\phi}_a(\mathbf{x}^\perp,t)=-\frac{1}{\epsilon_0 h\lambda_a^M}\tilde{\rho}_a(\mathbf{x}^\perp,t)\,. \tag{3.38}$$

This is called the Screened Poisson Equation or alternatively the modified Helmholtz equation. It has the screening constant $(k_a)^2=\lambda_a^D/(\lambda_a^M h^2)$; note that it depends on the index a. Now to solve this equation.

3.2.2 Green's Function

Since the modified Helmholtz equation is an inhomogeneous linear partial differential equation, it may be solved using the Green's function. Consider this equation for a general index a and a δ-function source term, let $\Phi_a(\mathbf{x}^\perp)$ be the solution that satisfies:

$$\left(\Delta_{\mathbf{x}^\perp} - k_a^2\right) \Phi_a(\mathbf{x}^\perp) = -\delta^{(2)}(\mathbf{x}^\perp)\,. \tag{3.39}$$

The Green's function, $\mathrm{G}_a(\mathbf{x}^\perp, \mathbf{y}^\perp)$, is written using the point source solution, $\Phi_a(\mathbf{x}^\perp)$:

$$\mathrm{G}_a(\mathbf{x}^\perp, \mathbf{y}^\perp) = \Phi_a(\mathbf{y}^\perp - \mathbf{x}^\perp)\,. \tag{3.40}$$

Now, to solve for $\Phi_a(\mathbf{x}^\perp)$. Let $\widetilde{\Phi}_a(\mathbf{k}^\perp)$ denote the two dimensional Fourier transform of $\Phi_a(\mathbf{x}^\perp)$ from $\mathbf{x}^\perp$ to $\mathbf{k}^\perp$. Then, taking the Fourier transform of (3.39) gives:

$$\left(-|\mathbf{k}^\perp|^2 - k_a^2\right) \widetilde{\Phi}_a(\mathbf{k}^\perp) = -1\,, \tag{3.41}$$

and dividing, assuming the denominator is non-zero:

$$\widetilde{\Phi}_a(\mathbf{k}^\perp) = \frac{1}{|\mathbf{k}^\perp|^2 + k_a^2}\,. \tag{3.42}$$

Taking the inverse Fourier transform gives a modified Bessel function of the second kind:

$$\Phi_a(\mathbf{x}^\perp) = \frac{1}{2\pi} K_0\left(k_a|\mathbf{x}^\perp|\right)\,, \tag{3.43}$$

this is the point source solution. For transverse boundary conditions which are zero at infinity, we have:

$$\mathrm{G}_a(\mathbf{x}^\perp, \mathbf{y}^\perp) = \Phi_a(\mathbf{y}^\perp - \mathbf{x}^\perp)\,. \tag{3.44}$$

The boundary conditions that arise more naturally in accelerator physics is a metallic pipe of radius R. Using the method of images, we add an additional source term outside of the pipe:

$$\mathrm{G}_a(\mathbf{x}^\perp, \mathbf{y}^\perp) = \Phi_a(\mathbf{y}^\perp - \mathbf{x}^\perp) - \Phi_a\left(\frac{|\mathbf{x}^\perp|}{R}\left(\mathbf{y}^\perp - \frac{R^2}{|\mathbf{x}^\perp|^2}\mathbf{x}^\perp\right)\right)\,, \tag{3.45}$$

this satisfies that the potential is zero at the pipe wall and there is no additional source term within the pipe.

3.2.3 Solution

Whichever set of boundary conditions is chosen, the solution in the diagonal basis using the Green's function is:

$$\tilde{\phi}_a(\mathbf{x}^\perp) = \frac{1}{\epsilon_0 h \lambda_a^M} \int \mathrm{d}^2\tilde{\mathbf{x}}^\perp \tilde{\rho}_a(\tilde{\mathbf{x}}^\perp) \mathrm{G}_a(\mathbf{x}^\perp, \tilde{\mathbf{x}}^\perp)\,. \tag{3.46}$$

The explicit solution for ϕ is found by contracting with $\mathbf{S}$ to return to the non-diagonal basis, and substituting the definition of $\tilde{\rho}$ to give:

$$\phi(\mathbf{x}) = \frac{1}{\epsilon_0 h} \sum_{n,a,\ell} \psi_n(z) S_{na} S_{a\ell} \left(\frac{1}{\lambda_a^M} \int \mathrm{d}^2\tilde{\mathbf{x}}^\perp \rho_\ell(\tilde{\mathbf{x}}^\perp) \mathrm{G}_a(\mathbf{x}^\perp, \tilde{\mathbf{x}}^\perp) \right)\,. \tag{3.47}$$

This is the semi-analytic solution for the self-potential.

3.3 External Potential Approximation

Ideally, this semi-analytic potential would be used like the discrete Green's function in the particle-in-cell method derived in Section 2.2. However, this straightforward approach would be computationally prohibitive. To evaluate the equations of motion, this would require the numerical integration of $\mathcal{O}({N_p}^2)$ four dimensional integrals.

To overcome this cost, I take inspiration from the work done by Cook et al. in Ref [27], in which they use the Hamiltonian formulation to describe the particle dynamics and where the self-field is subject to 'auxiliary-conditions' which are the equations of motion for the self field deriving from Lagrangian formulation. By writing the self-field as the explicit solution to the Lagrangian equations of motion, these 'auxiliary-conditions' are enforced explicitly.

The Hamiltonian term for the self-potential is then the negative of the Lagrangian interaction term, as in:

$$\mathrm{H}_\phi = q \int \mathrm{d}^3\mathbf{x}\, \mathrm{d}^3\mathbf{p} f(\mathbf{x}, \mathbf{p}) \phi(\mathbf{x})\,, \tag{3.48}$$

which is identical to the external field term.

This allows the Taylor expansion of the self-potential, as if it was an external potential. It follows that by making the same sets of assumptions,

the expanded self-potential gives the Hamiltonian term:

$$\mathrm{H}_\phi = \sum_i q w_i \int \mathrm{d}z R(z - Q_{zi}(t)) \left(\phi(z) + \frac{(Q_{xi})^2}{2} \phi_{xx}(z) + \frac{(Q_{yi})^2}{2} \phi_{yy}(z) \right). \tag{3.49}$$

Where, to reiterate, the potential is Taylor expanded to second order about the z-axis and the first order terms are assumed to be zero because of the uncorrelated assumption. The computation cost to evaluate the equation of motion requires only computing the self-potential and some of its derivatives on-axis. This reduces the computation cost to $\mathcal{O}(N_p N_g)$ two-dimensional integrals.

However, the enforcement of the 'auxiliary conditions' in this way violates the standard Hamiltonian formalism. The proper methods of formulating Hamiltonian systems with constraints, similar to Lagrange multipliers are described by Hairier et. al. at the start of Chapter VII. Non-Canonical Hamiltonian Systems from Ref [25]. Thus, this system will no longer be energy conserving. This assumption violates Hamiltonian mechanics by introducing an explicit asymmetry in how the charge is deposited into the potential compared to how the potential influences the charges. This asymmetry is typical for momentum-conserving particle-in-cell codes.

3.4 The Algorithm

The particle distribution function is a discrete sum of macro-particles:

$$f(\mathbf{x}, \mathbf{p}, t) = \sum_i w_i f_i^\perp(\mathbf{x}^\perp, \mathbf{p}^\perp, t) R(z - Q_{zi}) \delta \left(p_z - \frac{P_{zi}}{w_i} \right). \tag{3.50}$$

In the transverse dimensions, each macro-particle contains a distribution which is described by the system of second moments. The ith macro-particle is defined with respect to the following set of coordinates:

$$\tilde{\mathbf{y}}_i = (Q_{xi}, Q_{yi}, Q_{zi}, P_{xi}, P_{yi}, P_{zi}, \mathcal{E}_{xi}, \mathcal{E}_{yi}), \tag{3.51}$$

where the Q and P are canonically conjugate and the $\mathcal{E}$ are constants. The Hamiltonian of this system is:

$$\begin{aligned}\mathrm{H} = \sum_i \frac{1}{2mw_i}\left((P_{xi})^2 + \left(\frac{\mathcal{E}_{xi}}{Q_{xi}}\right)^2 + (P_{yi})^2 + \left(\frac{\mathcal{E}_{yi}}{Q_{yi}}\right)^2 + (P_{zi})^2\right) \\ + qw_i \int \mathrm{d}z\, R(z - Q_{zi})\left(\varphi(z) + \frac{(Q_{xi})^2}{2}\varphi_{xx}(z) + \frac{(Q_{yi})^2}{2}\varphi_{yy}(z)\right) \\ + qw_i \int \mathrm{d}z R(z - Q_{zi})\left(\phi(z) + \frac{Q_{xi}^2}{2}\phi_{xx}(z) + \frac{Q_{yi}^2}{2}\phi_{yy}(z)\right). \quad (3.52)\end{aligned}$$

Using Hamilton's equations, the equations of motion for the spatial coordinates are simple:

$$\frac{\mathrm{d}Q_{xi}}{\mathrm{d}t} = \frac{\partial H}{\partial P_{xi}} = \frac{P_{xi}}{mw_i}\,, \quad (3.53)$$

$$\frac{\mathrm{d}Q_{yi}}{\mathrm{d}t} = \frac{\partial H}{\partial P_{yi}} = \frac{P_{yi}}{mw_i}\,, \quad (3.54)$$

$$\frac{\mathrm{d}Q_{zi}}{\mathrm{d}t} = \frac{\partial H}{\partial P_{zi}} = \frac{P_{zi}}{mw_i}\,. \quad (3.55)$$

As for the momenta, it is more complicated:

$$\frac{\mathrm{d}P_{xi}}{\mathrm{d}t} = -\frac{\partial H}{\partial Q_{xi}} = \frac{1}{mw_i}\frac{\mathcal{E}_{xi}^2}{Q_{xi}^3} - qw_iQ_{xi}\int \mathrm{d}z\, R(z - Q_{zi})\left(\varphi_{xx}(z) + \left.\frac{\partial^2\phi(\mathbf{x},t)}{\partial x^2}\right|_{\mathbf{x}^\perp=\mathbf{0}}\right), \quad (3.56)$$

$$\frac{\mathrm{d}P_{yi}}{\mathrm{d}t} = -\frac{\partial H}{\partial Q_{yi}} = \frac{1}{mw_i}\frac{\mathcal{E}_{yi}^2}{Q_{yi}^3} - qw_iQ_{yi}\int \mathrm{d}z\, R(z - Q_{zi})\left(\varphi_{yy}(z) + \left.\frac{\partial^2\phi(\mathbf{x},t)}{\partial y^2}\right|_{\mathbf{x}^\perp=\mathbf{0}}\right), \quad (3.57)$$

$$\frac{\mathrm{d}P_{zi}}{\mathrm{d}t} = -\frac{\partial H}{\partial Q_{zi}}$$
$$= -qw_i \int \mathrm{d}z \, \frac{\partial R(z - Q_{zi})}{\partial Q_{zi}} \Bigg(\varphi(z) + \frac{(Q_{xi})^2}{2}\varphi_{xx}(z) + \frac{(Q_{yi})^2}{2}\varphi_{yy}(z)$$
$$+ \phi(\mathbf{x}, t)|_{\mathbf{x}^\perp = \mathbf{0}} + \frac{(Q_{xi})^2}{2} \left.\frac{\partial^2 \phi(\mathbf{x}, t)}{\partial x^2}\right|_{\mathbf{x}^\perp = \mathbf{0}} + \frac{(Q_{yi})^2}{2} \left.\frac{\partial^2 \phi(\mathbf{x}, t)}{\partial y^2}\right|_{\mathbf{x}^\perp = \mathbf{0}} \Bigg) . \tag{3.58}$$

As a detail pertaining to the code, to be able to use a δ-function particle kernel, we integrate the z-direction equation of motion by parts to instead calculate:

$$\frac{\mathrm{d}P_{zi}}{\mathrm{d}t} = -qw_i \int \mathrm{d}z \, R(z - Q_{zi}) \frac{\partial}{\partial z} \Bigg(\varphi(z) + \frac{(Q_{xi})^2}{2}\varphi_{xx}(z) + \frac{(Q_{yi})^2}{2}\varphi_{yy}(z)$$
$$+ \phi(\mathbf{x}, t)|_{\mathbf{x}^\perp = \mathbf{0}} + \frac{(Q_{xi})^2}{2} \left.\frac{\partial^2 \phi(\mathbf{x}, t)}{\partial x^2}\right|_{\mathbf{x}^\perp = \mathbf{0}} + \frac{(Q_{yi})^2}{2} \left.\frac{\partial^2 \phi(\mathbf{x}, t)}{\partial y^2}\right|_{\mathbf{x}^\perp = \mathbf{0}} \Bigg) . \tag{3.59}$$

The self-potential is computed each time the equations of motion of the momenta are evaluated. We have only to compute the following terms:

$$\phi(\mathbf{x}, t)|_{\mathbf{x}^\perp = \mathbf{0}} , \qquad \left.\frac{\partial^2 \phi(\mathbf{x}, t)}{\partial x^2}\right|_{\mathbf{x}^\perp = \mathbf{0}} , \qquad \left.\frac{\partial^2 \phi(\mathbf{x}, t)}{\partial y^2}\right|_{\mathbf{x}^\perp = \mathbf{0}} . \tag{3.60}$$

For details on how the self-potential terms are calculated numerically, refer to Appendix C. In the following chapter, we test the numerical evaluation of these terms against analytic solutions.

Macro-Particle Initialization

The interpretation of the coordinates of each macro-particle are the localized point or spatial distribution in longitudinal phase space (z, p_z) with an associated transverse distribution.

Each macro-particle must be initialized with a constant weight w_i as well as the initial coordinates:

$$(Q_{xi}, Q_{yi}, Q_{zi}, P_{xi}, P_{yi}, P_{zi}, \mathcal{E}_{xi}, \mathcal{E}_{yi}) , \tag{3.61}$$

at the initial time. It may be more natural however, to initialize using the non-canonical moment system. In this case, the user of the code needs to specify the following initial parameters:

$$(\langle x^2\rangle_i, \langle xp_x\rangle_i, \langle p_x^2\rangle_i, \langle y^2\rangle_i, \langle yp_y\rangle_i, \langle p_y^2\rangle_i, z_i, p_{z_i})\,, \tag{3.62}$$

where both sets of coordinates are related by the canonical coordinate transformation.

Either way, one must specify the initial longitudinal phase space distribution function $f(z, p_z)$ and the initial transverse moments as a function of the longitudinal phase space:

$$(\langle x^2\rangle(z,p_z), \langle xp_x\rangle(z,p_z), \langle p_x^2\rangle(z,p_z), \langle y^2\rangle(z,p_z), \langle yp_y\rangle(z,p_z), \langle p_y^2\rangle(z,p_z))\,. \tag{3.63}$$

This is the most general way to specify such initial conditions.

The process to initialize the set of macro-particles follows. Firstly, generate a set of longitudinal phase-space coordinates from $f(z, p_z)$ using a numerical method such as rejection sampling or Markov chain Monte Carlo. Then, for each macro-particle, given it's longitudinal phase-space coordinates assign the transverse moments from (3.63). Finally, if necessary, for each macro-particle transform the transverse moments to canonical coordinates.

For example, consider the three-dimensional distribution of the uniform sphere of charge, that is initially stationary. The distribution function can be expressed as:

$$f(\mathbf{x},\mathbf{p}) = \begin{cases} \frac{3N}{4\pi R^3}\delta^{(3)}(\mathbf{p}), & \sqrt{x^2+y^2+z^2} \le R\,, \\ 0, & \text{otherwise.} \end{cases} \tag{3.64}$$

To project this into the longitudinal phase-space, integrate over the transverse dimensions:

$$f(z,p_z) = \int \mathrm{d}^2\mathbf{x}^\perp\, \mathrm{d}^2\mathbf{p}^\perp\, f(\mathbf{x},\mathbf{p}) = \begin{cases} \frac{3N}{4R^3}(R^2-z^2)\delta(p_z), & |z| \le R\,, \\ 0, & \text{otherwise.} \end{cases} \tag{3.65}$$

Now, for the moments, since it is initially stationary all momentum moments are zero, and by symmetry: $\langle x^2\rangle(z,p_z) = \langle y^2\rangle(z,p_z)$. So, computing the

cross-sectional moment:

$$\langle x^2 \rangle(z, p_z) = \int \mathrm{d}^2\mathbf{x}^\perp \, \mathrm{d}^2\mathbf{p}^\perp \, x^2 \, f(\mathbf{x}, \mathbf{p}) = \begin{cases} \frac{3N}{4R^3} \frac{(R^2 - z^2)^2}{4} \delta(p_z), & |z| \leq R \,, \\ 0, & \text{otherwise.} \end{cases} \tag{3.66}$$

Which is all of the information needed to initialize a uniform sphere.

Following a similar procedure, the uniform cylinder of charge with longitudinal length L and transverse radius R has the distribution:

$$f(\mathbf{x}, \mathbf{p}) = \begin{cases} \frac{N}{\pi R^2 L} \delta^{(3)}(\mathbf{p}), & \sqrt{x^2 + y^2} \leq R \text{ and } |z| < L/2 \,, \\ 0, & \text{otherwise.} \end{cases} \tag{3.67}$$

So the projection onto the longitudinal phase space is:

$$f(z, p_z) = \int \mathrm{d}^2\mathbf{x}^\perp \, \mathrm{d}^2\mathbf{p}^\perp \, f(\mathbf{x}, \mathbf{p}) = \begin{cases} \frac{N}{L} \delta(p_z), & |z| \leq L/2 \,, \\ 0, & \text{otherwise,} \end{cases} \tag{3.68}$$

and the transverse second moments are:

$$\langle x^2 \rangle(z, p_z) = \int \mathrm{d}^2\mathbf{x}^\perp \, \mathrm{d}^2\mathbf{p}^\perp \, x^2 \, f(\mathbf{x}, \mathbf{p}) = \begin{cases} \frac{N}{L} \frac{R^2}{4} \delta(p_z), & |z| \leq L/2 \,, \\ 0, & \text{otherwise,} \end{cases} \tag{3.69}$$

where the same symmetry argument from the uniform sphere applies here to $\langle y^2 \rangle(z, p_z)$.

This process can be applied to any given analytic distribution function $f(\mathbf{x}, \mathbf{p})$ of the six dimensional phase-space. This approach is preferred when initializing distributions where $f(\mathbf{x}, \mathbf{p})$ may be written as a direct product of distributions in each dimension as in:

$$f(\mathbf{x}, \mathbf{p}) = f_1(x, p_x) f_2(y, p_y) f_3(z, p_z) \,, \tag{3.70}$$

which is the case for distributions with no correlations between the phase-space dimensions.

Another method of initialization is from the output of an envelope code such as `TRANSPORT` or `TRANSOPTR`. This arises when modelling a 2D continuous beam, since such envelope codes return the set of transverse moments as a function of the location. In the case of a continuous beam, the current and the longitudinal distribution function are assumed to be uniform in z

and some thermal distribution of appropriate temperature in p_z.

External Field Numerical Integration

The longitudinal particle kernel function $R(z)$ is implemented as a couple of options. The first is the δ-function kernel:

$$R_\delta(z) = \delta(z)\,, \tag{3.71}$$

the other kernel function is the uniform kernel:

$$R_1(z) = \begin{cases} \frac{1}{h}\,, & |z| \le h/2\,, \\ 0\,, & |z| > h/2\,, \end{cases} \tag{3.72}$$

where h is the width of the kernel. Both of these kernels are analytically integrated against the potential basis functions.

Conversely, the external potential must be numerically integrated against the kernel function. For R_δ, it is trivially the field evaluated at the macro-particle location. For R_1, there is a choice of some numerical integration scheme. For such a numerical integration scheme consider the integral:

$$\int_{-\infty}^{\infty} \mathrm{d}z\, R_1(z - Q_{zi})\Phi(z)\,, \tag{3.73}$$

where $\Phi(z)$ is some function representing the external fields. Then, by making a change of variables to $z' = z - Q_{zi}$ it becomes:

$$\int_{-h/2}^{h/2} \mathrm{d}z'\, R_1(z')\Phi(z' + Q_{zi})\,. \tag{3.74}$$

If h is small with respect to how quickly $\Phi(z)$ changes in both time and space, then only need a few numerical integration points are needed. In fact, if h is very small, compared to the change in $\Phi(z)$, then taking the rectangle rule over the full interval gives:

$$\int_{-h/2}^{h/2} \mathrm{d}z'\, R_1(z') f(z' + Q_{zi}) \approx f(Q_{zi})\,, \tag{3.75}$$

which is the same as the R_δ kernel.

For general external fields, I implemented the Trapezoidal rule for a more accurate integration by dividing the interval into N sub-intervals in $[-h/2, h/2]$. This gives:

$$\int_{-h/2}^{h/2} \mathrm{d}z'\, R_1(z') f(z'+Q_{zi}) \approx \frac{1}{2} \sum_{k=1}^{N} \left(f(Q_{zi} - h/2 + z_{k-1}) + f(Q_{zi} - h/2 + z_k) \right) , \tag{3.76}$$

where z_k is the left end point of of the kth interval.

In the implementation of the code, the following external potential terms must be specified as continuous functions:

$$\varphi_z(z,t)\,, \qquad \varphi_{xx}(z,t)\,, \qquad \varphi_{yy}(z,t)\,, \qquad \varphi_{xxz}(z,t)\,, \qquad \varphi_{yyz}(z,t)\,. \tag{3.77}$$

Numerical Integration

The implementation integrates using using the simplest explicit symplectic numerical integrators. However, since I made the approximation to the self-field, symplectic integrators will not be energy conserving. Even so, the implementation includes the first order Symplectic Euler method as well as the second order Störmer-Verlet method.

Let the time at the start of the simulation be $t = 0$. Then the time at any later step is given by $t = n\Delta t$, where Δt is the time incremented per integration step and n is the number of integration steps completed. Then, label the state of the coordinates at time $n\Delta t$ by the two vectors:

$$(\mathbf{q}^n, \mathbf{p}^n)\,, \tag{3.78}$$

where $\mathbf{p}^n$ denotes the vector of canonical momenta and $\mathbf{q}^n$ the vector of canonical positions both at at the nth time step. The Hamiltonian is a function of the phase space coordinates: $H(\mathbf{q}, \mathbf{p})$. Using this notation, the first order symplectic Euler method is:

$$\mathbf{p}^{n+1} = \mathbf{p}^n - \Delta t\, \nabla_{\mathbf{q}} H(\mathbf{q}^n, \mathbf{p}^{n+1})\,, \tag{3.79}$$

$$\mathbf{q}^{n+1} = \mathbf{q}^n + \Delta t\, \nabla_{\mathbf{p}} H(\mathbf{q}^n, \mathbf{p}^{n+1})\,. \tag{3.80}$$

And similarly, the second order symplectic Störmer-Verlet method:

$$\mathbf{p}^{n+1/2} = \mathbf{p}^n - \frac{\Delta t}{2}\nabla_{\mathbf{q}} H(\mathbf{q}^n, \mathbf{p}^{n+1/2})\,, \tag{3.81}$$

$$\mathbf{q}^{n+1} = \mathbf{q}^n + \frac{\Delta t}{2}\left(\nabla_{\mathbf{p}} H(\mathbf{q}^n, \mathbf{p}^{n+1/2}) + \nabla_{\mathbf{p}} H(\mathbf{q}^{n+1}, \mathbf{p}^{n+1/2})\right)\,, \tag{3.82}$$

$$\mathbf{p}^{n+1} = \mathbf{p}^{n+1/2} - \frac{\Delta t}{2}\nabla_{\mathbf{q}} H(\mathbf{q}^{n+1}, \mathbf{p}^{n+1/2})\,. \tag{3.83}$$

These integration schemes are explicit for separable Hamiltonian systems.

Chapter 4

Validation and Application

4.1 Simple Geometries

To test the field solver as well as the integration scheme I start with looking at idealized distributions. To test the field solver, its output is compared to analytic solutions for the on-axis potential and second transverse derivatives. The derivation of the analytic solutions is found in Appendix D.

These artificial distributions have zero initial temperature. This makes the calculations in this section susceptible to an artificially high level of numerical noise. Many more macro-particles and grid points are used for these calculations than is necessary for a more realistic beam, as will be shown in the next section.

4.1.1 Uniform Sphere of Charge

The first test of the field solver is to model a uniformly distributed sphere of charge. The uniform sphere contains 10^8 protons in a radius of 1 cm. To create a uniform spherical distribution 1024 macro-particles were initialized uniformly throughout the sphere with varying sizes and weights. The potential grid of length 10 cm centred on the sphere was initialized with metallic boundary conditions and constructed with 104 grid points. Fig. 4.1 shows the calculated potential and radial second derivative of the potential from the field solver compared to the analytic solution. Since the analytic solution is for free space boundary conditions, the method of images was used to find the solution with metallic boundary conditions. The calculated potential shows excellent agreement with the analytic solution in contrast with the transverse

second derivatives which show some disagreement. The calculation near the edge of the sphere shows a smoothing effect. This effect may be due to the finite resolution of the grid which is not able to resolve the relatively 'sharp' edge where the linear density and size rapidly decrease to zero.

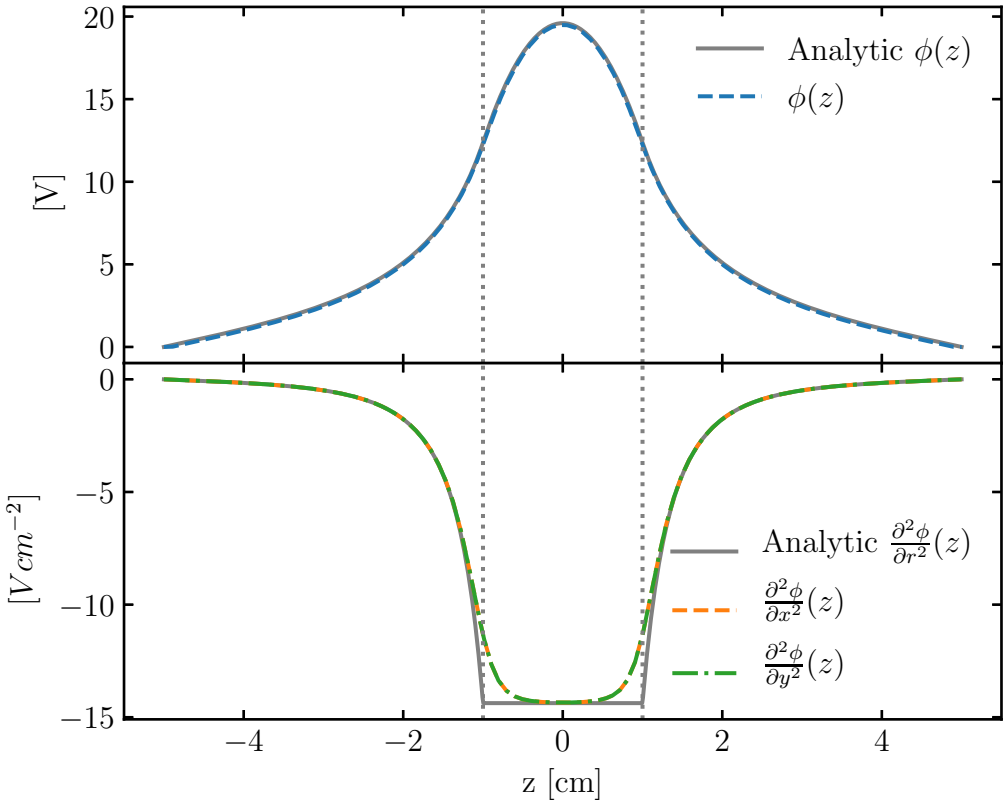

Figure 4.1: The potential and second transverse derivative of the potential (in this case in the x-direction) is compared to the analytic solution for a uniform sphere of charge. The vertical dotted lines indicate the edge of the sphere.

4.1.2 Expanding Uniform Sphere of Charge

The distribution of macro-particles is tracked over the time it takes for the sphere to double in size. The distribution of 1024 macro-particles was initialized in the same manner as the static sphere of uniform charge. This

sphere contained 10^8 charges in an initial radius of 1 cm. The potential grid is constructed with 250 points and metallic boundary conditions, with a grid length of 10 cm. Fig. 4.2 shows the time evolution of the edge of the sphere in each of the Cartesian directions. The sphere doubles in size in the correct amount of time in each of the directions, and there is no symmetry breaking in any direction. Fig. 4.3 shows a more detailed look at the expansion of the distribution. The scale of the distribution changes appropriately in time, while it maintains the same shape.

For the purposes of Fig. 4.2, the edge is calculated from the time dependent second moments. Consider the normalized spatial distribution for the uniform sphere:

$$f(\mathbf{x}) = \begin{cases} \frac{3}{4\pi R^3}\,, & \sqrt{x^2+y^2+z^2} \leq R\,, \\ 0, & \text{otherwise.} \end{cases} \tag{4.1}$$

The second moment in the x direction is:

$$\langle x^2 \rangle = \int \mathrm{d}^3\mathbf{x}\,\mathrm{d}^3\mathbf{p}\,x^2 f(\mathbf{x},\mathbf{p}) = \frac{R^2}{5}\,, \tag{4.2}$$

and by symmetry this is the same for $\langle y^2 \rangle$ and $\langle z^2 \rangle$. Therefore given that the sphere maintains uniformity, the second moments are related to the edge of the sphere by:

$$R_x = \sqrt{5\langle x^2 \rangle}\,, \qquad R_y = \sqrt{5\langle y^2 \rangle}\,, \qquad R_z = \sqrt{5\langle z^2 \rangle}\,, \tag{4.3}$$

where a separate radius is specified in each Cartesian direction to observe any symmetry breaking in the expanding sphere.

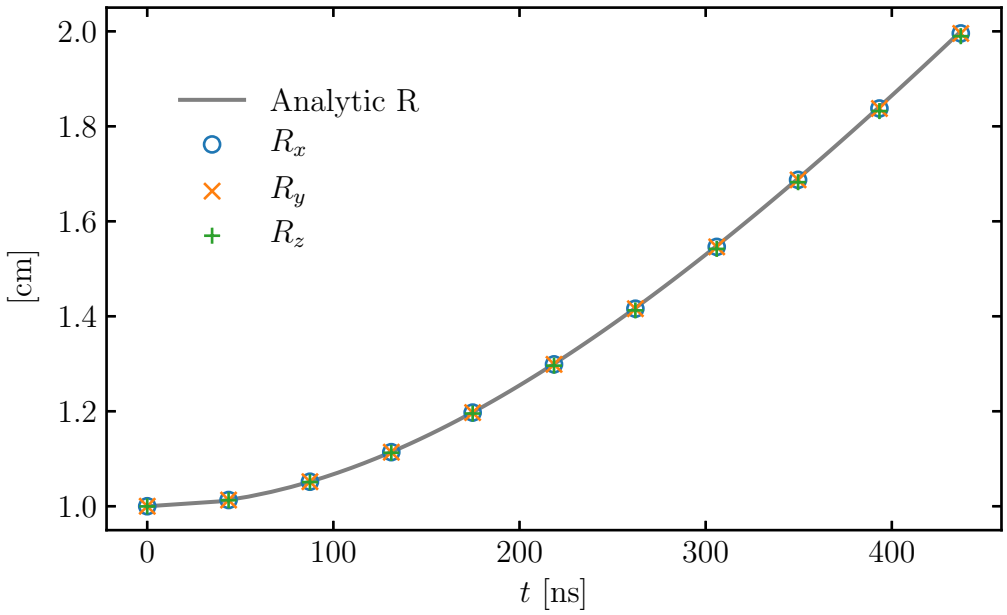

Figure 4.2: The Cartesian edges of the uniform sphere of charge as it expands, plotted against the analytic solution. The analytic solution is indicated by the grey line.

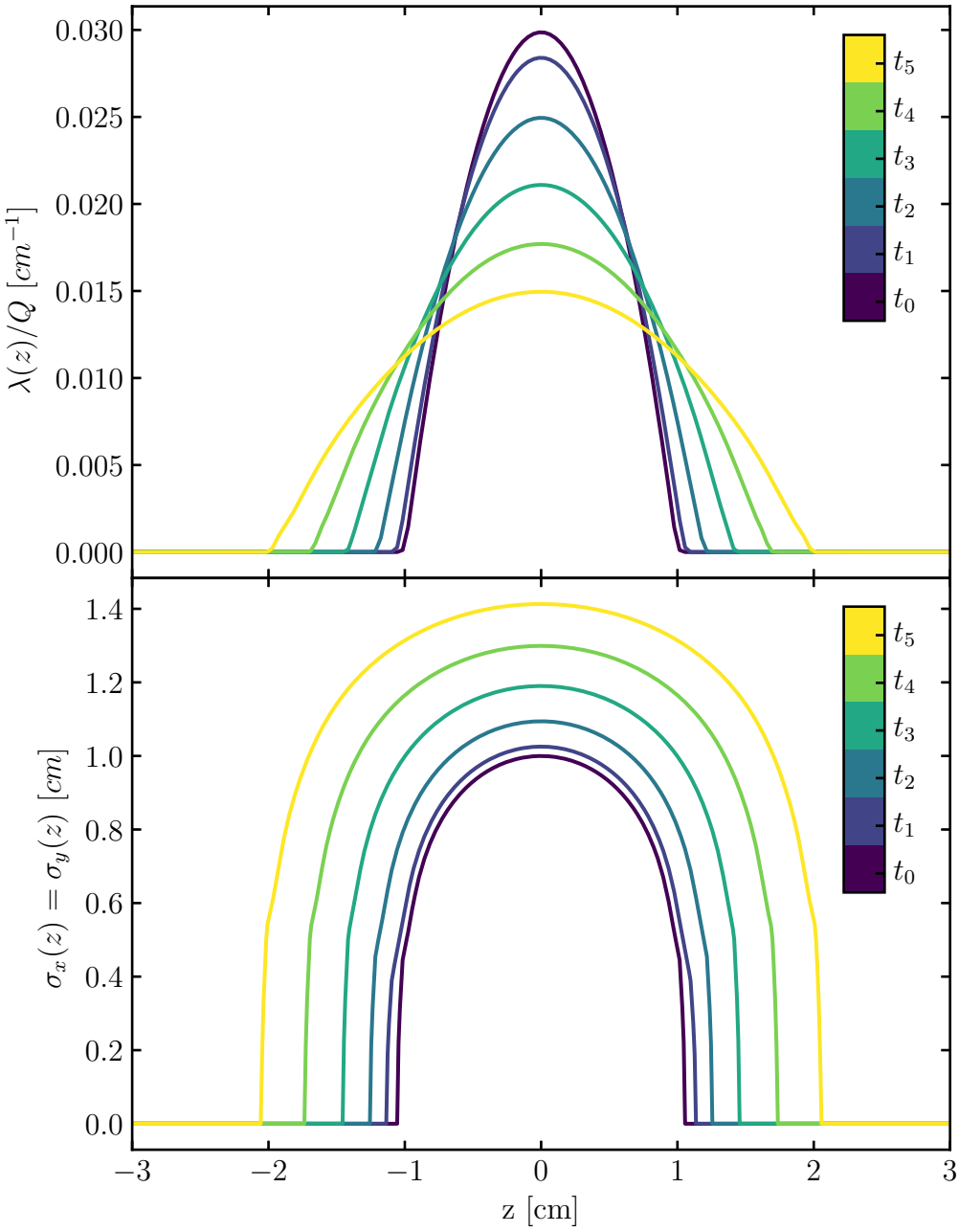

Figure 4.3: The deposited charge and shape on the self-field grid are shown at evenly spaced times. On top is the projected linear charge density, normalized by the total charge. Below that, the projected transverse 1-σ width in the x-direction is shown. The width in the y-direction, not shown, is identical.

4.1.3 Uniform Cylinder of Charge

The next simple geometry test is the uniform cylinder of charge. The distribution of 10^{10} protons has a radius of 5 cm and length 20 cm. To create a uniform cylindrical distribution 1024 macro-particles were initialized uniformly along the cylinder with a constant size and weight. The potential grid of length 100 cm centred on the cylinder was initialized with metallic boundary conditions and was constructed with 104 nodes. Fig. 4.4 shows the calculated potential and radial second derivatives of the potential. The field solver shows excellent agreement for both the potential and the second transverse derivative.

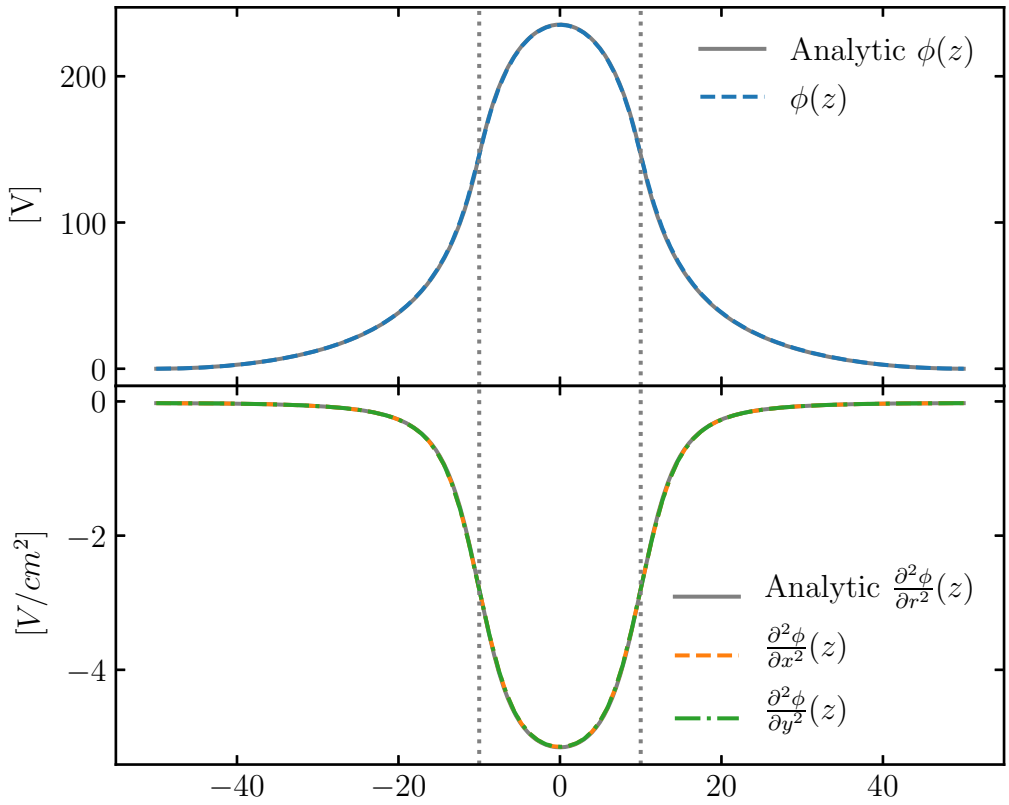

Figure 4.4: The potential and second transverse derivative of the potential (in this case in the x-direction) are compared to the analytic solution for a uniform cylinder of charge. The vertical dotted lines indicate the edge of the cylinder.

4.1.4 Expanding Uniform Cylinder of Charge

Compared to the expanding sphere of charge, a cylinder of charge features less symmetry so there is no analytic expression for its expansion. Instead, I choose to compute the expansion using the three dimensional moment code `TRANSOPTR`. `TRANSOPTR` uses the longitudinal position as the independent variable so the protons are initialized with an initial 1 MeV kinetic energy in the longitudinal direction with no initial momentum spread. The self

potential grid maintains a constant length but is repositioned to be centred on the centre of mass of the distribution.

The distribution of 1024 macro-particles was initialized in the same manner as the static cylinder of uniform charge, with different parameters. This distribution contains $5 \cdot 10^{10}$ protons in an initial radius of 1 cm and length 4 cm. The potential grid is constructed with 250 points and metallic boundary conditions, with a grid length of 10 cm. Fig. 4.5 compares the second moments in each of the Cartesian directions against the position of the centre of mass in the longitudinal direction. The moment tracking shows excellent agreement with `TRANSOPTR`. Fig. 4.3 shows a more detailed look at the expansion of the distribution. The scale of the distribution changes appropriately in time, while the shape of the distribution expands to be more sphere-like.

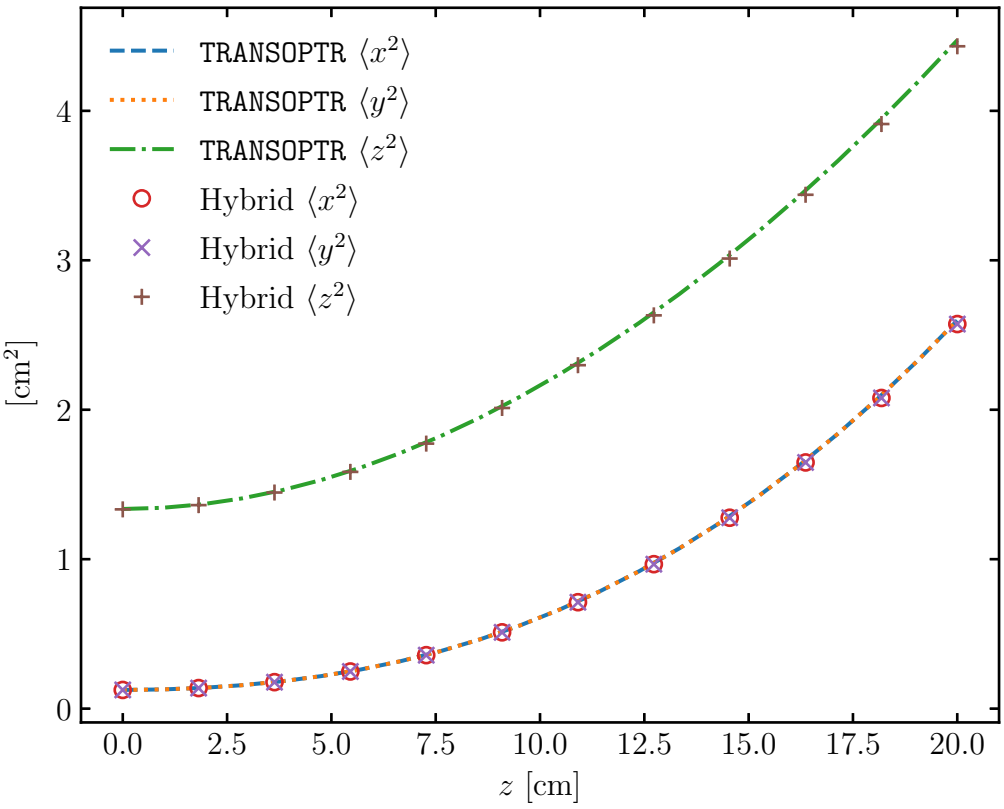

Figure 4.5: The second moments the uniform cylinder of charge as it expands. The Hybrid implementation is plotted against the moment code `TRANSOPTR`.

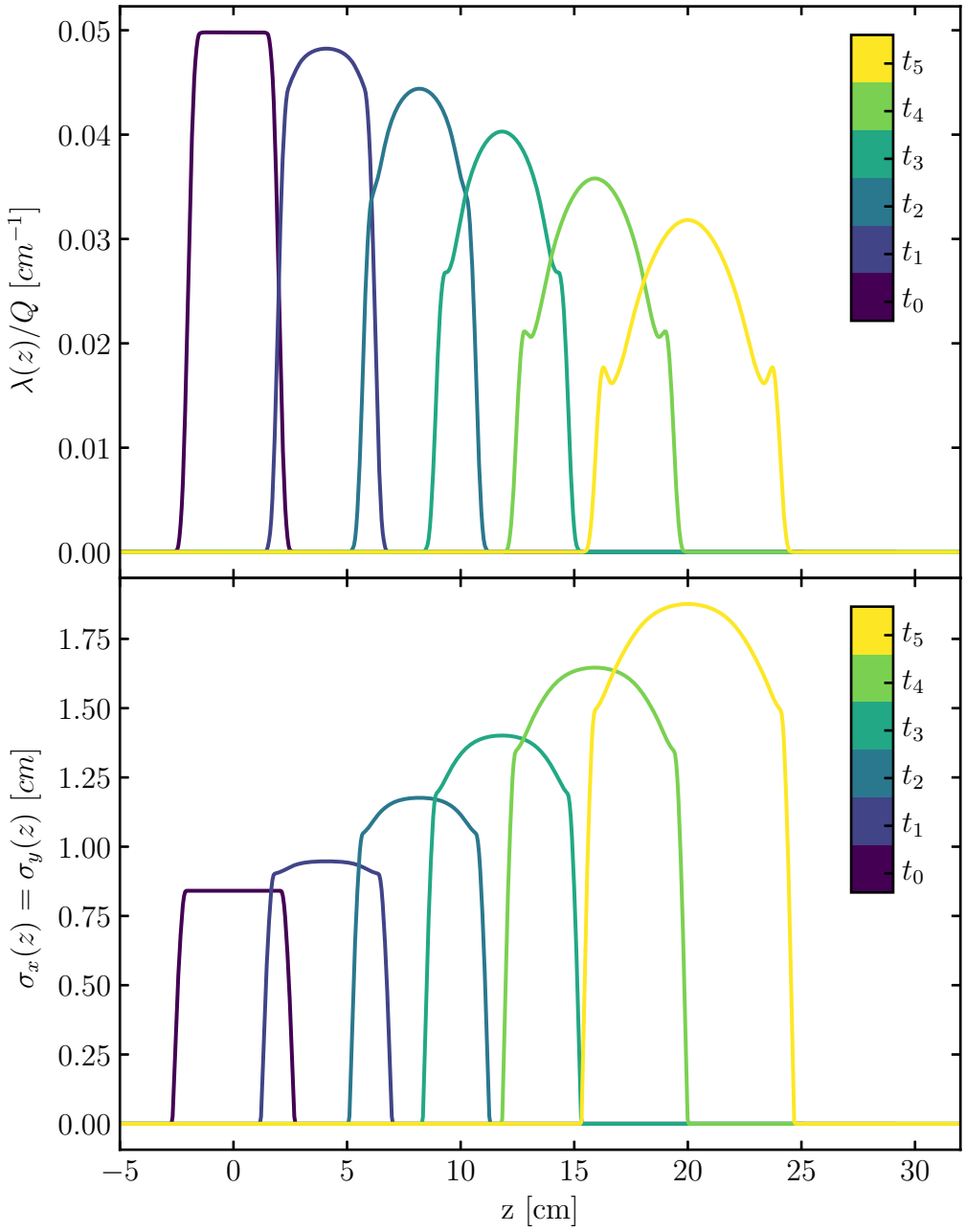

Figure 4.6: The deposited charge and shape on the self-field grid are shown at different times. On top is the projected linear charge density, normalized by the total charge. Below that, the projected transverse 1-σ width in the x-direction is shown. The width in the y-direction, not shown, is identical.

4.2 Code Comparison

With the current set of assumptions, the algorithm is suited to systems with only external electric fields with space charge effects. One such system is the Ion Source Injection System (ISIS) for the TRIUMF cyclotron which provides a high current beam of 300 keV H^- ions. Focusing is provided by electrostatic quadrupoles and bunching is done by two bunchers, a first and a second harmonic, each of which are the two-gap type.

Due to the limitations of the current set of assumptions, many specifics of the injection line can not be modelled. For simplicity, I choose to use the uniform quadrupole lattice instead of the realistic focusing lattice which has different periodic sections with matching sections between them. Since the model does not track first moments and correlations, and the field solver does not work for curvature, it cannot model the two sets of electrostatic cylindrical benders which bend the beam out from the source and then down into the vertical section. For the same reasons, the spiral inflector which bends the beam into the mid-plane of the cyclotron cannot be included. Also, since correlations are neglected, the main magnet fringe-field which acts like a solenoidal field cannot be modelled either. This field rotates the beam axially while the beam travels down the vertical section into the cyclotron.

First I start by tracking the beam through the electrostatic quadrupole lattice. This will let us check the numerical stability of the scheme. I then include a model for the first and second harmonic bunchers to compare the results to a one dimensional code `SPUNCH` written by Baartman Ref. [28] to study the process of bunching in the injection system to the TRIUMF Cyclotron.

4.2.1 Matched Quadrupole Lattice

To verify the numerical stability of the algorithm, I test the long-term tracking behaviour through a periodic quadrupole lattice. This calculation tracks 500 µA of 300 keV protons through a periodic lattice of electrostatic quadrupoles. The parameters of the quadrupoles are chosen to be the most common species found in the ISIS beamline. The quadrupoles have an aperture radius of 2.54 cm and a length of 12.08 cm, they are placed 25.0 cm apart. The voltage is set to ±3.5 kV on the vanes and they are wired in a focus-drift-defocus-drift pattern. One period of this lattice consists of one focus and one defocus quadrupole.

The on-axis fields of the quadrupoles are modelled using a one-parameter Enge function. That is the quadrupole strength is a soft-edge model where the edge is parametrized by:

$$k(z) = \frac{1}{2}\left(1 + \tanh\left(\frac{a_0 z}{4r_a}\right)\right) , \tag{4.4}$$

for an edge at $z = 0$. The variable r_a is the aperture radius of the quad and a_0 is the lowest order Enge parameter, which parametrizes the slope of the fringe field. The 3D potential for the quad is then:

$$V(x, y, z) = G_0(x^2 - y^2)\left[k(z + L/2) - k(z - L/2)\right] , \tag{4.5}$$

where G_0 is the electric field gradient and L is the length of the quad. The quads are modelled with the Enge parameter $a_0 = 6.5169$.

To model a direct current beam the self-potential is taken to be periodic in the longitudinal direction where the period is the length of one quadrupole lattice period. The distribution of macro-particles is randomly uniformly distributed over the length of one lattice. The longitudinal momentum is derived from the energy expression given by a thermal distribution for one degree of freedom at 2000 °C in addition to the initial accelerating potential of 300 kV. Since some macro-particles are initialized inside quadrupoles, the potential energy for those is taken into account as well. The matched distribution is calculated using `TRANSOPTR` and then used to initialize the transverse moments of the macro-particles. The calculation uses 1920 macro-particles and 64 grid points. Which is 30 macro-particles per grid point. The second order Stromer Verlet scheme is used with a step size which is equivalent to 50 steps per period.

Figure 4.7 shows the envelope, or transverse beam size over the first 5 periods of the lattice compared to the 2D moment code `TRANSOPTR`. The envelopes show excellent agreement. Figure 4.8 plots the emittance growth relative to the initial emittance over the integration interval. The emittance in each transverse direction is conserved precisely, as it is an exact conserved quantity of the discretization scheme. The longitudinal emittance grows sharply initially before fluctuating about 5 % to 8 % of the initial value. The initial growth is explained by the initial randomly sampled distribution having some structure that is inconsistent with a thermalized distribution. Once the distribution is thermalized, it reaches stability.

Lastly, Figure 4.9 plots the longitudinal phase space portraits at the first, half-way and final view screen locations along the lattice. The colour of the points indicates the estimated local density in phase space, with lighter colours being more dense. The distribution maintains the appropriate shape and scale.

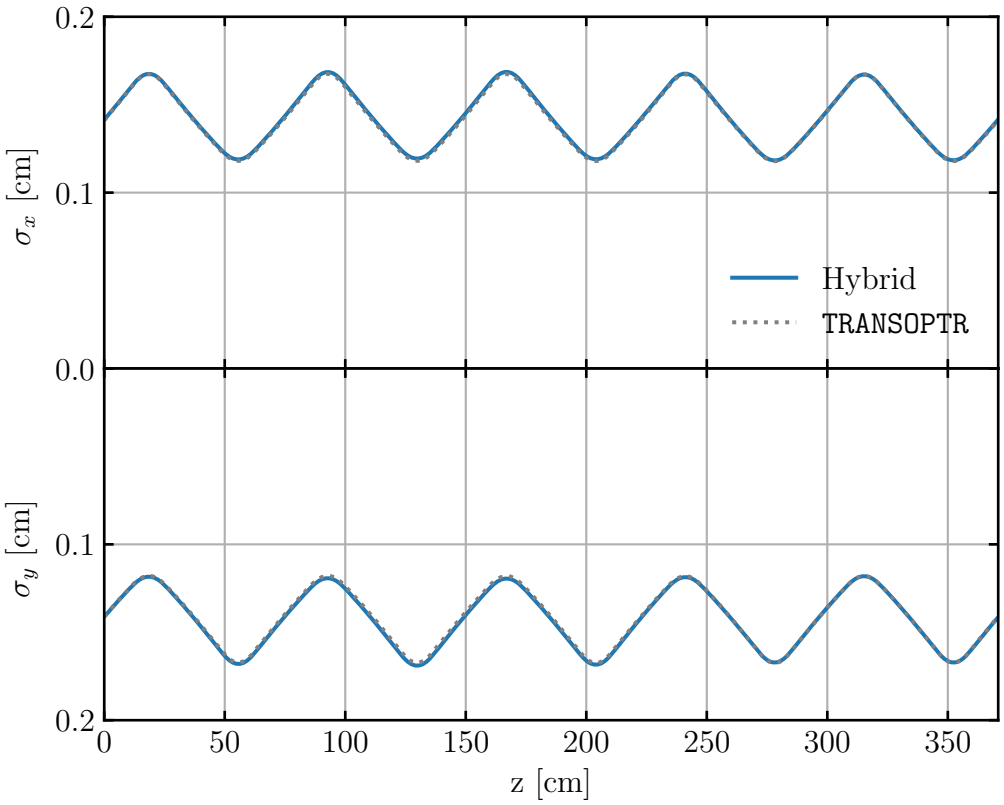

Figure 4.7: The cross-sectional width, the one standard deviation width, over the first 5 periods of the lattice. Above is the width in the x-direction and below is the negative width in the y-direction. This layout highlights the feature of matched distributions in a FODO lattice, having a constant cross-sectional area.

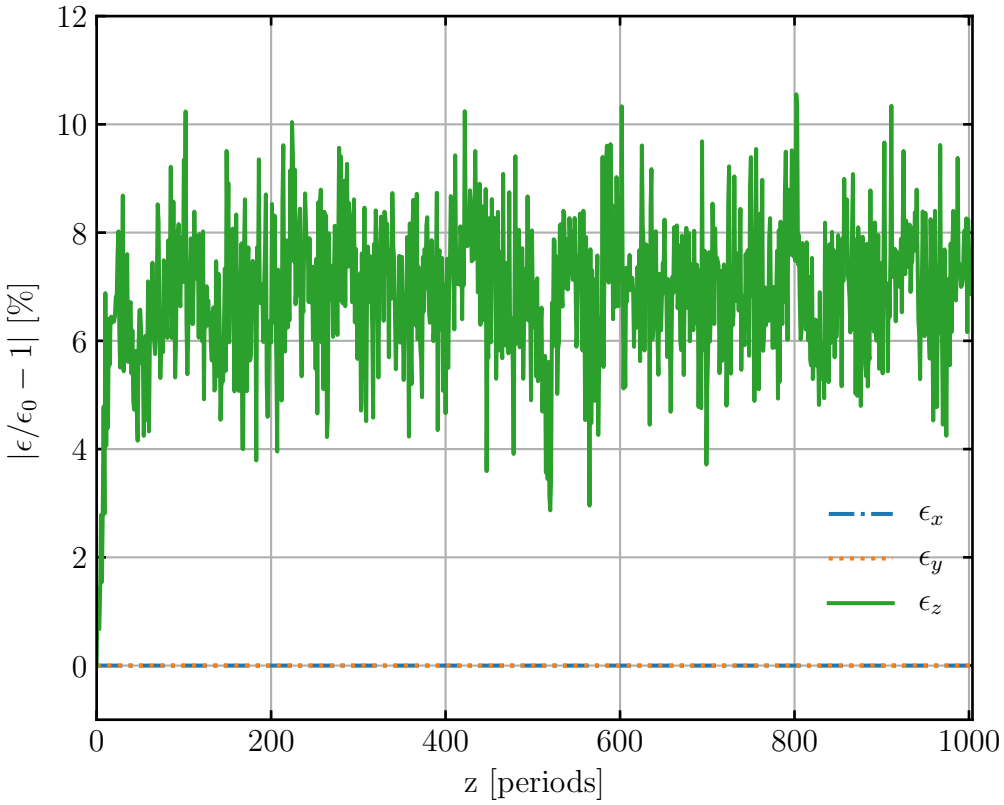

Figure 4.8: The percentage relative emittance growth in each direction is plotted over the integration time. The observations are measured by a simulated view screen placed at the end of each cell. The transverse emittance is conserved. The longitudinal emittance grows initially and then fluctuates but remains bounded.

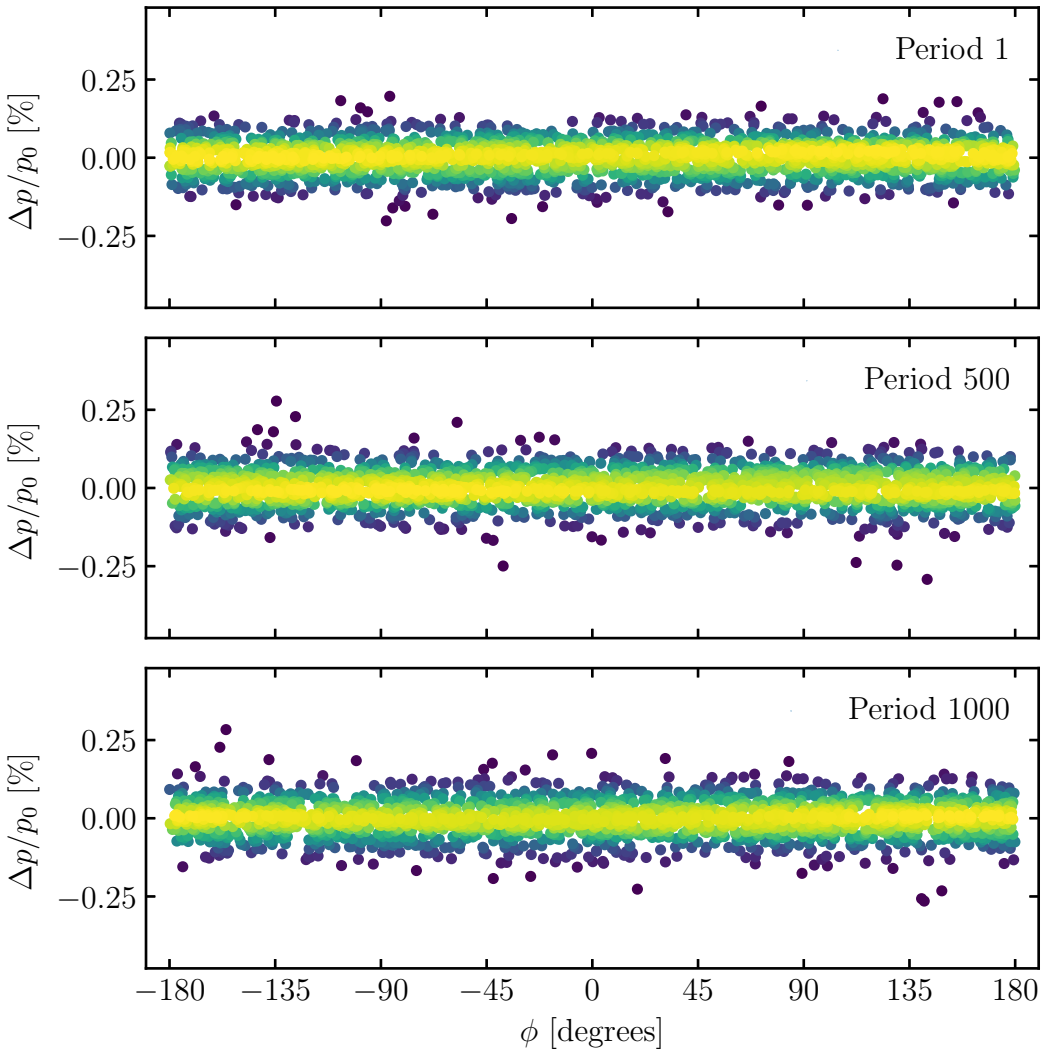

Figure 4.9: Longitudinal phase space portraits of the beam at three view screens placed at the end of the first, cell the five-hundredth cell and the one-thousandth cell (respectively from top to bottom). Each point is an individual macro-particle phase space location, the colour indicates a local approximate density of macro-particles.

4.2.2 Quadrupole Lattice with Bunching

Comparing the results to a one dimensional code `SPUNCH` written by Baartman [28] to study the process of bunching in the injection system to the TRIUMF Cyclotron. This code tracks the momentum and phase of many uniform discs of charge, but cannot track the transverse envelope; the discs are artificially given a fixed radius. The model can track the bunch through drifts and idealized thin-lens bunchers. The forces between the discs are derived from an analytic expression which includes the effect of the beam pipe. Mirror charge terms are included in the longitudinal direction.

Buncher Model

Since the model only requires linearised transverse fields I choose to use an expanded three dimensional potential, with azimuthal symmetry. Assuming that the value of the potential has been specified exactly along the central axis by a function $\varphi(z)$ and that it satisfies the Laplace equation in free space, then the potential has approximate form [29]:

$$\Phi(r,z) = \varphi(z) - \frac{r^2}{4}\frac{\mathrm{d}^2\varphi(z)}{\mathrm{d}z^2} + \mathcal{O}(r^4)\,. \tag{4.6}$$

To compute the on-axis potential, the bunchers are modelled using `OPERA-2D` based on the original design drawings. The model is shown in Figure 4.10. The longitudinal on-axis electric field of each buncher is computed at a fixed voltage, in this case 1 kV. The code then appropriately splines and scales the resulting electric potentials to a varying radio-frequency voltage. The relative phases and transit time factors are computed numerically by integrating the equation of motion of an on-axis non-relativistic reference particle through the bunchers.

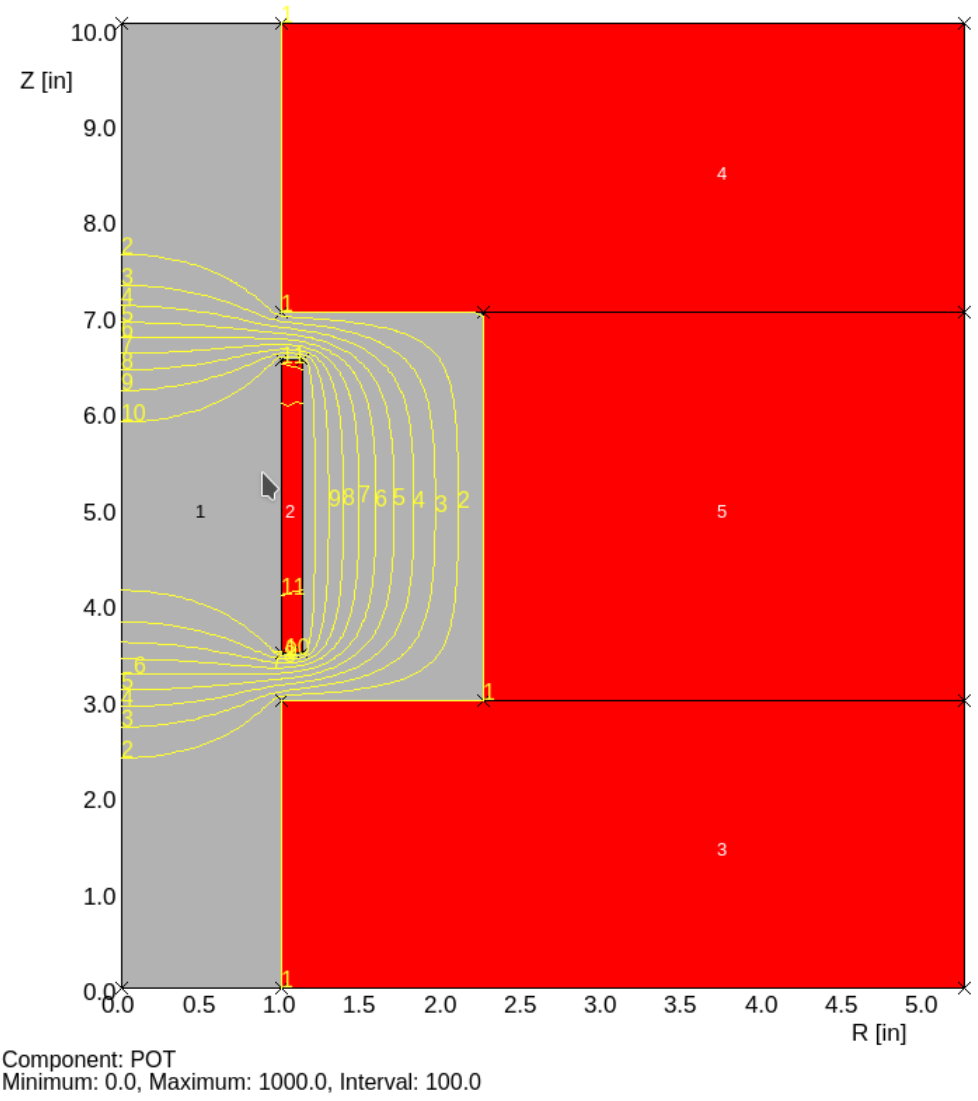

Figure 4.10: The OPERA-2D model of the second harmonic buncher in the radial-longitudinal plane with azimuthal symmetry. The central drift tube is held at a fixed voltage and the equipotential lines in free space are plotted over the geometry. Vacuum is drawn in the grey regions and metal in red.

Code Comparison

Since the bunchers have two gaps, the particles gain energy from twice the effective voltage. In SPUNCH, however the idealized thin buncher imparts a sinusoidal energy gain from a given voltage. The buncher voltage of SPUNCH is hence related to the hybrid algorithm by the following:

$$V_{\texttt{SPUNCH}} = 2TV_{\text{hybrid}} \,, \tag{4.7}$$

where T is the dimensionless transit time factor that depends on the normalized velocity β, the phase of the RF and the geometry of the gap.

Similar to the quadrupole lattice section this example tracks 500 µA of 300 keV H^- ions. The quadrupole lattice is held at the same ±3.5 kV. The lattice is now 28 periods long with the first buncher placed after the first cell and the second harmonic buncher placed after the seventh cell. The relative distances between the bunchers and the end is equal to the spacing in the ISIS beam line.

For the hybrid implementation, the macro-particles are initialized as in the previous section. The transverse moments of the macro-particles are initialized to the matched solution for the focussing lattice. The initial longitudinal phase space is randomly uniformly distributed over the length of one period of the first harmonic, instead of the quadrupole lattice. The longitudinal momentum spread is given by a thermal distribution at 2000 °C. The analogous SPUNCH distribution is initialized over one period of the first harmonic with an equivalent momentum spread. To make the comparison as close as possible, the transverse beam size parameter in the input to SPUNCH is computed from the output of the hybrid code.

The hybrid method is initialized with 1860 macro-particles and 62 self-potential grid points. The SPUNCH calculation is run with 500 discs, the maximum due to memory constraints of the computer when it was implemented.

To compare the two codes the bunchers are run with the same parameters $V_1 = 4.740\,\text{kV}$ and $V_2 = -2.450\,\text{kV}$ which is a result of a previous SPUNCH optimization by Baartman and Rao Ref [30]. Figure 4.11 shows the beam envelope produced by the hybrid algorithm. The transverse beam envelope is the time-integrated width of the beam, one standard deviation, at a particular location. The longitudinal beam envelope is tracked over the integration time. For consistent plotting it is plotted against the longitudi-

nal position of the centre of mass. Figure 4.12 compares the phase space portraits, produced by the two codes, at regularly spaced locations along the beam line. The phase space is observed at a fixed location at the end of the indicated quadrupole lattice period. The final phase space distribution from Figure 4.12 produced by the hybrid code is shown in Figure 4.13 with additional histograms for the one dimensional projections.

The phase space portraits show excellent agreement, with all of the same features present with identical scales. Note that the difference in macro-particle number may make the local density difficult to compare visually.

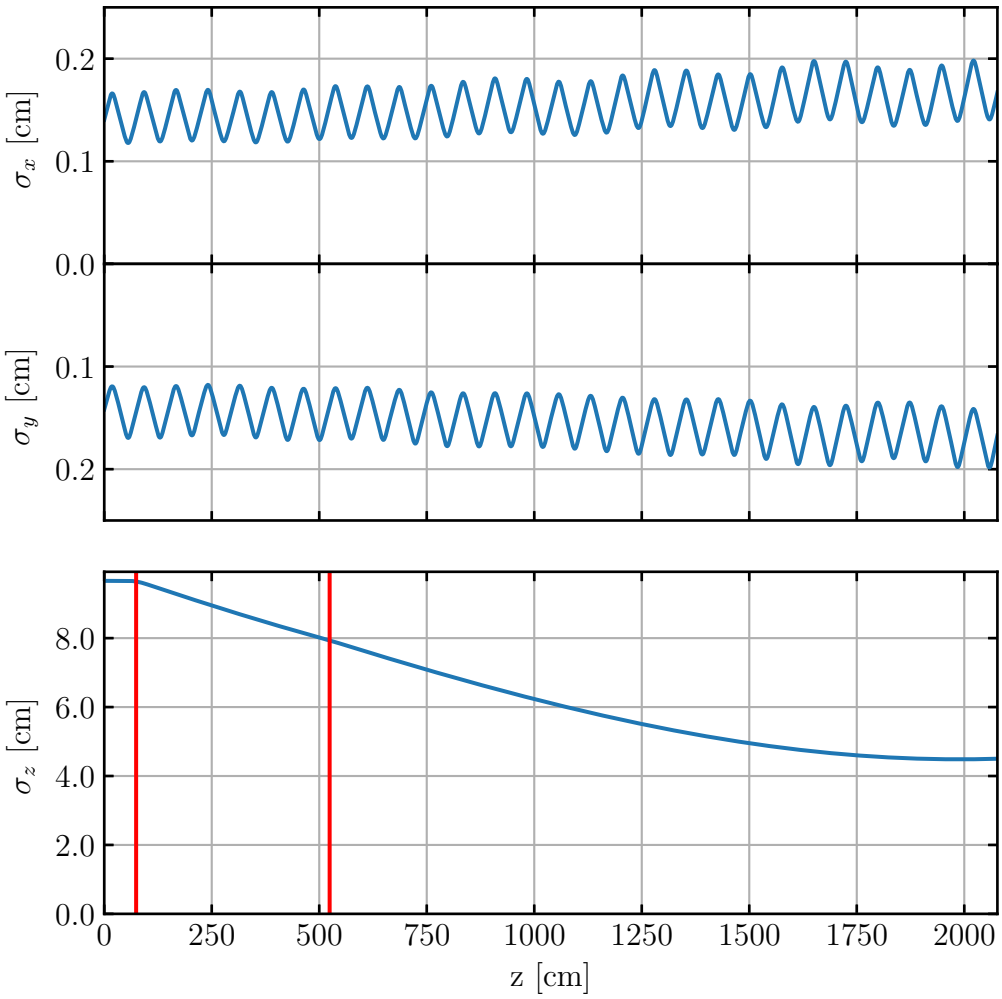

Figure 4.11: The cross-sectional, one standard deviation width, over the lattice. Top is the width in the x-direction, middle is the width in the y-direction, bottom is the longitudinal width. The buncher locations are indicated by the vertical red lines.

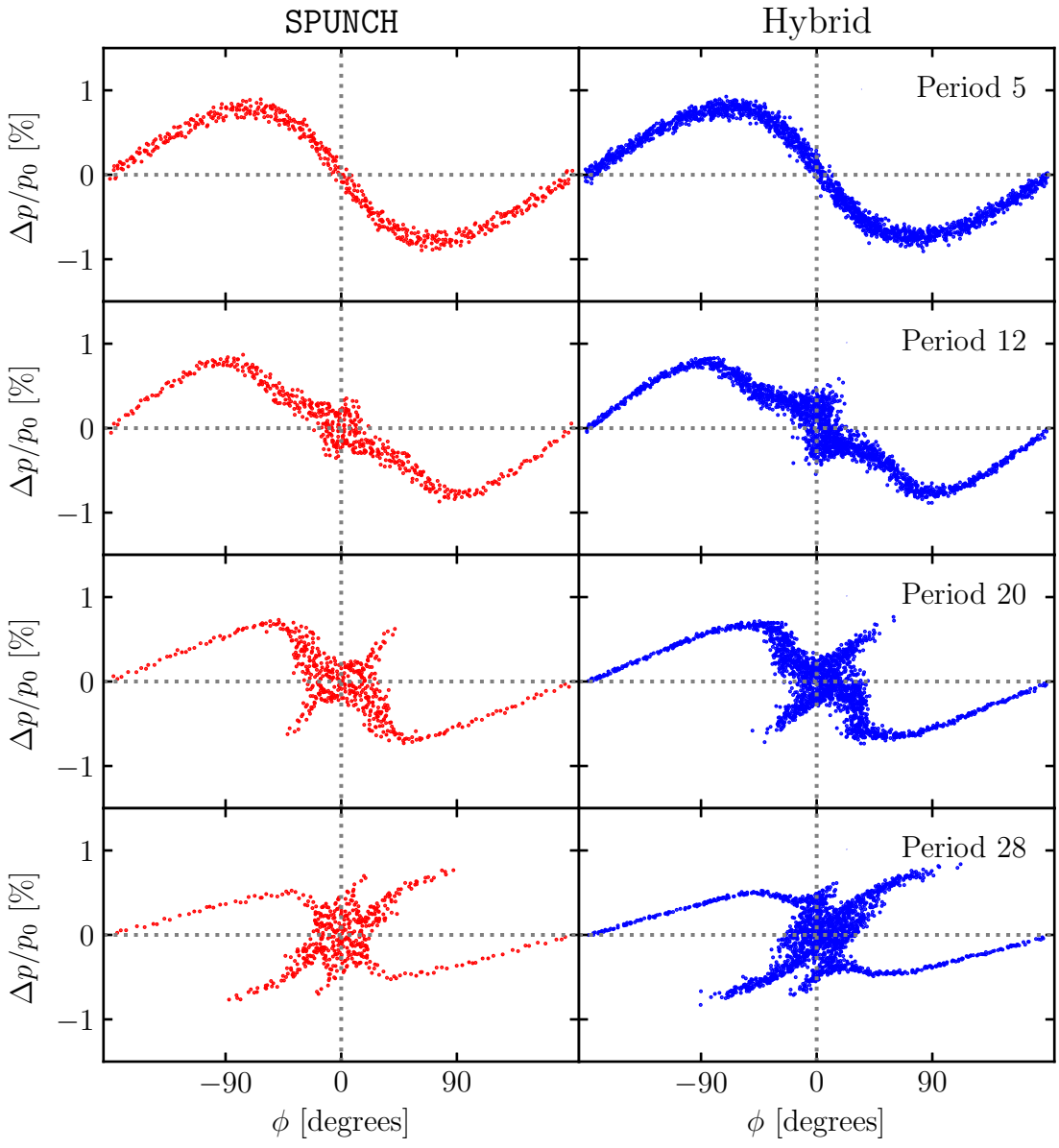

Figure 4.12: Longitudinal phase space portraits of the beam at the end of the indicated period. The left column is the code SPUNCH compared to the hybrid implementation in the right column. The last portrait corresponds to the end of the lattice.

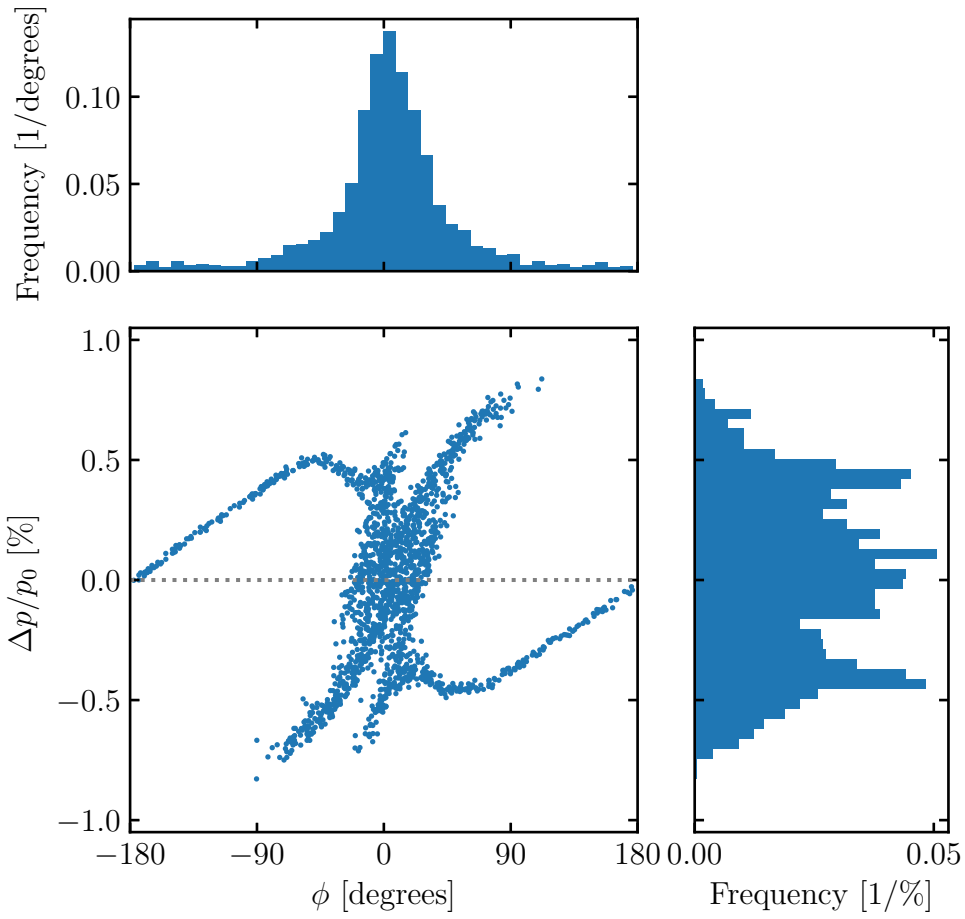

Figure 4.13: Longitudinal phase space portrait of the beam at the end of the lattice. Each point is an individual macro-particle phase space location. The histogram of the projection onto each axis is displayed as well.

Chapter 5

Conclusions

This model is the first in accelerator physics used to study conversion of a DC beam into a bunched one, that reduces the complexity in some dimensions by linearisation, instead of reducing the dimension. Models with reduced dimension, cannot self-consistently include the effects of the transverse dynamics. Compared to a full 3D macro-particle code, this method is able to describe the relevant three dimensional dynamics but with many fewer macro-particles. It also requires a significantly less detailed description of the optics.

The variational approach to deriving discrete systems of equations produces algorithms with many desirable traits. This approach was able to serve as a common mathematical language describing both moment and macro-particle algorithms.

The method of moment expansion reduces the number of model inputs, and thus, model input error significantly. For example, the quadrupole model required only four discrete parameters per quadrupole. The bunchers were modelled in greater detail, with the electric field on-axis given as a field map. The reduction in the total number of inputs to a simulation reduces friction for the users of the code. The lesser friction can mean faster prototyping and less time spent debugging.

The macro-particle discretization scheme is very useful for detailed modelling of non-linear effects. The statistical limitations for requiring high numbers of macro-particles can be lessened by reducing the number of phase space dimensions that are discretized in this way.

The as-implemented algorithm is inadequate for fully modelling most realistic systems. The hybrid macro-particle discretization scheme has potential

for making useful codes. The extensions of the macro-particle discretization scheme from the current set of assumptions to a relativistic beam, off-axis with cross-dimension correlations will be the topic of future work.

Further investigation should be done on the feasibility of extending the field solver to curved reference trajectories with off-axis particles. The decision to sacrifice the symplecticity of the system, by making the external field approximation, led to grid-heating, a flaw of many particle-in-cell codes. Future investigations into alternate schemes should seek to maintain symplecticity to avoid this.

Bibliography

[1] A. Saltelli, *A short comment on statistical versus mathematical modelling*, Nature communications, 10 (2019), pp. 1–3.

[2] H. A. Lorentz, *Attempt of a theory of electrical and optical phenomena in moving bodies*, Leiden: EJ Brill, Leiden, (1895).

[3] A. Vlasov, *Theory of vibrations properties of electron gas and its application*, JETF, 8 (1938), p. 291.

[4] R. W. Hockney and J. W. Eastwood, *Computer simulation using particles*, crc Press, 1988.

[5] R. D. Ryne, *Advanced computing tools and models for accelerator physics*, , Lawrence Berkeley National Lab.(LBNL), Berkeley, CA (United States), 2008.

[6] I. Kapchinskij and V. Vladimirskij, *Limitations of proton beam current in a strong focusing linear accelerator associated with the beam space charge*, (1959).

[7] F. Sacherer, *RMS envelope equations with space charge*, CERN-SI-Int-DL-70-12., 1970.

[8] K. L. Brown, F. Rothacker, D. C. Carey, and C. Iselin, *Transport-a computer program for designing charged particle beam transport systems*, , European Organization for Nuclear Research, 1980.

[9] E. Heighway and R. Hutcheon, *TRANSOPTR—a second order beam transport design code with optimization and constraints*, Nuclear Instruments and Methods in Physics Research, 187 (1981), pp. 89–95.

[10] R. Baartman, *TRANSOPTR: Changes since 1984*, TRI-BN-16-06, TRIUMF, 2016.

[11] R. Baartman, *Fast envelope tracking for space charge dominated injectors. to be published proc*, in 28th Linear Accelerator Conference, 2016.

[12] P. Channell, *The moment approach to charged particle beam dynamics*, IEEE Transactions on Nuclear Science, 30 (1983), pp. 2607–2609.

[13] F. Low, *A lagrangian formulation of the boltzmann-vlasov equation for plasmas*, Proceedings of the Royal Society of London. Series A. Mathematical and Physical Sciences, 248 (1958), pp. 282–287.

[14] P. J. Morrison, *The maxwell-vlasov equations as a continuous hamiltonian system*, Physics Letters A, 80 (1980), pp. 383–386.

[15] P. J. Morrison, *Poisson brackets for fluids and plasmas*, in AIP Conference proceedings, vol. 88, AIP, 1982, pp. 13–46.

[16] A. Weinstein and P. J. Morrison, *Comments on: The maxwell-vlasov equations as a continuous hamiltonian system*, Physics Letters A, 86 (1981), pp. 235–236.

[17] E. G. Evstatiev and B. A. Shadwick, *Variational formulation of particle algorithms for kinetic plasma simulations*, Journal of Computational Physics, 245 (2013), pp. 376–398.

[18] B. A. Shadwick, A. B. Stamm, and E. G. Evstatiev, *Variational formulation of macro-particle plasma simulation algorithms*, Physics of Plasmas, 21 (2014), p. 055708.

[19] B. Shadwick and J. Wurtele, *General moment model of beam transport*, in Proceedings of the 1999 Particle Accelerator Conference (Cat. No. 99CH36366), vol. 4, IEEE, 1999, pp. 2888–2890.

[20] B. Shadwick, G. Tarkenton, E. Esarey, and F. M. Lee, *Hamiltonian reductions for modeling relativistic laser-plasma interactions*, Communications in Nonlinear Science and Numerical Simulation, 17 (2012), pp. 2153–2160.

[21] R. Salmon, *Hamiltonian fluid mechanics*, Annual review of fluid mechanics, 20 (1988), pp. 225–256.

[22] G. B. Arfken and H. J. Weber, *Mathematical methods for physicists 6th ed.*, Elsevier Academic Press, 2005.

[23] J. Qiang, *Symplectic particle-in-cell model for space-charge beam dynamics simulation*, Physical Review Accelerators and Beams, 21 (2018), p. 054201.

[24] J. Qiang, *Symplectic multiparticle tracking model for self-consistent space-charge simulation*, Physical Review Accelerators and Beams, 20 (2017), p. 014203.

[25] E. Hairer, C. Lubich, and G. Wanner, *Geometric Numerical integration: structure-preserving algorithms for ordinary differential equations*, Springer, 2006.

[26] F. J. Sacherer, *RMS envelope equations with space charge*, IEEE Transactions on Nuclear Science, 18 (1971), pp. 1105–1107.

[27] N. Cook, D. Abell, D. Bruhwiler, J. Edelen, S. Webb, and C. Hall, *An s-based symplectic spectral space charge algorithm*, (2018).

[28] R. Baartman, *Spunch: a space charge bunching computer code*, in Eleventh international conference on cyclotrons and their applications, 1987.

[29] R. Baartman, *Bunch dynamics through accelerator column*, TRI-BN-10-01, TRIUMF, 2010.

[30] R. Baartman and Y.-N. Rao, *Investigation of space charge effect in triumf injection beamline*, in Proceedings of the 2003 Particle Accelerator Conference, vol. 3, IEEE, 2003, pp. 1578–1580.

[31] L. D. Landau and E. M. Lifshitz, *The classical theory of fields*, (1971).

[32] E. Engel and R. M. Dreizler, *Density functional theory*, Springer, 2013.

[33] J. D. Jackson, *Classical electrodynamics*, 1999.

[34] O. Ciftja, *Coulomb self-energy and electrostatic potential of a uniformly charged square in two dimensions*, Physics Letters A, 374 (2010), pp. 981–983.

Appendix A

Hamiltonian Formulation of the Vlasov Poisson System

A.1 Calculus of Variations

In discrete classical mechanics, our quantities of interest are functions of time which are the solutions to ordinary differential equations. In Hamiltonian mechanics, these differential equations are Hamilton's equations which are partial derivatives of the Hamiltonian.

In the variational formulation of the Vlasov system, our quantities of interest are fields: multivariate functions which are the solutions to partial differential equations. The systems of partial differential equations are produced by a generalized set of Hamilton's equations using functional derivatives.

Functionals can be understood as maps from functions to numbers, often expressed as an integral. The functional derivative calculates how the functional varies when its dependent function changes.

The functional derivative exhibits the familiar properties of linearity and has an associated chain rule and product rule. For the extension of mechanics to classical field theory, see Landau and Lifshitz Ref. [31]. For a helpful resource on properties of more complicated of functional derivatives, refer to the first appendix of the book by Engel and Dreizler Ref. [32]. The following section reviews the few properties of the functional derivative used in this thesis.

A.1.1 Functional Derivatives

Consider a general functional $J[g]$ that depends on the multivariate function $g(\mathbf{x})$ that maps $\mathbb{R}^n$ to $\mathbb{R}$. The functional is an integral over the domain $\mathcal{D}$ in $\mathbb{R}^n$ and can be written as:

$$J[g] = \int_{\mathcal{D}} \mathrm{d}^n\mathbf{x}\, \mathcal{L}(g, \nabla_{\mathbf{x}} g, \ldots, \mathbf{x})\,, \tag{A.1}$$

where $\mathcal{L}(g, \nabla_{\mathbf{x}} g, \ldots, \mathbf{x})$ is called the Lagrangian density of $J[g]$, in this case it just refers to the fact that it is the integrand of the functional. It may have explicit dependence on $\mathbf{x}$, $g(\mathbf{x})$, and any number of its higher partial derivatives.

To find the variational derivative of $J[g]$ with respect to $g(\mathbf{x})$, we consider a general function $\eta(\mathbf{x})$. If the function vanishes at the boundary:

$$\eta(\mathbf{x})|_{\partial\mathcal{D}} = 0\,, \tag{A.2}$$

then we may add it as a small perturbation in g. Let us parametrize the size of the perturbation by ϵ, a small positive real number. The functional derivative is defined implicitly by:

$$\int_{\mathcal{D}} \mathrm{d}^n\mathbf{x}\, \frac{\delta J}{\delta g}\eta(\mathbf{x}) = \left.\frac{d}{d\epsilon} J[g + \epsilon\eta]\right|_{\epsilon=0}\,, \tag{A.3}$$

where $\frac{\delta J}{\delta g}$ is the functional derivative, it does not depend on $\eta(\mathbf{x})$.

Throughout this thesis the only functionals of interest are functionals of the particle density function $f(\mathbf{x}, \mathbf{p}, t)$, with no dependence on its derivatives. Consider such a functional $J[f]$, it can be written:

$$J[f] = \int_{\mathcal{P}} \mathrm{d}^3\mathbf{x}\, \mathrm{d}^3\mathbf{p}\, f(\mathbf{x}, \mathbf{p}, t) j(\mathbf{x}, \mathbf{p}, t)\,, \tag{A.4}$$

where $j(\mathbf{x}, \mathbf{p}, t)$ a function of phase space variables and $\mathcal{P}$ is some phase-space volume. Since we assume the functional has no dependence on any partial

derivatives of f, it follows:

$$\begin{aligned}\int_{\mathcal{P}} \mathrm{d}^3\mathbf{x}\,\mathrm{d}^3\mathbf{p}\ \frac{\delta J}{\delta f}\eta(\mathbf{x},\mathbf{p}) &= \frac{d}{d\epsilon}J[f+\epsilon\eta]\bigg|_{\epsilon=0} \\ &= \frac{d}{d\epsilon}\int_{\mathcal{P}} \mathrm{d}^3\mathbf{x}\,\mathrm{d}^3\mathbf{p}\ \left(f(\mathbf{x},\mathbf{p},t)+\epsilon\eta(\mathbf{x},\mathbf{p},t)\right) j(\mathbf{x},\mathbf{p},t)\bigg|_{\epsilon=0} \\ &= \int_{\mathcal{P}} \mathrm{d}^3\mathbf{x}\,\mathrm{d}^3\mathbf{p}\, j(\mathbf{x},\mathbf{p},t)\eta(\mathbf{x},\mathbf{p},t)\,.\end{aligned} \tag{A.5}$$

From the implicit definition, (A.3) the functional derivative is the phase space function:

$$\frac{\delta J}{\delta f(\mathbf{x},\mathbf{p},t)} = j(\mathbf{x},\mathbf{p},t)\,. \tag{A.6}$$

Consider the expression: $f(\mathbf{x}',\mathbf{p}',t)$, the density function evaluated at a specified point. It may be written as a functional in the form of $J[f]$ using Dirac δ-functions:

$$f(\mathbf{x}',\mathbf{p}',t) = \int_{\mathcal{P}} \mathrm{d}^3\mathbf{x}\mathrm{d}^3\mathbf{p}\, f(\mathbf{x},\mathbf{p},t)\delta^{(3)}(\mathbf{x}-\mathbf{x}')\delta^{(3)}(\mathbf{p}-\mathbf{p}')\,. \tag{A.7}$$

Now, using (A.6) to directly write the functional derivative:

$$\frac{\delta f(\mathbf{x}',\mathbf{p}',t)}{\delta f(\mathbf{x},\mathbf{p},t)} = \delta^{(3)}(\mathbf{x}-\mathbf{x}')\delta^{(3)}(\mathbf{p}-\mathbf{p}')\,. \tag{A.8}$$

The relations (A.6) and (A.8) will be used commonly throughout this thesis. The other properties we will need for calculating functional derivatives are the chain rule and the product rule. The product rule is given by A.29 from the texbook of Engel and Dreizler [32] which follows.

$$\frac{\delta(J_1J_2)}{\delta g(\mathbf{x})} = \frac{\delta J_1}{\delta g(\mathbf{x})}J_2 + J_1\frac{\delta J_2}{\delta g(\mathbf{x})} \tag{A.9}$$

for functionals $J_1[g]$ and $J_2[g]$.

The chain rule is much more complicated because of the many possible ways functionals may be nested. For our case, however, consider that the functional $J[g(\mathbf{x})]$ maps the functions $g(\mathbf{x})$ to the real numbers. Since J is real number valued we may construct a function of J, written $F(J[g(\mathbf{x})])$, which through its dependence on J, is also a functional with respect to $g(\mathbf{x})$;

expressed as $F[g(\mathbf{x})]$. The variational derivative with respect to $g(\mathbf{x})$ is then:

$$\frac{\delta F[g]}{\delta g(\mathbf{x})} = \frac{\partial F(J)}{\partial J}\frac{\delta J[g]}{\delta g(\mathbf{x})}\,, \tag{A.10}$$

which follows from A.38 from Engel and Dreizler [32]. This has the familiar form of a normal function chain rule.

A.2 Continuous Equations of Motion

To find the set of continuous equations of motion of this system, consider the density function at a particular point $f(\mathbf{x}', \mathbf{p}', t)$. Since the Poisson bracket is bilinear, the equation of motion simplifies to:

$$\frac{\partial f(\mathbf{x}', \mathbf{p}', t)}{\partial t} = \{f(\mathbf{x}', \mathbf{p}', t), \mathrm{H}_p\} + \{f(\mathbf{x}', \mathbf{p}', t), \mathrm{H}_\phi\}\,. \tag{A.11}$$

Firstly, for the kinetic energy term of the Hamiltonian, we have:

$$\{f(\mathbf{x}', \mathbf{p}', t), \mathrm{H}_p\} = \int \mathrm{d}^3\mathbf{x}\,\mathrm{d}^3\mathbf{p}\, f(\mathbf{x}, \mathbf{p}) \left[\frac{\delta f(\mathbf{x}', \mathbf{p}', t)}{\delta f(\mathbf{x}, \mathbf{p}, t)}, \frac{\delta \mathrm{H}_p}{\delta f(\mathbf{x}, \mathbf{p}, t)}\right]\,. \tag{A.12}$$

The first functional derivative is identically (A.8). To compute the second functional derivative recall (A.6), to find:

$$\frac{\delta \mathrm{H}_p}{\delta f(\mathbf{x}, \mathbf{p}, t)} = \frac{\mathbf{p}^2}{2m}\,, \tag{A.13}$$

then the Poisson bracket is:

$$\{f(\mathbf{x}', \mathbf{p}', t), \mathrm{H}_p\} = \int \mathrm{d}^3\mathbf{x}\,\mathrm{d}^3\mathbf{p}\, f(\mathbf{x}, \mathbf{p}) \left[\delta^{(3)}(\mathbf{x} - \mathbf{x}')\delta^{(3)}(\mathbf{p} - \mathbf{p}'), \frac{\mathbf{p}^2}{2m}\right]\,. \tag{A.14}$$

Computing the canonical Poisson bracket yields:

$$= \int \mathrm{d}^3\mathbf{x}\,\mathrm{d}^3\mathbf{p}\, f(\mathbf{x}, \mathbf{p})\Big(\delta^{(3)}(\mathbf{p} - \mathbf{p}')\nabla_{\mathbf{x}}\delta^{(3)}(\mathbf{x} - \mathbf{x}') \cdot \frac{\mathbf{p}}{m}\Big)\,. \tag{A.15}$$

Then, integrating by parts to move the gradient from the delta function and

dropping the boundary term, simplifies to:

$$= -\int \mathrm{d}^3\mathbf{x}\,\mathrm{d}^3\mathbf{p}\,\delta^{(3)}(\mathbf{p}-\mathbf{p}')\delta^{(3)}(\mathbf{x}-\mathbf{x}')\nabla_{\mathbf{x}} f(\mathbf{x},\mathbf{p})\cdot\frac{\mathbf{p}}{m}\,. \tag{A.16}$$

The δ-functions are then integrated over to find:

$$\{f(\mathbf{x}',\mathbf{p}',t),\mathrm{H}_p\} = -\frac{\mathbf{p}'}{m}\cdot\nabla_{\mathbf{x}'} f(\mathbf{x}',\mathbf{p}')\,, \tag{A.17}$$

the drift term in the Vlasov equation.

Now, to look at the contribution from the self-field. The first functional derivative is the same as before, the second functional derivative is more complicated this time so, breaking down the steps. Consider:

$$\frac{\delta \mathrm{H}_\phi}{\delta f(\mathbf{x},\mathbf{p},t)} = \\ -\frac{q^2}{2\epsilon_0}\frac{\delta}{\delta f(\mathbf{x},\mathbf{p},t)}\int \mathrm{d}^3\mathbf{x}'\,\mathrm{d}^3\mathbf{x}''\,\mathrm{d}^3\mathbf{p}'\,\mathrm{d}^3\mathbf{p}''\,G(\mathbf{x}',\mathbf{x}'')f(\mathbf{x}',\mathbf{p}',t)f(\mathbf{x}'',\mathbf{p}'',t)\,. \tag{A.18}$$

The functional derivative will commute with the integrals and the Green's function. So, the variational derivative will apply to only the two f terms. Note that the two instances of f each have different arguments than $f(\mathbf{x},\mathbf{p},t)$. So, the rule for taking derivatives in (A.6) is not directly applicable. Instead, the product rule, (A.9), can be used along with (A.8) as follows.

$$\frac{\delta\left(f(\mathbf{x}',\mathbf{p}',t)f(\mathbf{x}'',\mathbf{p}'',t)\right)}{\delta f(\mathbf{x},\mathbf{p},t)} = \left(\frac{\delta f(\mathbf{x}',\mathbf{p}',t)}{\delta f(\mathbf{x},\mathbf{p},t)}f(\mathbf{x}'',\mathbf{p}'',t) + f(\mathbf{x}',\mathbf{p}',t)\frac{\delta f(\mathbf{x}'',\mathbf{p}'',t)}{\delta f(\mathbf{x},\mathbf{p},t)}\right) \\ = \delta^{(3)}(\mathbf{p}-\mathbf{p}')\delta^{(3)}(\mathbf{x}-\mathbf{x}')f(\mathbf{x}'',\mathbf{p}'',t) + \delta^{(3)}(\mathbf{p}-\mathbf{p}'')\delta^{(3)}(\mathbf{x}-\mathbf{x}'')f(\mathbf{x}',\mathbf{p}',t)\,. \tag{A.19}$$

Putting this result back into (A.18), integrate over the δ-functions giving:

$$= -\frac{q^2}{2\epsilon_0}\int \mathrm{d}^3\mathbf{x}''\,\mathrm{d}^3\mathbf{p}''\,f(\mathbf{x}'',\mathbf{p}'',t)G(\mathbf{x},\mathbf{x}'') - \frac{q^2}{2\epsilon_0}\int \mathrm{d}^3\mathbf{x}'\,\mathrm{d}^3\mathbf{p}'f(\mathbf{x}',\mathbf{p}',t)G(\mathbf{x}',\mathbf{x})\,. \tag{A.20}$$

To further simplify, use the fact that the Green's function of the Poisson equation is symmetric. See Section 9.7 of the textbook by Arfken and Weber

Ref. [22]. Therefore, re-label one of these terms to become identical to the other, combining them to find:

$$\frac{\delta \mathrm{H}_\phi}{\delta f(\mathbf{x},\mathbf{p},t)} = -\frac{q^2}{\epsilon_0}\int \mathrm{d}^3\mathbf{x}''\,\mathrm{d}^3\mathbf{p}'' f(\mathbf{x}'',\mathbf{p}'',t)G(\mathbf{x},\mathbf{x}'') = q\phi(\mathbf{x},t)\,, \tag{A.21}$$

this is (1.11), the definition of the electrostatic potential written in terms of the Green's function. From here onwards, we will use $\phi(\mathbf{x},t)$ to denote the self-field.

Now, the equation of motion of f from this Hamiltonian will be:

$$\begin{aligned}\{f(\mathbf{x}',\mathbf{p}',t),\mathrm{H}_\phi\} &= \int \mathrm{d}^3\mathbf{x}\,\mathrm{d}^3\mathbf{p}\, f(\mathbf{x},\mathbf{p},t)\left[\delta^{(3)}(\mathbf{x}-\mathbf{x}')\delta^{(3)}(\mathbf{p}-\mathbf{p}'), q\phi(\mathbf{x},t)\right] \\ &= -q\int \mathrm{d}^3\mathbf{x}\,\mathrm{d}^3\mathbf{p}\, f(\mathbf{x},\mathbf{p},t)\delta^{(3)}(\mathbf{x}-\mathbf{x}')\nabla_{\mathbf{p}}\delta^{(3)}(\mathbf{p}-\mathbf{p}')\cdot\nabla_{\mathbf{x}}\phi(\mathbf{x},t)\,.\end{aligned} \tag{A.22}$$

Integrating by parts and dropping the boundary term once again gives:

$$= q\int \mathrm{d}^3\mathbf{x}\,\mathrm{d}^3\mathbf{p}\,\delta^{(3)}(\mathbf{x}-\mathbf{x}')\delta^{(3)}(\mathbf{p}-\mathbf{p}')\nabla_{\mathbf{p}} f(\mathbf{x},\mathbf{p},t)\cdot\nabla_{\mathbf{x}}\phi(\mathbf{x},t) \tag{A.23}$$

Then, integrating over the δ-functions,

$$\{f(\mathbf{x}',\mathbf{p}',t),\mathrm{H}_\phi\} = q\nabla_{\mathbf{x}'}\phi(\mathbf{x},t)\cdot\nabla_{\mathbf{p}'} f(\mathbf{x}',\mathbf{p}',t)\,. \tag{A.24}$$

which describes the force from the self-potential acting on the charge distribution.

The final equation of motion is then found by substituting the results (A.17) and (A.24) into (A.11) to find:

$$\frac{\partial f(\mathbf{x}',\mathbf{p}',t)}{\partial t} = -\frac{\mathbf{p}'}{m}\cdot\nabla_{\mathbf{x}'} f(\mathbf{x}',\mathbf{p}') + q\nabla_{\mathbf{x}'}\phi(\mathbf{x}',t)\cdot\nabla_{\mathbf{p}'} f(\mathbf{x}',\mathbf{p}')\,. \tag{A.25}$$

Now, since the choice of test coordinate was arbitrary, we recover the Vlasov Poisson system.

$$\frac{\partial f}{\partial t} + \frac{\mathbf{p}}{m}\cdot\nabla_{\mathbf{x}} f - q\nabla_{\mathbf{x}}\phi\cdot\nabla_{\mathbf{p}} f = 0\,. \tag{A.26}$$

Thus, the variational formulation of the Vlasov Poisson system contains the physics of the Vlasov Poisson system.

Appendix B

Poisson Systems

The process of discretization is one by which the continuous system is reduced to a finite set of discrete equations. This chapter covers how such a reduction may be done using the Poisson bracket formalism for both canonical and non-canonical systems. This section follows from Chapter VII of the textbook "Geometric Numerical Integration" by Hairer; Ref. [25].

This chapter starts by presenting the basic theory of general Poisson systems. I then show that discretizing the continuous Vlasov Poisson system gives a discrete general Poisson system with respect to the discrete coordinates. In Section B.1.1, I show that the macro-particle discretization presented in Section 2.2 has a canonical Hamiltonian structure. Lastly, in Section B.2 I show the derivation of the Poisson structure matrix used in the moment discretization method Section 2.3.

B.1 Hamiltonian and Poisson systems

Canonical Poisson Bracket

Let us start with the Poisson bracket of a canonical Hamiltonian system with N discrete degrees of freedom. For such a canonical system, consider the phase-space coordinates to be $\mathbf{y} = (x_1, x_2, \ldots, x_N, p_1, p_2, \ldots, p_N)$ where the positions x_i are canonically conjugate to the momenta p_i for all $i = 1, 2, \ldots, N$. The Poisson bracket can be written:

$$\{F, G\} = \sum_{i=1}^{N} \left(\frac{\partial F}{\partial x_i} \frac{\partial G}{\partial p_i} - \frac{\partial F}{\partial p_i} \frac{\partial G}{\partial x_i} \right) . \tag{B.1}$$

Alternatively, this can be expressed using vector notation with respect to the $2N$-dimensional phase-space vector $\mathbf{y}$ as:

$$\{F, G\} = (\nabla_{\mathbf{y}} F)^T \cdot \mathbf{J} \cdot \nabla_{\mathbf{y}} G \,, \tag{B.2}$$

where the matrix $\mathbf{J}$ is called the 'structure matrix' given by,

$$\mathbf{J} = \begin{bmatrix} 0 & \mathbf{I} \\ -\mathbf{I} & 0 \end{bmatrix} , \tag{B.3}$$

and $\mathbf{I}$ is the N-dimensional identity matrix. The matrix $\mathbf{J}$ is known as the symplectic matrix.

For a given Hamiltonian, $\mathrm{H}(\mathbf{y})$, the equations of motion are then:

$$\frac{\mathrm{d}\mathbf{y}}{\mathrm{d}t} = \{\mathbf{y}, \mathrm{H}(\mathbf{y})\} = (\nabla_{\mathbf{y}} \mathbf{y})^T \cdot \mathbf{J} \cdot \nabla_{\mathbf{y}} \mathrm{H}(\mathbf{y}) = \mathbf{J} \cdot \nabla_{\mathbf{y}} \mathrm{H}(\mathbf{y}) \,. \tag{B.4}$$

General Poisson Bracket

A general Poisson structure is one defined with a structure matrix that is not $\mathbf{J}$ but where the important properties of the Poisson bracket are maintained. Let the vector of non-canonical coordinates be $\mathbf{y}$. The generalized Poisson bracket is then given by:

$$\{F, G\} = (\nabla_{\mathbf{y}} F)^T \cdot \mathbf{B}(\mathbf{y}) \cdot \nabla_{\mathbf{y}} G \,, \tag{B.5}$$

where $\mathbf{B}(\mathbf{y})$ is the general structure matrix, which may be a function of the state of the system. For such a system, the individual elements $B_{ij}(\mathbf{y})$ may be found by taking:

$$\{y_i, y_j\} = B_{ij}(\mathbf{y}) \,, \tag{B.6}$$

where y_i and y_j are ith and jth components of $\mathbf{y}$ and $B_{ij}(\mathbf{y})$ is the component of the ith row and jth column of the matrix $\mathbf{B}(\mathbf{y})$.

However, there are some restrictions on the matrix $\mathbf{B}(\mathbf{y})$. Lemma 2.3 of Hairer in Ref. [25] states that for this to be a valid Poisson bracket structure $\mathbf{B}(\mathbf{y})$ must be anti-symmetric, that is:

$$B_{ij}(\mathbf{y}) = -B_{ji}(\mathbf{y}) \,, \tag{B.7}$$

and it must satisfy the following equation relating to Jacobi's identity:

$$\sum_{l=1}^{N}\left(\frac{\partial B_{ij}(\mathbf{y})}{\partial q_j}B_{lk}(\mathbf{y})+\frac{\partial B_{jk}(\mathbf{y})}{\partial q_l}B_{li}(\mathbf{y})+\frac{\partial B_{ki}(\mathbf{y})}{\partial q_l}B_{lj}(\mathbf{y})\right)=0\,, \tag{B.8}$$

for all indices i, j, k ranging from 1 to N. For a given matrix, these may be shown straightforwardly using symbolic algebra software.

The equations of motion, for a given Hamiltonian, $\mathrm{H}(\mathbf{y})$, are then:

$$\frac{\mathrm{d}\mathbf{y}}{\mathrm{d}t}=\{\mathbf{y},\mathrm{H}(\mathbf{y})\}=(\nabla_{\mathbf{y}}\mathbf{y})^T\cdot\mathbf{B}(\mathbf{y})\cdot\nabla_{\mathbf{y}}\mathrm{H}(\mathbf{y})=\mathbf{B}(\mathbf{y})\cdot\nabla_{\mathbf{y}}\mathrm{H}(\mathbf{y})\,, \tag{B.9}$$

which is very similar to the canonical Hamiltonian equations of motion.

B.1.1 Vlasov Poisson Discretization

This section derives the explicit form of the Poisson structure matrix that comes from discretizing the continuous Vlasov Poisson system. Discretization involves approximating the continuous state of the system by a finite number of coordinates. The choice of these coordinates is specific to the particular approach, but will remain general for this section. It is important to note that these coordinates must be representable as functionals of the particle density function. Since the coordinates are functionals, one can use the Poisson bracket of the continuous system to find the equations of motion for the discrete system. To simplify working with the discrete system, the Poisson bracket can be expressed in terms of the new closed system of coordinates. This Poisson bracket highlights the underlying canonical structure of the non-canonical coordinates.

Reduced Poisson Bracket

Assume that a general functional $F[f]$, by some means, may be written in terms of our discrete variables, labelled with the vector $\mathbf{y}$. That is: $F[f]=\widetilde{F}(\mathbf{y})$. If each of the components of $\mathbf{y}$ are functionals of f, that is $y_i[f]$ for all i. Then we may use the chain rule of functional derivatives given by (A.10) to expand:

$$\frac{\delta F}{\delta f}=\frac{\partial\widetilde{F}}{\partial\mathbf{y}}\cdot\frac{\delta\mathbf{y}}{\delta f}=\sum_i\frac{\partial\widetilde{F}}{\partial y_i}\frac{\delta y_i}{\delta f}\,. \tag{B.10}$$

This may be substituted into the Poisson bracket, (1.6) and simplified:

$$\begin{aligned}
\{F, G\} &= \int \mathrm{d}^3\mathbf{x}\,\mathrm{d}^3\mathbf{p}\, f(\mathbf{x},\mathbf{p},t)\left[\frac{\delta F}{\delta f}, \frac{\delta G}{\delta f}\right] \\
&= \int \mathrm{d}^3\mathbf{x}\,\mathrm{d}^3\mathbf{p}\, f(\mathbf{x},\mathbf{p},t)\left[\sum_i \frac{\partial \widetilde{F}}{\partial y_i}\frac{\delta y_i}{\delta f}, \sum_j \frac{\partial \widetilde{G}}{\partial y_j}\frac{\delta y_j}{\delta f}\right] \\
&= \int \mathrm{d}^3\mathbf{x}\,\mathrm{d}^3\mathbf{p}\, f(\mathbf{x},\mathbf{p},t)\sum_{ij} \frac{\partial \widetilde{F}}{\partial y_i}\frac{\partial \widetilde{G}}{\partial y_j}\left[\frac{\delta y_i}{\delta f}, \frac{\delta y_j}{\delta f}\right] \\
&= \sum_{ij} \frac{\partial \widetilde{F}}{\partial y_i}\frac{\partial \widetilde{G}}{\partial y_j}\int \mathrm{d}^3\mathbf{x}\,\mathrm{d}^3\mathbf{p}\, f(\mathbf{x},\mathbf{p},t)\left[\frac{\delta y_i}{\delta f}, \frac{\delta y_j}{\delta f}\right] \\
&= \sum_{ij} \frac{\partial \widetilde{F}}{\partial y_i}\frac{\partial \widetilde{G}}{\partial y_j}\{y_i, y_j\}\,,
\end{aligned} \tag{B.11}$$

where the derivation used the fact that, $\widetilde{F}(\mathbf{y})$ and $\widetilde{G}(\mathbf{y})$ did not depend on the canonical coordinates $(\mathbf{x}, \mathbf{p})$ as well as the bilinear property of the Poisson bracket. This is the explicit form of (B.5), the general Poisson bracket structure. We see that the components of the Poisson structure matrix are given by:

$$B_{ij} = \{y_i, y_j\}\,, \tag{B.12}$$

as shown in the previous section. This shows how the continuous Poisson bracket becomes a general Poisson system when discretized.

Using this property, we only need to use the continuous Poisson bracket once to compute the Poisson structure matrix. Then, we can use the general Poisson structure matrix to compute equations of motion in much more simple manner.

B.2 Reduced Macro-particle Poisson Bracket

For the one-dimensional macro-particle methods presented in Section 2.2 the Poisson bracket may be simplified using the discretization scheme (2.6). Since the macro-particles define separate groups that only interact through

the self-field, the Poisson bracket becomes a sum over the macro-particles:

$$\{F, G\} = \sum_i \int \mathrm{d}x\, \mathrm{d}p\, f_i(x,p,t) \left[\frac{\delta F}{\delta f_i}, \frac{\delta G}{\delta f_i}\right] , \tag{B.13}$$

where each macro-particle has a separate Poisson bracket.

Since this discretization scheme is an explicit representation of the density function $f(x,p,t)$, then for any functional, $F[f]$ we may directly substitute (2.6) into the functional $F[f]$. After substitution $F[f]$ becomes the function $\widetilde{F}(w_1, \ldots w_{N_p}, x_1, , \ldots x_{N_p}, p_1, \ldots, p_{N_p})$, simply denoted $\widetilde{F}$. This process of discretization reduces functionals which are integrals over probability density functions to sums over the macro-particles.

First note that the discrete coordinates can be written as functionals of f_i:

$$\begin{aligned} w_i &= \int \mathrm{d}x\, \mathrm{d}p\, f_i(x,p,t)\,, \\ x_i &= \frac{1}{w_i} \int \mathrm{d}x\, \mathrm{d}p\, f_i(x,p,t)\, x\,, \\ p_i &= \int \mathrm{d}x\, \mathrm{d}p\, f_i(x,p,t)\, p\,. \end{aligned} \tag{B.14}$$

That is w_i is the total number of particles contained in each macro-particle. The coordinate x_i is the centroid of the macro-particle, and p_i is the average momentum of the macro-particle multiplied by the total number of real particles it contains; it is the mechanical momentum of the macro-particle.

The remaining variational derivatives may be computed given that the new coordinates depend on f_i as functionals, as shown by (B.14). Firstly, the macro-particle weight:

$$\frac{\delta w_i}{\delta f_i} = \frac{\delta}{\delta f_i} \left(\int \mathrm{d}x\, \mathrm{d}p\, f_i(x,p,t) \right) = 1\,, \tag{B.15}$$

directly from (A.6). Similarly, the momentum:

$$\frac{\delta p_i}{\delta f_i} = \frac{\delta}{\delta f_i} \left(\int \mathrm{d}x\, \mathrm{d}p\, f_i(x,p,t)\, p \right) = p\,. \tag{B.16}$$

Note that x_i depends on a product of the normalizing factor and another functional, this requires using the product rule. But first, the functional

derivative of the normalizing factor $1/w_i$ can be computed using the chain rule. It follows:

$$\frac{\delta(1/w_i)}{\delta f_i} = \frac{\partial(1/w_i)}{\partial w_i}\frac{\delta w_i}{\delta f_i} = -\frac{1}{w_i^2}\,. \tag{B.17}$$

where we used (B.15) to simplify. Each functional derivative is either given by (B.17) or (A.6) which gives:

$$\begin{aligned}\frac{\delta x_i}{\delta f_i} &= \left(\int \mathrm{d}x\,\mathrm{d}p\, f_i(x,p,t)\, x\right)\frac{\delta(1/w_i)}{\delta f_i} + \frac{1}{w_i}\frac{\delta}{\delta f_i}\left(\int \mathrm{d}x\,\mathrm{d}p\, f_i(x,p,t)\, x\right)\\ &= -\frac{1}{w_i^2}\left(\int \mathrm{d}x\,\mathrm{d}p\, f_i(x,p,t)\, x\right) + \frac{1}{w_i}x\\ &= \frac{x - x_i}{w_i}\,,\end{aligned} \tag{B.18}$$

where I substituted the definition of x_i. These explicit variational derivatives can now be used to compute the Poisson bracket between each of the coordinates.

Trivially, since the Poisson bracket between any functionals of f_i and f_j where $i \neq j$ is zero, only the following may be non-zero:

$$\begin{aligned}&\{w_i,w_i\}\,, \quad \{w_i,x_i\}\,, \quad \{w_i,p_i\}\,,\\ &\{x_i,w_i\}\,, \quad \{x_i,x_i\}\,, \quad \{x_i,p_i\}\,,\\ &\{p_i,w_i\}\,, \quad \{p_i,x_i\}\,, \quad \{p_i,p_i\}\,.\end{aligned} \tag{B.19}$$

However, recall that the non-canonical Poisson bracket is written using a canonical Poisson bracket with respect to $\mathbf{x}, \mathbf{p}$. Using this fact, the canonical Poisson bracket of w_i will yield zero. Thus, w_i is a constant of motion. Also, the Poisson bracket of a quantity with itself is identically zero. Which leaves:

$$\{x_i,p_i\}\,, \qquad\qquad \{p_i,x_i\}\,. \tag{B.20}$$

Computing these explicitly, we have:

$$\begin{aligned}
\{x_i, p_i\} &= \sum_j \int \mathrm{d}x\, \mathrm{d}p\, f_j(x,p,t) \left[\frac{\delta x_i}{\delta f_j}, \frac{\delta p_i}{\delta f_j}\right] \\
&= \int \mathrm{d}x\, \mathrm{d}p\, f_i(x,p,t) \left[\frac{x - x_i}{w_i}, p\right] \\
&= \frac{1}{w_i} \int \mathrm{d}x\, \mathrm{d}p\, f_i(x,p,t)\, [x,p] \\
&= \frac{1}{w_i} \int \mathrm{d}x\, \mathrm{d}p\, f_i(x,p,t) \\
&= 1\,.
\end{aligned} \tag{B.21}$$

$$\begin{aligned}
\{p_i, x_i\} &= \sum_j \int \mathrm{d}x\, \mathrm{d}p\, f_j(x,p,t) \left[\frac{\delta p_i}{\delta f_j}, \frac{\delta x_i}{\delta f_j}\right] \\
&= \int \mathrm{d}x\, \mathrm{d}p\, f_i(x,p,t) \left[p, \frac{x - x_i}{w_i}\right] \\
&= \frac{1}{w_i} \int \mathrm{d}x\, \mathrm{d}p\, f_i(x,p,t)\, [p,x] \\
&= \frac{1}{w_i} \int \mathrm{d}x\, \mathrm{d}p\, f_i(x,p,t)(-1) \\
&= -1\,.
\end{aligned} \tag{B.22}$$

The results may be expressed as:

$$\{x_i, p_j\} = \delta_{ij}\,, \qquad \{p_i, x_j\} = -\delta_{ij}\,, \tag{B.23}$$

which means that x_i is canonically conjugate to p_i.

So, the fully simplified Poisson bracket is expressed as:

$$\{F, G\} = \sum_i \left(\frac{\partial \widetilde{F}}{\partial x_i} \frac{\partial \widetilde{G}}{\partial p_i} - \frac{\partial \widetilde{F}}{\partial p_i} \frac{\partial \widetilde{G}}{\partial x_i} \right)\,, \tag{B.24}$$

which is the canonical Poisson bracket for discrete particles. This Poisson bracket is relatively general, since the macro-particle shape function, $R(x)$ has an arbitrary form. Also, note that the simplification of this Poisson bracket did not involve the Hamiltonian. The next step will be to see how

this mathematical structure may be used to derive well known algorithms for specific choices of the Hamiltonian.

B.3 Reduced Moment Poisson Bracket

The structure matrix, (2.51) is derived by taking the continuous Poisson bracket, (2.2) of each pair of coordinates. Before proceeding with calculation, note that each of the moments is a simpler phase-space function so (A.6) can be used to compute the functional derivative. This will leave the canonical Poisson bracket between each of these second order polynomial phase space functions. Since the canonical Poisson bracket is skew symmetric the diagonal terms will be zero. The upper triangular components of the matrix will differ from the lower triangular components by a sign. Hence, only three terms need to be computed.

$$\begin{aligned}\{\langle x^2\rangle, \langle xp\rangle\} &= \int \mathrm{d}x\,\mathrm{d}p\, f(x,p,t)\left[x^2, xp\right] \\ &= \int \mathrm{d}x\,\mathrm{d}p\, f(x,p,t)\, 2x^2 \\ &= 2\langle x^2\rangle\,,\end{aligned} \tag{B.25}$$

$$\begin{aligned}\{\langle x^2\rangle, \langle p^2\rangle\} &= \int \mathrm{d}x\,\mathrm{d}p\, f(x,p,t)\left[x^2, p^2\right] \\ &= \int \mathrm{d}x\,\mathrm{d}p\, f(x,p,t)\, 4xp \\ &= 4\langle xp\rangle\,,\end{aligned} \tag{B.26}$$

$$\begin{aligned}\{\langle xp\rangle, \langle p^2\rangle\} &= \int \mathrm{d}x\,\mathrm{d}p\, f(x,p,t)\left[xp, p^2\right] \\ &= \int \mathrm{d}x\,\mathrm{d}p\, f(x,p,t)\, 2p^2 \\ &= 2\langle p^2\rangle\,.\end{aligned} \tag{B.27}$$

Appendix C

Self-Field Implementation Details

C.1 Uniform Finite Element Discretization

The potential is discretized in the longitudinal direction by depositing it onto a set of basis functions. I choose to use linear finite elements which interpolate with second order accuracy in the grid spacing. The basis function $\psi_n(z)$ centred about z_n is:

$$\psi_n(z) = \begin{cases} 1 - \frac{|z-z_n|}{h}, & |z - z_n| < h/2 \\ 0, & \text{otherwise} \end{cases}, \tag{C.1}$$

where h is the width of the basis function and z_n is the centre of the nth grid-point. The arrangement of the basis functions is illustrated in Figure C.1.

C.1.1 Boundary Conditions

Consider the longitudinal domain to be given over an interval from $z \in [0, L]$. The most commonly used boundary conditions in such a basis is the Galerkin method where the configuration of node points is shown in Fig. C.2. The node points are labelled z_n where $n = 1, 2, \ldots, N_g$ and the open node points denote the absence of nodes on the boundary. Since the potential is exactly zero at $z = 0$ and $z = L$ this corresponds to metallic walls at these points.

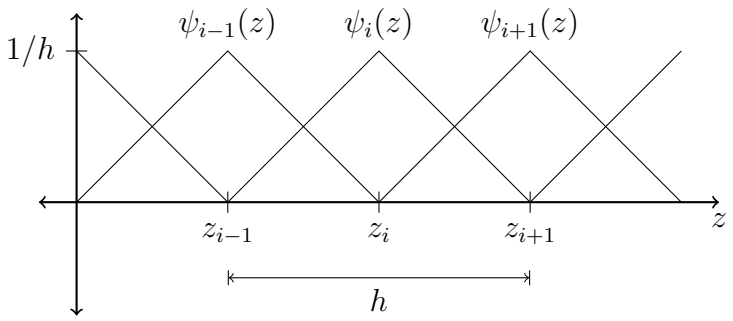

Figure C.1: Illustration of the basis of linear finite elements.

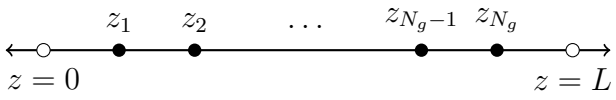

Figure C.2: Uniform grid with metallic boundary conditions. The nodes at the boundary are set to zero.

In accelerator physics, longitudinally metallic boundaries are not often useful as the beam travels through an open unobstructed pipe. However, by taking L to be large compared to the charge distribution we may approximate the potential in free space.

For other problems in accelerator physics, the beam has some periodic structure longitudinally, so a useful set of boundary conditions is periodic. The node configuration to construct a periodic grid with length L is shown in Fig. C.3. The open node locations denote the nearest neighbours on either side of the interval.

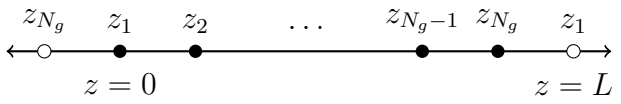

Figure C.3: Uniform grid with periodic boundary conditions. The nodes to the left and right of the interval are identified with nodes inside of the interval.

Choosing either set of boundary conditions will determine the specifics of the node mass and differentiation matrices. We will look at these in the next section.

C.1.2 Mass and Stiffness Matrices

Recall (3.21), the components arising from substituting the finite elements into the Lagrangian. Let us consider these components to define two square matrices $\mathbf{M}$ and $\mathbf{D}$ which are $N_g \times N_g$ real matrices. $\mathbf{M}$ may be identified as a mass matrix and $\mathbf{D}$ a stiffness matrix which has the interpretation of a second order central finite difference.

The explicit form of $\mathbf{M}$ and $\mathbf{D}$ for the linear finite elements are symmetric tri-diagonal matrices with components:

$$M_{nm} = \left(\frac{1}{6}\delta_{n,m+1} + \frac{2}{3}\delta_{n,m} + \frac{1}{6}\delta_{n,m-1}\right) , \tag{C.2}$$

$$D_{k\ell} = \left(-\delta_{n,m+1} + 2\delta_{n,m} - \delta_{n,m-1}\right) , \tag{C.3}$$

for the case of metallic boundary conditions. The periodic boundary conditions have additional terms:

$$M_{nm}^{\text{periodic}} = M_{nm} + \frac{1}{6}\left(\delta_{n,1}\delta_{m,N_g} + \delta_{n,N_g}\delta_{m,1}\right) , \tag{C.4}$$

$$D_{k\ell}^{\text{periodic}} = D_{k\ell} - \left(\delta_{k,1}\delta_{\ell,N_g} + \delta_{k,N_g}\delta_{\ell,1}\right) , \tag{C.5}$$

these are interaction terms between the first and last node. In matrix form

these are tri-diagonal matrices:

$$\mathbf{M} = \frac{1}{6}\begin{bmatrix} 4 & 1 & & & & & \\ 1 & 4 & 1 & & & & \\ & 1 & 4 & 1 & & & \\ & & & \ddots & & & \\ & & & 1 & 4 & 1 & \\ & & & & 1 & 4 & 1 \\ & & & & & 1 & 4 \end{bmatrix}, \tag{C.6}$$

$$\mathbf{D} = \begin{bmatrix} 2 & -1 & & & & & & \\ -1 & 2 & -1 & & & & & \\ & -1 & 2 & -1 & & & & \\ & & & \ddots & & & & \\ & & & -1 & 2 & -1 & & \\ & & & & -1 & 2 & -1 & \\ & & & & & -1 & 2 \end{bmatrix}, \tag{C.7}$$

as well as the periodic matrices, with additional coupling terms on the main skew diagonal:

$$\mathbf{M}^{\text{periodic}} = \frac{1}{6}\begin{bmatrix} 4 & 1 & & & & & & 1 \\ 1 & 4 & 1 & & & & & \\ & 1 & 4 & 1 & & & & \\ & & & \ddots & & & & \\ & & & 1 & 4 & 1 & & \\ & & & & 1 & 4 & 1 & \\ & & & & & 1 & 4 & 1 \\ 1 & & & & & & 1 & 4 \end{bmatrix}, \tag{C.8}$$

$$\mathbf{D}^{\text{periodic}} = \begin{bmatrix} 2 & -1 & & & & & & -1 \\ -1 & 2 & -1 & & & & & \\ & -1 & 2 & -1 & & & & \\ & & & \ddots & & & & \\ & & & -1 & 2 & -1 & & \\ & & & & -1 & 2 & -1 & \\ & & & & & -1 & 2 & -1 \\ -1 & & & & & & -1 & 2 \end{bmatrix}, \tag{C.9}$$

where the other components are zero.

To solve the system we need to simultaneously diagonalize **M** and **D**. If two matrices commute, then we can simultaneously diagonalize them.

Let us determine if these matrices commute. Note that **M** and **D** are symmetric matrices. If we assume that their product **MD** is symmetric then:

$$\mathbf{MD} = (\mathbf{MD})^T = \mathbf{D}^T\mathbf{M}^T = \mathbf{DM}\,, \tag{C.10}$$

the two matrices commute. So to verify for both metallic and periodic boundary conditions the matrix product was computed for arbitrary grid size using symbolic algebra software.

Firstly, the metallic boundary condition product is:

$$\begin{aligned}(MD)_{nm} &= \sum_k M_{nk}D_{km} \\ &= \left(-\frac{N_g}{6}\delta_{n,m+1} + \frac{4N_g}{3}\delta_{n,m} - \frac{N_g}{6}\delta_{n,m-1}\right)\,,\end{aligned} \tag{C.11}$$

as for the periodic boundary condition matrices, it is the same with additional terms:

$$\begin{aligned}(MD)^{\text{periodic}}_{nm} = (MD)_{nm} &- \frac{1}{2}\left(\delta_{n,1}\delta_{m,1} + \delta_{n,N_g}\delta_{m,N_g}\right) \\ &+ \frac{1}{6}\left(\delta_{n,1}\delta_{m,2} + \delta_{n,2}\delta_{m,1} + \delta_{n,N_g}\delta_{m,N_g-1} + \delta_{n,N_g-1}\delta_{m,N_g}\right)\,,\end{aligned} \tag{C.12}$$

these are both symmetric tri-diagonal matrices. Therefore, for these sets of boundary conditions **M** and **D** commute. This property is important for simultaneously diagonalizing both matrices to solve the system.

Note that the simultaneous diagonalization of these matrices is not a property that holds true for other sets of basis functions. The requirement for simultaneous diagonalization may prevent this scheme to be generalized to a higher order basis function or to other geometries.

C.2 Evaluating the Self-Field

To evaluate the self-potential requires solving a number of numerical convolutions which will take the majority of the CPU time per integration step.

C.2.1 Charge Density

Recall (3.30), the equation for the deposited charge density on node ℓ. Substituting the discretization scheme for the particle density function gives:

$$\rho_\ell(\mathbf{x}^\perp) = \sum_i w_i \int \mathrm{d}^2\mathbf{p}^\perp f_i^\perp(\mathbf{x}^\perp, \mathbf{p}^\perp) \int \mathrm{d}z\, R(z - Q_{zi})\psi_\ell(z)\,, \tag{C.13}$$

where the transverse spatial distribution is left general and the longitudinal direction is discrete. As in Chapter 2, Section 2.3, to calculate the potential values, we need to assume that the charge density has an explicit form.

The most straightforward assumption is that each macro-particle is uniformly distributed. Namely, consider the ith distribution to be a uniformly distributed ellipse with the standard deviation in x and y being given by the corresponding coordinates Q_{xi} and Q_{yi} respectively. Then:

$$\int \mathrm{d}^2\mathbf{p}^\perp f_i^\perp(\mathbf{x}^\perp, \mathbf{p}^\perp) = U(Q_{xi}, Q_{yi}, \mathbf{x}^\perp)\,. \tag{C.14}$$

The computational time complexity of evaluating the potential at a single point is $\mathcal{O}(N_p {N_g}^2)$, with $N_p \times N_g$ convolutions needing to be computed. This is approximately equivalent to a full 3D spectral method. We would prefer to have a 3D PIC-like scaling of $\mathcal{O}(N_p + {N_g}^2)$ so we will use a different assumption about the transverse density.

Instead, of each macro-particle having a definite shape, the transverse distribution of the entire beam on each basis node is assumed to be uniform. The total charge and transverse size of this uniform distribution is given by:

$$q_\ell = \sum_i q W_{i\ell}\,, \tag{C.15}$$

$$\langle x^2 \rangle_\ell = \frac{\sum_i (Q_{xi})^2 W_{i\ell}}{\sum_j W_{j\ell}}\,, \tag{C.16}$$

$$\langle y^2 \rangle_\ell = \frac{\sum_i (Q_{yi})^2 W_{i\ell}}{\sum_j W_{j\ell}}\,, \tag{C.17}$$

that is, q_ℓ is the charge at grid point ℓ, and $\langle x^2 \rangle_\ell$ and $\langle y^2 \rangle_\ell$ are the moments of the overall uniform distribution at that grid point. We call the matrix $\mathbf{W}$,

the longitudinal weight matrix defined by:

$$W_{i\ell} = w_i \int \mathrm{d}z\, R(z - Q_{zi}) K(z - z_\ell)\,. \tag{C.18}$$

So the charge density at each node is:

$$\rho_\ell(\mathbf{x}^\perp) = q_\ell U(\langle x^2\rangle_\ell, \langle y^2\rangle_\ell, \mathbf{x}^\perp)\,. \tag{C.19}$$

Using this charge density separates the sum over the particles in the field evaluation into a deposition step, which takes $\mathcal{O}(N_p)$, so this does scale like $\mathcal{O}(N_p + {N_g}^2)$. Now with ${N_g}^2$ convolutions needing to be computed, this reduces in the number of convolutions needed overall.

C.2.2 Convolutions

Consider an uncorrelated, uniform, transverse charge distribution function with half-width in the x-direction to be s_x and the half-width the y-direction to be s_y. The total number of charges in this transverse distribution is N. This distribution is given by:

$$\rho(x, y) = \frac{N}{\pi s_x s_y}\left[1 - \Theta\left(\frac{x^2}{s_x^2} + \frac{y^2}{s_y^2} - 1\right)\right]\,, \tag{C.20}$$

where $\Theta(x)$ is the Heaviside step function:

$$\Theta(x) = \int_{-\infty}^{x} \delta(x')dx'\,. \tag{C.21}$$

The convolution that needs to be evaluated is:

$$\int \mathrm{d}^2\tilde{\mathbf{x}}^\perp \rho_\ell(\tilde{\mathbf{x}}^\perp)\mathrm{G}_a(\mathbf{x}^\perp, \tilde{\mathbf{x}}^\perp)\,. \tag{C.22}$$

On-axis Self-Potential

Recall the external potential approximation described in Section 3.3. Since the self-field was Taylor expanded we only need to evaluate the self-potential

on-axis. This simplifies the integrals:

$$\int \mathrm{d}^2\tilde{\mathbf{x}}^\perp \rho_\ell(\tilde{\mathbf{x}}^\perp)\mathrm{G}_a(\mathbf{0}^\perp, \tilde{\mathbf{x}}^\perp)$$
$$= \frac{N}{2\pi^2 s_x s_y}\int \mathrm{d}x\mathrm{d}y K_0\left(k_a\sqrt{x^2+y^2}\right)\left[1-\Theta\left(\frac{x^2}{s_x^2}+\frac{y^2}{s_y^2}-1\right)\right]. \quad \text{(C.23)}$$

Transforming to normalized coordinates $s_x u = x$ and $s_y v = y$ simplifies to:

$$= \frac{N}{2\pi^2}\int \mathrm{d}u\mathrm{d}v K_0\left(k_a\sqrt{s_x^2u^2+s_y^2v^2}\right)\left[1-\Theta\left(u^2+v^2-1\right)\right]. \quad \text{(C.24)}$$

Now, transforming to polar coordinates (r,θ),

$$= \frac{N}{2\pi^2}\int \mathrm{d}r\mathrm{d}\theta\, r K_0\left(rk_a\sqrt{s_x^2\cos^2\theta+s_y^2\sin^2\theta}\right)\left[1-\Theta\left(r^2-1\right)\right]. \quad \text{(C.25)}$$

Integrating over r, gives the solution:

$$= \frac{N}{2\pi^2}\int \mathrm{d}\theta\,\frac{1-a(\theta)K_1\left(a(\theta)\right)}{(a(\theta))^2}, \quad \text{(C.26)}$$

where the function $a(\theta)$ is defined by:

$$a(\theta) = k_a\sqrt{s_x^2\cos^2\theta+s_y^2\sin^2\theta}, \quad \text{(C.27)}$$

for simplicity. Notice, that if $s_x = s_y$, there is cylindrical symmetry, then $a(\theta)$ is a constant and the integral is trivial. This integral is left to be done numerically.

Second Transverse Derivatives of the Self-Field

Now, because of the external potential approximation described in Section 3.3 the the second transverse derivatives of the potential need to be computed as well.

Note that (C.22), the integral between the charge distribution function and the Green's function, is a convolution. Hence, we may use the following property of convolutions. Let $f(x)$ and $g(x)$ be functions, and $*$ be the

convolution operation, then the derivative of their convolution is:

$$\frac{\mathrm{d}}{\mathrm{d}x}(f*g)(x) = \left(\frac{\mathrm{d}f}{\mathrm{d}x} * g\right)(x) = \left(f * \frac{\mathrm{d}g}{\mathrm{d}x}\right)(x)\,, \tag{C.28}$$

so we may write the second derivative as:

$$\frac{\mathrm{d}^2}{\mathrm{d}x^2}(f*g)(x) = \left(\frac{\mathrm{d}f}{\mathrm{d}x} * \frac{\mathrm{d}g}{\mathrm{d}x}\right)(x)\,. \tag{C.29}$$

Notice that the derivative of the charge density function gives a Dirac δ-function:

$$\frac{\partial\rho(x,y)}{\partial x} = -\frac{N}{\pi s_x s_y}\frac{2x}{s_x^2}\,\delta\left(\frac{x^2}{s_x^2}+\frac{y^2}{s_y^2}-1\right)\,. \tag{C.30}$$

Also, the derivative of the source term of the Green's function is a higher order Bessel function:

$$\frac{\partial\Phi_a(x,y)}{\partial x} = -\frac{1}{2\pi}k_a\frac{x}{\sqrt{x^2+y^2}}K_1\left(k_a\sqrt{x^2+y^2}\right)\,. \tag{C.31}$$

Following the same procedure as with the on-axis potential. This integral is transformed to normalized coordinates, then to polar coordinates. In this case, the Dirac delta function makes the radial integral trivial, and we are left with the following simplified angular integrals:

$$\left[\frac{\partial^2}{\partial x^2}\int \mathrm{d}^2\tilde{\mathbf{x}}^\perp\rho_\ell(\tilde{\mathbf{x}}^\perp)\mathrm{G}_a(\mathbf{x}^\perp,\tilde{\mathbf{x}}^\perp)\right]_{\mathbf{x}^\perp=\mathbf{0}} = \frac{N}{2\pi^2}k_a^2\int \mathrm{d}\theta\,\cos^2\theta\,\frac{K_1(a(\theta))}{a(\theta)}\,, \tag{C.32}$$

$$\left[\frac{\partial^2}{\partial y^2}\int \mathrm{d}^2\tilde{\mathbf{x}}^\perp\rho_\ell(\tilde{\mathbf{x}}^\perp)\mathrm{G}_a(\mathbf{x}^\perp,\tilde{\mathbf{x}}^\perp)\right]_{\mathbf{x}^\perp=\mathbf{0}} = \frac{N}{2\pi^2}k_a^2\int \mathrm{d}\theta\,\sin^2\theta\,\frac{K_1(a(\theta))}{a(\theta)}\,, \tag{C.33}$$

with the same $a(\theta)$ as before.

C.2.3 Computing the Image Charge

Recall (3.45), the image charge term in the Green's function for metallic boundary conditions with radius R. Taking the limit as either $|\mathbf{y}^\perp|\to 0$ or

$|\mathbf{x}^\perp| \to 0$, yields the potential term:

$$\begin{aligned} G_{\text{image}}(x,y) &= \lim_{|\mathbf{x}^\perp|\to 0} -\Phi_a\left(\frac{|\mathbf{x}^\perp|}{R}\left(\mathbf{y}^\perp - \frac{R^2}{|\mathbf{x}^\perp|^2}\mathbf{x}^\perp\right)\right) \\ &= -\Phi_a(R) \\ &= -\frac{1}{2\pi}K_0(k_a R)\,. \end{aligned} \tag{C.34}$$

Intuitively, this is a potential shift at the centre of the pipe by the total charge deposited on the pipe. The fact that this term is a constant means that computing the boundary conditions does not take appreciably more computation time.

The transverse derivative terms simplify as well. Starting from the second derivative of the image charge component of the Green's function, then taking the on-axis limit gives:

$$\frac{\partial^2 G_{\text{image}}}{\partial x^2}(x,y) = -\frac{k_a}{2\pi R^2}\left(x^2 k_a K_0(k_a R) + \frac{(x^2-y^2)}{R}K_1(k_a R)\right)\,, \tag{C.35}$$

$$\frac{\partial^2 G_{\text{image}}}{\partial y^2}(x,y) = -\frac{k_a}{2\pi R^2}\left(y^2 k_a K_0(k_a R) + \frac{(y^2-x^2)}{R}K_1(k_a R)\right)\,. \tag{C.36}$$

Integrating these terms against the charge density will give dependence on the second moments in x and y, and a difference of the moments, which is a quadrupole term.

Appendix D

Analytic Potentials

D.1 Uniform Sphere of Charge

The natural test of the field solver is of a uniformly distributed sphere of charge with total charge Q and radius R. To calculate the potential we refer to Chapter 1 of Jackson [33] to write the free-space solution for an arbitrary charge distribution:

$$\Phi(\mathbf{x}) = \frac{1}{4\pi\epsilon_0} \int \mathrm{d}\mathbf{x}' \frac{\rho(\mathbf{x}')}{|\mathbf{x} - \mathbf{x}'|}\,, \tag{D.1}$$

to take advantage of rotational symmetry we transform to spherical coordinates, (r, θ, φ) where θ is the polar angle and φ is the azimuthal angle. We put the centre of the sphere of charge at the origin. To transform the volume integral, the determinant of the Jacobian is $r^2 \sin\theta$. The distance between the test point (r, θ, φ) and the integration point (r', θ', φ') may be simplified by orienting the axis such that that the test point lies on the z-axis so $\theta = \varphi = 0$. Then the distance between the test and integration point is:

$$\sqrt{(r')^2 + r^2 - 2r'r\cos\theta'}\,. \tag{D.2}$$

Now, for a uniformly charged sphere, the charge density is the total charge Q over the volume of the sphere with radius R:

$$\rho(r) = \begin{cases} \frac{3Q}{4\pi R^3}, & r \leq R \\ 0, & \text{otherwise} \end{cases}\,. \tag{D.3}$$

Substituting these gives the volume integral over the sphere:

$$\Phi(r) = \frac{3Q}{16\pi^2\epsilon_0 R^3}\int_0^R \mathrm{d}r' \int_0^\pi \mathrm{d}\theta' \int_{-\pi}^\pi \mathrm{d}\varphi' \frac{(r')^2 \sin\theta'}{\sqrt{(r')^2 + r^2 - 2r'r\cos\theta'}}\,, \tag{D.4}$$

the integral over φ' is trivial, leaving us with:

$$\Phi(r) = \frac{3Q}{8\pi\epsilon_0 R^3}\int_0^R \mathrm{d}r'(r')^2 \int_0^\pi \mathrm{d}\theta' \frac{\sin\theta'}{\sqrt{(r')^2 + r^2 - 2r'r\cos\theta'}}\,. \tag{D.5}$$

To integrate over the polar angle, let $u = \sqrt{(r')^2 + r^2 - 2r'r\cos\theta'}$ then,

$$\mathrm{d}u = \frac{rr'\sin\theta'}{\sqrt{(r')^2 + r^2 - 2r'r\cos\theta'}}\mathrm{d}\theta'\,. \tag{D.6}$$

The bounds of integration become $\sqrt{(r')^2 + r^2 - 2r'r}$ and $\sqrt{(r')^2 + r^2 + 2r'r}$ for 0 and π respectively. Therefore the integration over the polar angle is as follows:

$$\begin{aligned}\Phi(r) &= \frac{3Q}{8\pi\epsilon_0 R^3}\int_0^R \mathrm{d}r'(r')^2 \int_{\sqrt{(r')^2+r^2-2r'r}}^{\sqrt{(r')^2+r^2+2r'r}} \frac{1}{rr'}\mathrm{d}u \\ &= \frac{3Q}{8\pi\epsilon_0 R^3}\int_0^R \mathrm{d}r'\frac{r'}{r}\left(\sqrt{(r')^2 + r^2 + 2r'r} - \sqrt{(r')^2 + r^2 - 2r'r}\right)\,,\end{aligned} \tag{D.7}$$

where we may factor the arguments of the square roots to find:

$$\Phi(r) = \frac{3Q}{8\pi\epsilon_0 R^3}\int_0^R \mathrm{d}r'\frac{r'}{r}\left(|r + r'| - |r - r'|\right)\,, \tag{D.8}$$

which may be simplified by considering the cases where $r' < r$ and $r' > r$. This splits the integral:

$$\Phi(r) = \frac{3Q}{8\pi\epsilon_0 R^3}\left(\int_0^r \mathrm{d}r'\,\frac{2(r')^2}{r} + \int_r^R \mathrm{d}r'\,2r'\right)\,, \tag{D.9}$$

and finally integrating the polynomials in r' this leaves us with:

$$\Phi(r) = \begin{cases} \frac{Q}{4\pi\epsilon_0}\frac{1}{R}\left(\frac{3}{2} - \frac{r^2}{2R^2}\right), & r \leq R \\ \frac{Q}{4\pi\epsilon_0}\frac{1}{r}, & \text{otherwise} \end{cases}. \tag{D.10}$$

Now, consider the potential in Cartesian coordinates:

$$\Phi(x,y,z) = \begin{cases} \frac{Q}{4\pi\epsilon_0}\frac{1}{R}\left(\frac{3}{2} - \frac{x^2+y^2+z^2}{2R^2}\right), & r \leq R \\ \frac{Q}{4\pi\epsilon_0}\frac{1}{\sqrt{x^2+y^2+z^2}}, & \text{otherwise} \end{cases}. \tag{D.11}$$

Evaluating the potential along the z-axis gives:

$$\varphi(z) = \Phi(0,0,z) = \begin{cases} \frac{Q}{4\pi\epsilon_0}\frac{1}{R}\left(\frac{3}{2} - \frac{z^2}{2R^2}\right), & r \leq R \\ \frac{Q}{4\pi\epsilon_0}\frac{1}{|z|}, & \text{otherwise} \end{cases}. \tag{D.12}$$

Now, the transverse derivatives along the z-axis are:

$$\varphi_{xx}(z) = \left.\frac{\partial^2}{\partial x^2}\Phi(x,y,z)\right|_{x=y=0} = \begin{cases} -\frac{Q}{4\pi\epsilon_0}\frac{1}{R^3}, & r \leq R \\ -\frac{Q}{4\pi\epsilon_0}\frac{1}{|z|^3}, & \text{otherwise} \end{cases}. \tag{D.13}$$

for x and $\varphi_{yy}(z)$ is identical. The particles are uniformly distributed in z with zero initial momentum in p_z. The particle weight is given by the linear charge density of the sphere:

$$\lambda(z) = \frac{3Q}{4}\,\frac{R^2 - z^2}{R^3}\,, \tag{D.14}$$

the transverse moments are initialized according to the longitudinal position.

D.2 Uniform Cylinder of Charge

We now consider a uniform cylinder with total charge Q of length L and radius R. In cylindrical coordinates, (r, θ, z) it is centred on the z-axis about

$z = 0$. The charge density:

$$\rho(r) = \begin{cases} \frac{Q}{\pi R^2 L}, & r \leq R,\, |z| < L/2 \\ 0, & \text{otherwise} \end{cases}, \tag{D.15}$$

and the Jacobian for cylindrical coordinates is r'. Once again let, r, z define the location of the test charge where the axis is defined such that $\theta = 0$. And let (r', θ', z') be the integration variables. The distance between the test and integration point is:

$$\sqrt{r^2 + (r')^2 - 2rr'\cos\theta' + (z - z')^2}\,. \tag{D.16}$$

So the potential is now:

$$\Phi(r, z) = \frac{Q}{4\pi^2\epsilon_0 R^2 L} \int_0^R \mathrm{d}r' \int_0^{2\pi} \mathrm{d}\theta' \int_{-L/2}^{L/2} \mathrm{d}z' \, \frac{r'}{\sqrt{r^2 + (r')^2 - 2rr'\cos\theta' + (z - z')^2}}\,. \tag{D.17}$$

In the pedagogical note, Ciftja et. al. in Ref. [34] present a trick to integrate over an angle between any pair of vectors in a cylindrical coordinate system, Equation 9 from that paper applied to our integral gives:

$$\int_0^{2\pi} \frac{\mathrm{d}\theta'}{\sqrt{r^2 + (r')^2 - 2rr'\cos\theta' + (z - z')^2}} = 2\pi \int_0^\infty \mathrm{d}k J_0(kr) J_0(kr') e^{-k|z - z'|}\,, \tag{D.18}$$

substituting and simplifying leaves us with:

$$\Phi(r, z) = \frac{Q}{2\pi\epsilon_0 R^2 L} \int_0^\infty \mathrm{d}k \int_0^R \mathrm{d}r' \int_{-L/2}^{L/2} \mathrm{d}z' \, r' J_0(kr) J_0(kr') e^{-k|z - z'|}\,. \tag{D.19}$$

This may not be integrated analytically, however, we only need the potential along the z-axis, so we will set $r = 0$ so that $J_0(kr) = 1$ and we may now integrate over r'. Using the recurrence property of derivatives of Bessel functions we have:

$$\frac{\partial}{\partial r'} J_1(kr') = k J_0(kr') - \frac{1}{r'} J_1(kr') \tag{D.20}$$

$$\implies J_0(kr') = \frac{1}{k} \frac{\partial}{\partial r'} J_1(kr') + \frac{1}{kr'} J_1(kr')\,. \tag{D.21}$$

So substituting into the integral, we find:

$$\begin{aligned}\int_0^R \mathrm{d}r'\, r' J_0(kr') &= \frac{1}{k}\int_0^R \mathrm{d}r'\, r' \frac{\partial}{\partial r'} J_1(kr') + \frac{1}{k}\int_0^R \mathrm{d}r' J_1(kr') \\ &= \frac{1}{k}\left([r' J_1(kr')]_0^R - \int_0^R \mathrm{d}r'\, J_1(kr') \right) + \frac{1}{k}\int_0^R \mathrm{d}r' J_1(kr') \\ &= \frac{1}{k}\left([r' J_1(kr')]_0^R \right) \\ &= \frac{R}{k} J_1(kR)\,,\end{aligned} \tag{D.22}$$

by integration by parts. Now, integrating over k using symbolic integration software to find:

$$\int_0^\infty \mathrm{d}k\, \frac{R}{k} J_1(kR) e^{-k|z-z'|} = \sqrt{R^2 + (z-z')^2} - |z-z'|\,, \tag{D.23}$$

which leaves an integral over z:

$$\Phi(z) = \frac{Q}{2\pi\epsilon_0 R^2 L}\int_{-L/2}^{L/2} \mathrm{d}z' \left(\sqrt{R^2 + (z-z')^2} - |z-z'| \right). \tag{D.24}$$

Once again using the integration software, the solution is given by the expression:

$$\begin{aligned}\Phi(z) = \frac{Q}{16\pi\epsilon_0 R^2 L}\Bigg[& 4R^2 \log\left(\frac{\sqrt{(L+2z)^2 + 4R^2} + L + 2z}{\sqrt{(L-2z)^2 + 4R^2} - L + 2z} \right) \\ & + (L+2z)\sqrt{(L+2z)^2 + 4R^2} \\ & + (L-2z)\sqrt{(L-2z)^2 + 4R^2} \\ & + \begin{cases} -2(L^2 + 4z^2), & |z| \le L/2 \\ -8L|z|, & |z| > L/2 \end{cases} \Bigg],\end{aligned} \tag{D.25}$$

where one term in the brackets is a piecewise polynomial in z and L. We also want to compute the second radial derivative of the potential along the z-axis. So, we return to Eq. D.19, the simplified expression for the potential,

with radial dependence:

$$\frac{\partial^2}{\partial r^2}\Phi(r,z)\bigg|_{r=0} = \frac{Q}{2\pi\epsilon_0 R^2 L}\int_0^\infty \mathrm{d}k \int_0^R \mathrm{d}r' \int_{-L/2}^{L/2} \mathrm{d}z'\, r' \left.\frac{\partial^2 J_0(kr)}{\partial r^2}\right|_{r=0} J_0(kr')e^{-k|z-z'|}\,, \tag{D.26}$$

but using the recurrence relation the term simplifies to:

$$\left.\frac{\partial^2 J_0(kr)}{\partial r^2}\right|_{r=0} = \lim_{r\to 0}\left[\frac{k}{r}J_1(kr) - k^2 J_0(kr)\right] = -\frac{k^2}{2}\,. \tag{D.27}$$

So the potential now simplifies in a similar way to before:

$$\frac{\partial^2\Phi}{\partial r^2}(z) = -\frac{Q}{4\pi\epsilon_0 R^2 L}\int_0^\infty \mathrm{d}k \int_0^R \mathrm{d}r' \int_{-L/2}^{L/2} \mathrm{d}z'\, k^2 r' J_0(kr')e^{-k|z-z'|}\,. \tag{D.28}$$

The integral over r' carries out as before:

$$\frac{\partial^2\Phi}{\partial r^2}(z) = -\frac{Q}{4\pi\epsilon_0 R^2 L}\int_0^\infty \mathrm{d}k \int_{-L/2}^{L/2} \mathrm{d}z'\, RkJ_1(kR)e^{-k|z-z'|}\,. \tag{D.29}$$

Now, integrating over k using the symbolic integration software:

$$\frac{\partial^2\Phi}{\partial r^2}(z) = -\frac{Q}{4\pi\epsilon_0 R^2 L}\int_{-L/2}^{L/2} \mathrm{d}z'\, \frac{R^2}{(R^2+(z-z')^2)^{3/2}}\,, \tag{D.30}$$

and integrating over z' leaves the final solution:

$$\frac{\partial^2\Phi}{\partial r^2}(z) = -\frac{Q}{4\pi\epsilon_0 R^2 L}\left(\frac{L-2z}{\sqrt{4R^2+(L-2z)^2}} + \frac{L+2z}{\sqrt{4R^2+(L+2z)^2}}\right)\,, \tag{D.31}$$

which gives the second transverse derivatives in the x and y directions.

D.3 Expanding Uniform Sphere of Charge

Consider the uniform sphere of charge to be composed of a sphere of particles initially at rest. We are interested in the time evolution of the sphere.

Recall Eq D.10, the potential for the uniform sphere of charge. The radial

electric field inside the sphere is:

$$E_r(r) = -\frac{\partial}{\partial r}\Phi(r) = \frac{Q}{4\pi\epsilon_0}\frac{r}{R^3}\,, \tag{D.32}$$

this will cause the distribution of particles to be repelled from each other, and the sphere to expand.

Due to the rotational symmetry of the problem, only the radial distribution of particles can change over time. Also, the consequence of assuming rotational symmetry is that the magnetic field is zero. To illustrate, consider the general solution to the vector potential in the Lorentz gauge:

$$\mathbf{A}(\mathbf{x},t) = \frac{\mu_0}{4\pi}\int \mathrm{d}^3\mathbf{x}'\frac{\mathbf{J}(\mathbf{x}',t')}{|\mathbf{x}-\mathbf{x}'|}\,, \tag{D.33}$$

due to the symmetry the only non-zero component of $\mathbf{J}(\mathbf{x}',t')$ is the radial component $J_r(r,t)$. Therefore the only non-zero component of the vector potential is radial as well; $A_r(r,t)$. Computing the magnetic field by calculating the curl of this quantity gives a zero magnetic field.

$$\mathbf{B}(r,\theta,\varphi,t) = \frac{1}{r}\left(\frac{1}{\sin\theta}\frac{\partial A_r}{\partial\varphi}\hat{\theta} - \frac{\partial A_r}{\partial\theta}\hat{\varphi}\right) = \mathbf{0}\,. \tag{D.34}$$

Since gauge transformations do not change the magnetic field, this is true for all gauges. Because the force applied to the distribution by the electric field is linear in radius, the sphere will maintain uniformity.

Therefore as the sphere expands the potential is simply re-scaled by the radius. To track the expansion of the sphere consider the force applied to the particle with charge q at the edge of the sphere:

$$\mathrm{F} = \frac{qQ}{4\pi\epsilon_0 R^2}\,. \tag{D.35}$$

So as the sphere expands the particle gains non-relativistic kinetic energy:

$$\mathrm{T} = \frac{1}{2}m\left(\frac{\mathrm{d}R}{\mathrm{d}t}\right)^2\,. \tag{D.36}$$

Even though the force is changing in time, we may equate the infinitesimal

change in kinetic energy to the work done for this particle:

$$\mathrm{dT} = \mathrm{F} \cdot \mathrm{d}R \tag{D.37}$$

We will integrate time from the initial time $t = 0$ to an arbitrary time $t > 0$:

$$\int_0^t \mathrm{dT} = \int_{R(0)}^{R(t)} \mathrm{F} \cdot \mathrm{d}R \tag{D.38}$$

$$\left[\frac{1}{2}m\left(\frac{\mathrm{d}R}{\mathrm{d}t}\right)^2\right]_0^t = \int_{R(0)}^{R(t)} \frac{qQ}{4\pi\epsilon_0 R^2}\mathrm{d}R \tag{D.39}$$

$$\left[\left(\frac{\mathrm{d}R}{\mathrm{d}t}\right)^2\right]_0^t = \frac{qQ}{2\pi\epsilon_0 m}\int_{R(0)}^{R(t)} \frac{1}{R^2}\mathrm{d}R\,. \tag{D.40}$$

Now, we can apply the condition that the sphere is initially stationary and the initial radius is R_0:

$$\left(\frac{\mathrm{d}R}{\mathrm{d}t}\right)^2 = \frac{qQ}{2\pi\epsilon_0 m}\left[\frac{1}{R_0} - \frac{1}{R(t)}\right] \tag{D.41}$$

$$\frac{\mathrm{d}R}{\mathrm{d}t} = \pm\sqrt{\frac{qQ}{2\pi\epsilon_0 m}\left[\frac{1}{R_0} - \frac{1}{R(t)}\right]}\,, \tag{D.42}$$

from which we choose the positive solution, since the sphere is expanding. Notice, that the integrated work done is simply the difference in the potentials between the two points. This is unexpected for a system with time-varying fields. It may be understood that the only energy exchange is between the kinetic energy of the particles and the electric field energy, since there is no radiation.

We now have a differential equation for the velocity of the particle at the edge of the sphere. We may integrate its inverse to find the time it takes to double in size:

$$\int_0^{t_2} \mathrm{d}t = \int_{R_0}^{2R_0} \frac{1}{\sqrt{\frac{qQ}{2\pi\epsilon_0 m}\left[\frac{1}{R_0} - \frac{1}{R(t)}\right]}}\mathrm{d}R\,. \tag{D.43}$$

The integral is calculated using symbolic integration software:

$$\int_{R_0}^{2R_0} \left(\frac{1}{R_0} - \frac{1}{R}\right)^{-1/2} \mathrm{d}R = {R_0}^{3/2} \left(\sqrt{2} + \sinh^{-1}(1)\right) . \tag{D.44}$$

So the time for the sphere to double in size is given by:

$$t_2 = \left(\sqrt{2} + \sinh^{-1}(1)\right) \sqrt{\frac{2\pi\epsilon_0 m {R_0}^3}{qQ}} . \tag{D.45}$$

In fact, integrating from the initial radius to any larger radius given by aR_0 where $a > 1$ corresponds to a time:

$$t(R = aR_0) = \left(\frac{1}{2}\log\left(2a - 1 + 2\sqrt{a(a-1)}\right) + \sqrt{a(a-1)}\right) \sqrt{\frac{2\pi\epsilon_0 m {R_0}^3}{qQ}} . \tag{D.46}$$